



## **Deliverable 8.1: State-of-the-art report**

Work Package 8

This project has received funding from the European Union's Horizon 2020 research and innovation programme under grant agreement No 847593.



## Document information

Project Acronym	<b>EURAD</b>
Project Title	<b>European Joint Programme on Radioactive Waste Management</b>
Project Type	<b>European Joint Programme (EJP)</b>
EC grant agreement No.	<b>847593</b>
Project starting / end date	<b>1<sup>st</sup> June 2019 – 30 May 2024</b>
Work Package No.	<b>8</b>
Work Package Title	<b>Spent Fuel Characterization and Evolution Until Disposal</b>
Work Package Acronym	<b>SFC</b>
Deliverable No.	<b>8.1</b>
Deliverable Title	<b>State-of-the-art report</b>
Lead Beneficiary	<b>Nagra</b>
Contractual Delivery Date	<b>November 2019</b>
Actual Delivery Date	<b>14 March 2022</b>
Type	<b>Report</b>
Dissemination level	<b>PU</b>
Authors	<b>Stefano Caruso (Nagra/KKG), Efstathios Vlassopoulos (Nagra), Ron Dagan (KIT), Luca Fiorito (SCK CEN), Michel Herm (KIT), Peter Jansson (UU), Marjan Kromar (JSI), Márton Király (MTA-EK), Jaakko Leppanen (VTT), Francisco Feria Marquez (CIEMAT), Volker Metz (KIT), Dimitrios Papaioannou (JRC KA), to Luis E. Herranz (CIEMAT), Dimitri Rochman (PSI), Peter Schillebeeckx (JRC ), Marcus Seidl (EON), Augusto Hernandez Solis (SCK CEN), Alexey Stankovskiy (SCK CEN), Francisco Alvarez Velarde (CIEMAT), Marc Verwerft (SCK CEN), M<sup>a</sup> Nieves Rodriguez Villagra (CIEMAT), Uwe Zencker (BAM), Gasper Žerovnik (JRC)</b>

### To be cited as:

Final version as of 14.03.2022 of deliverable D8.1 of the HORIZON 2020 project EURAD. EC Grant agreement no: 847593

### Disclaimer

All information in this document is provided "as is" and no guarantee or warranty is given that the information is fit for any particular purpose. The user, therefore, uses the information at its sole risk and liability. For the avoidance of all doubts, the European Commission has no liability in respect of this document, which is merely representing the authors' view.

### Acknowledgement

This document is a deliverable of the European Joint Programme on Radioactive Waste Management (EURAD). EURAD has received funding from the European Union's Horizon 2020 research and innovation programme under grant agreement No 847593.

Status of deliverable		
	By	Date
Delivered (Lead Beneficiary)	Nagra	31.01.2020
Verified (WP Leader)	SKB (UU)	31.01.2020
Reviewed (Reviewers)	David Hambley (NNL, UK) Laura McManniman (IAEA)	15.02.2021
Verified (WP Leader)	SKB	17.12.2021
Reviewed (PMO)	Paul Carbol	08.02.2022
Verified (WP Leader)	SKB	14.03.2022
Approved (PMO)	Paul Carbol	14.03.2022
Submitted to EC (Coordinator)	Andra	15.03.2022

## EURAD SFC – Project Overview

EURAD is an EC-funded project with a programme of integrated work packages (WPs) spanning many domains of radioactive waste management based on the needs and views of the mandated actors of the Member States. The EURAD scope seeks to be beneficial to national waste management programmes at all stages of advancement by supporting them in their RD&D activities. For that purpose, EURAD has a strong focus on knowledge management with a view to making existing information easily available and to provide means for transfer knowledge.

The project Spent Fuel Characterization and Evolution Until Disposal (SFC) is WP8 within the framework of the EURAD programme, aiming to provide a better understanding of spent nuclear fuel (SNF) properties from the perspective of pre-disposal activities, but also exploring aspects having an impact on long-term safety. The EURAD/SFC consortium brings together more than 20 partners with a range of skills and competences in spent fuel assessment, from management to experimental work. The consortium consists of national waste management organisations, research institutes, universities, technical support organisations and commercial organisations.

The results obtained within the WP will provide a rigorous scientific approach to developing the technical bases for continued safe and secure storage of spent nuclear fuel, in terms of transport, retrieval and pre-disposal options. These achievements are intended to support national programmes and safety assessments and are made available to all interested stakeholders. Safety aspects (i.e. better acknowledgement of safety-related parameter uncertainties, the contribution and further development of guidance on operational safety for both interim storage and fuel packaging facilities) and optimisation aspects (i.e. optimisation of the number of assemblies for the loading of disposal canisters based on precise determination of decay heat and reactivity of spent fuel assemblies) are intended to be addressed by the WP. Extremely valuable will be the combination of both numerical calculations and experimental methods, which aims to provide a complete and thorough understanding of the mechanisms driving the behaviour of the SNF in pre-disposal activities, for both normal and accident conditions.

For more information, please visit the EURAD website at: <https://www.ejp-eurad.eu/>

## Executive Summary

The first task of WP8 is dedicated to the state-of-the-art (SOTA) report and related know-how transfer and distribution. The SOTA report is the first product of the SFC research programme, which offers an overview of the status of knowledge in the field of spent nuclear fuel characterisation and assessment during the pre-disposal phase. The document aims to focus on the current safety-significant gaps and related challenges, providing a direct link to the goals of the mandated actors of EURAD. The report is expected to be used by all EURAD colleagues in their national programmes. However, this SOTA report is intended as an initial version, to be updated at the end of the WP to become the final SOTA report. The aim of the final report is to become a key reference in the field and to gain high recognition and visibility as a key resource for knowledge management programmes and to contribute to demonstrating and documenting the state-of-the-art.

Depending on individual back-end country strategies, being programme-based within the framework of their national strategy, spent nuclear fuel (SNF) can be destined for direct geological disposal, for reprocessing or for long-term interim storage followed by disposal. For all cases, a proper characterisation of the spent fuel is required.

A state-of-the-art review on characterisation of SNF properties in terms of source term and inventory assessment (neutron, gamma-ray emission, decay heat, radionuclide inventory, elemental content) and in terms of out-of-core fuel performance (cladding performance and fuel integrity in view of the safety criteria for SNF interim storage, transport and canister packaging) using several numerical and experimental approaches and methodologies is presented.

The ability to reliably predict spent nuclear fuel composition and SNF properties, namely radionuclide inventory and source term, is relevant for both operational and long-term safety assessment in geological disposal, as well as for disposal cost key factors, and relies on ad-hoc calculation schemes.

The calculations require a particle transport code coupled with a depletion solver. A large proportion of the available depletion codes has been reviewed in this work. However, since the results also depend on nuclear data and operational data as well as assay data, nuclear data libraries and uncertainty aspects have also been discussed. More specifically, the uncertainty of the fuel inventory can be dominated by several factors: irradiation history of the fuel, exact composition of the fresh fuel/cladding especially the level of impurities, and the large heterogeneities in the fuel design discharged from reactors, as well as modelling limitations, nuclear data libraries and reactor core characteristics such as, e.g., void fractions (in BWR's) and mechanical changes of fuel during irradiation. Therefore, the treatment of all related uncertainties (quantification and propagation) has been part of this review. The availability of experimental data enables testing and validation of codes and models in order to understand how closely the models replicate reality. The SOTA report also focuses on experimental verification techniques, i.e. Non-Destructive Analysis (NDA) methods (e.g. neutron and gamma spectrometry, gamma tomography, calorimetry, etc.) and Destructive Analysis (DA). Other non-conventional techniques (e.g. muon tomography) are also reviewed.

Furthermore, when considering operational safety cases for the surface facilities where the fuel must be encapsulated in special disposal canisters, studies and research activities are required to assess spent fuel performance as well as developing concepts for handling of consequence scenarios. Therefore, another part of the SOTA report reviews experimental campaigns developed to investigate fuel integrity. Conventional techniques for investigating the effect of hydrogen load, hydride distribution and fuel/cladding interaction, mechanical performance of the cladding and cladding integrity, deterioration of the mechanical properties of the cladding material resulting from Delayed Hydride Cracking (DHC) for high burnup are also reviewed, all with the focus on (extended) dry storage conditions.

Finally, the status of knowledge on definition and screening of accident scenarios with respect to pre-disposal activities, such as fuel packaging and transport, is provided on the basis of IAEA general assumptions.

## List of Figures

<a href="#"><u>Figure 1 – Specific thermal power (or decay heat rate) of an irradiated fuel sample as a function of cooling time</u></a> .....	20
<a href="#"><u>Figure 2 – Relative contribution of radionuclides to the thermal power of an irradiated fuel sample as a function of cooling time</u></a> .....	20
<a href="#"><u>Figure 3 – Comparison of the <math>^{134}\text{Cs}(n,\gamma)</math> cross-sections as a function of neutron energy which are recommended in the ENDF/B-V, ENDF/B-VII.0, JEFF-3.3 and JENDL-4.0 libraries</u></a> .....	35
<a href="#"><u>Figure 4 – Relative sensitivity of the nuclide inventory to the initial enrichment (IE) and burnup (BU)</u></a> .....	37
<a href="#"><u>Figure 5 – Comparison of the <math>^{147}\text{Nd}(n,\gamma)</math> cross-sections as a function of neutron energy that are recommended in the ENDF/B-VIII.0, JEFF-3.3, JENDL-4.0 and TENDL-2017 libraries</u></a> .....	39
<a href="#"><u>Figure 6 – Concentration of <math>^{244}\text{Cm}</math> as a function of burnup for a <math>\text{UO}_2</math> sample with initial enrichment of 4.8 wt.-% irradiated in a PWR to a burnup of 45 GWd/t</u></a> .....	47
<a href="#"><u>Figure 7 – Schematic representation of pellet cracking, evolution of the "hourglass" shape, and pellet-cladding gap during operation</u></a> .....	60
<a href="#"><u>Figure 8 – The three stages of creep</u></a> .....	62
<a href="#"><u>Figure 9 – The mandrel test performed with a ductile (left) and a brittle sample (right)</u></a> .....	64
<a href="#"><u>Figure 10 – Overview of the 3-point bending apparatus (a) and impact tower (b)</u></a> .....	66
<a href="#"><u>Figure 11 – Scheme of the specimen positioning in the bending (a) and impact (b) device</u></a> .....	66
<a href="#"><u>Figure 12 – A gastight specimen assembly connected to the pressure gauge and with the attached pressure transducer, ready for mechanical testing</u></a> .....	67
<a href="#"><u>Figure 13 – Measured deflection and maximum fracture load as a function of hydrogen concentration in the cladding during the cold 3-point bending test</u></a> .....	67
<a href="#"><u>Figure 14 – Load-displacement curves of high and low BU samples during the 3-point bending test</u></a> .....	68
<a href="#"><u>Figure 15 – Representative selected frames of the image sequence during an impact test on a SNF rod</u></a> .....	69
<a href="#"><u>Figure 16 – The hammer velocity change is used to calculate the transmitted energy that caused the specimen rupture</u></a> .....	69
<a href="#"><u>Figure 17 – Typical hydride distribution in a cladding tube</u></a> .....	70
<a href="#"><u>Figure 18 – Ring compression test experimental setup (left) and typical load-displacement curves (right)</u></a> .....	72
<a href="#"><u>Figure 19 – Different orientations of the TSC for the drop from a 9-m height</u></a> .....	85
<a href="#"><u>Figure 20 – Different loading modes of the fuel rod</u></a> .....	86

## List of Tables

<a href="#"><u>Table 1 – Burnup codes used in the comparison exercise reported by Žerovnik et al.</u></a> .....	29
<a href="#"><u>Table 2 – Comparison of the abundance of key nuclides present in a spent nuclear fuel sample of after a cooling time of 5 years</u></a> .....	31
<a href="#"><u>Table 3 – Cross-section for neutron-induced fission of <sup>235</sup>U and <sup>239</sup>Pu recommended in the latest versions of the main data libraries</u></a> .....	34
<a href="#"><u>Table 4 – Cumulative fission yields of <sup>90</sup>Sr, <sup>137</sup>Cs and <sup>148</sup>Nd for neutron-induced fission of <sup>235</sup>U and <sup>239</sup>Pu at thermal energy (or 2'200 m/s)</u></a> .....	34
<a href="#"><u>Table 5 – Total recoverable energy (Er) together with that resulting from charged particle (Er,cp) and <math>\gamma</math>-ray (Er,<math>\gamma</math>) emission due to the decay of the <sup>90</sup>Sr/<sup>90</sup>Y and <sup>137</sup>Cs/<sup>137m</sup>Ba chains</u></a> .....	35
<a href="#"><u>Table 6 – Total cross-section and cross-section for neutron elastic scattering and capture of <sup>103</sup>Rh at thermal energy</u></a> .....	36
<a href="#"><u>Table 7 – Recoverable energy due to neutron-induced interaction with <sup>235</sup>U and <sup>239</sup>Pu</u></a> .....	38
<a href="#"><u>Table 8 – Recoverable energy for some important neutron absorption reactions</u></a> .....	38
<a href="#"><u>Table 9 – Uncertainties of the inventory due to the propagation of nuclear data uncertainties</u></a> .....	42
<a href="#"><u>Table 10 – Uncertainty evaluation of the decay heat estimated by theoretical calculations</u></a> .....	43
<a href="#"><u>Table 11 – Synthesis of fuel performance codes and key phenomena simulated in dry storage</u></a> .....	79

## Glossary

ARIANE	Actinide Research In A Nuclear Element
ATF	Accident Tolerant Fuels
BDBA	Beyond Design Base Accident
BU	Burnup
BUC	Burnup Credit
BWR	Boiling Water Reactor
CIRFT	Cyclic Integrated Reversible-bending Fatigue Tester
CRAM	Chebyshev Rational Approximation Method
DA	Destructive Analysis
DBA	Design Basis Accidents
DBTT	Ductile-to-Brittle Transition Temperature
DDEP	Decay Data Evaluation Project
DHC	Delayed Hydride Cracking
DBRC	Doppler-Broadening Rejection Correction
EGADSNF	Expert Group on Assay Data of Spent Nuclear Fuel
EGBCC	Expert Group on Burnup Credit Criticality
ENDF	Evaluated Nuclear Data Files
EOL	End Of Life
ESARDA	European Safeguards Research and Development Association
FA	Fuel Assembly
FCCI	Fuel/Cladding Chemical Interaction
FDC	Final Disposal Canister
FEA/FEM	Finite Element Analysis/Finite Element Modelling
FIP	Fuel Integrity Project
FP	Fission Product
IAEA	International Atomic Energy Agency
ICP-SF-MS	Inductively Coupled Plasma – Sector Field – Mass Spectrometer
ICPS	Inductively Coupled Plasma Spectrometer
IE	Initial Enrichment
INL	Idaho National Laboratory
JRC	Joint Research Center
LWR	Light Water Reactor
MCNP	Monte Carlo N-Particle Transport Code
NDA	Non-Destructive Analysis
NEA	Nuclear Energy Agency

NPP	Nuclear Power Plants
ORNL	Oak Ridge National Laboratory
PGET	Passive Gamma Emission Tomography
PCI	Pellet-Cladding Interaction
PCMI	Pellet-Cladding Mechanical Interaction
PIE	Post-Irradiation Examination
PNNL	Pacific Northwest National Laboratory
PWR	Pressurised Water Reactor
RCT	Ring Compression Test
RHCF	Radial Hydride Continuity Factor
SCC	Stress Corrosion Cracking
SCIP	Studsвик Cladding Integrity Project
SNF	Spent Nuclear Fuel
SPAR	Spent fuel Performance Assessment and Research
TIMS	Thermal Ionisation Mass Spectrometer
TSC	Transport Storage Cask
UFDC	Used Fuel Disposition Campaign

## Table of Content

EURAD SFC – Project Overview.....	4
Executive Summary.....	5
List of Figures.....	6
List of Tables.....	7
Glossary.....	8
Table of Content.....	10
7. Introduction.....	12
2. Characterisation of the fuel, fuel inventory and source term.....	14
2.1. Observables and nuclides of interest.....	14
2.2. Theoretical calculation of the nuclide inventory and observables.....	16
2.2.1. Principles.....	17
2.2.2. Burnup codes.....	19
2.2.3. Code comparison.....	24
2.3. Sources of bias effects and uncertainties.....	27
2.3.1. Methodology.....	27
2.3.2. Nuclear data.....	28
2.3.3. Fuel history.....	33
2.4. Uncertainty evaluation and sensitivity analysis.....	36
2.4.1. Methods.....	36
2.4.2. Examples.....	38
2.5. Experimental determination of SNF source terms and observables.....	40
2.5.1. Analysis of fuel rods and segments.....	41
2.5.2. Non-destructive assay of spent fuel assemblies.....	43
2.5.3. Verification of transport and storage casks.....	47
2.6. Code validation.....	47
2.6.1. ALEPH2.....	47
2.6.2. CASMO and SIMULATE.....	48
2.6.3. DRAGON.....	49
2.6.4. EVOLCODE.....	49
2.6.5. SCALE.....	50
2.6.6. SERPENT.....	50
2.7. Summary and conclusions.....	51
3. Performance of spent nuclear fuel during pre-disposal activities and experimental characterisation.....	52
3.1. Introduction about spent nuclear fuel degradation.....	52

3.2. Key phenomena .....	52
3.2.1. UO <sub>2</sub> oxidation.....	53
3.2.2. Pellet-Cladding Interaction .....	54
3.3. Experimental characterisation .....	56
3.3.1. Radiochemical and chemical analysis of irradiated fuel rod components.....	56
3.3.2. Fuel-cladding chemical interaction analysis .....	56
3.3.3. Thermo-mechanical creep test.....	57
3.3.4. Mandrel ductility test.....	58
3.3.5. Three-point bending and impact tests .....	60
3.3.6. Ring compression test .....	66
3.4. Numerical methods and analysis .....	69
3.4.1. Finite element analysis and mechanical state of the fuel.....	69
3.4.2. Fuel performance codes.....	72
4. Accident scenarios.....	76
4.1. Safety standards for pre-disposal management of SNF .....	76
4.2. Accident scenarios for fuel in interim storage.....	77
4.3. Accident scenarios for SNF during transport.....	79
4.4. Other accident scenarios and the way forward to the final SOTA report .....	81
5. Acknowledgements .....	82
6. Conclusions .....	83
A. Relevant Radionuclides .....	84
References .....	87

## 7. Introduction

The ability to reliably predict spent nuclear fuel composition in terms of radionuclide inventory, elemental content, decay heat and radiation source term is relevant for both operational and long-term safety assessment in geological disposal and has an important influence on the cost of disposal. Calculations are thus required to fully characterise the SNF. The calculations involve a neutron transport code coupled with a depletion solver. The results depend on nuclear data and assay data. More specifically, the uncertainty of the fuel inventory can be dominated by several factors: irradiation history of the fuel, exact composition of the fresh fuel/cladding, such as the level of impurities, and the large heterogeneities in the fuel design discharged from reactors, as well as code modelling limitations and reactor physics code characteristics themselves. However, the availability of experimental data allows testing and validation of codes and models in order to be able to simulate the irradiation conditions quite closely to reality, or at least to assess a solid baseline as a starting point for further uncertainty assessments. If the baseline (i.e. code and fuel model) is known, being properly characterised by a well determined uncertainty, further assumptions can be analysed and incorporated in such a way as to encompass variables in a conservative way, but avoiding bringing the final estimates to a level of over-conservatism.

Depending on individual back-end country strategies, being programme-based within the framework of their national strategy, spent nuclear fuel (SNF) can be destined for direct geological disposal, for reprocessing or for long-term interim storage followed by disposal. For all cases, a proper characterisation of the spent fuel is required, even if the fuel changes its basic form, as in the reprocessing case where the final waste form is a glass and/or compacted metals.

For the case of geological disposal, safety assessments are required to cover a temporal spectrum typically of 1 million years, which implies the development of a qualification process using appropriate research programmes to reasonably reduce the level of uncertainties in the characterisation of the SNF. In particular, the spent nuclear fuel composition must be determined in terms of radionuclide inventory, elemental content, decay heat and radiation source term. Some observables can be determined by Non-Destructive Analysis (NDA) methods (such as decay heat by calorimetric measurements); however, such assays are time-consuming and are almost impracticable for addressing the entire SNF inventory produced over the lifetime of one or more Nuclear Power Plants (NPPs). Therefore, the ability to reliably simulate and predict the SNF source term are extremely important.

Nevertheless, the assessment can have different levels of relevance when considering operational safety cases at the level of surface facilities where the fuel must be encapsulated in special disposal canisters, or for long-term safety assessment where the SNF is encapsulated in canisters embedded in bentonite (or other buffer materials), surrounded by a host rock (in caverns).

Pre-disposal activities such as SNF transport after interim storage and/or unloading/loading and handling operations for the packaging of the SNF from the transport/storage casks (TSC) into the final disposal canisters (FDC) are safety-relevant operations. Therefore, studies and research activities aimed at assessing spent fuel performance, and developing concepts for handling of consequence scenarios, are required by many countries. Experimental campaigns to investigate fuel integrity are extremely valuable. Many aspects are indeed under observation: effect of hydrogen load, hydride distribution and fuel/cladding interaction, mechanical performance of the cladding and cladding integrity, deterioration of the mechanical properties of the cladding material resulting from Delayed Hydride Cracking (DHC) for high burnup, whilst all are relevant for long term dry storage, many aspects are also relevant to other back end activities such as post storage recovery and transport.

## Scope and structure of the SOTA report

The state-of-the-art (SOTA) report aims to provide an overview of the status of knowledge in the field of spent nuclear fuel characterisation and assessment during the pre-disposal phase. In particular, the document focuses on the current limitations and related challenges and it is expected to be relevant to all EU members with nuclear programs and the wider nuclear industry.

This SOTA report is intended as an initial version, to be updated at the end of the WP to become the final SOTA report. The target of the final report is to become a key reference in the field and to gain high recognition and visibility as a key resource for knowledge management programmes and to contribute to demonstrating and documenting the state-of-the-art character from a neutral and purely scientific viewpoint.

The report is composed of three main sections: 1) Characterisation of the fuel, fuel inventory and source term; 2) Performance of spent nuclear fuel during pre-disposal activities and experimental characterisation; 3) Accident scenarios.

The first section, Chapter 2, is a state-of-the-art review of characterisation of SNF properties in terms of source term and inventory assessment. The following parameters and related uncertainties (quantification and propagation) are considered in the review: neutron and gamma-ray emission, decay heat, radionuclide inventory and elemental content. Experimental verification techniques, i.e. Non-Destructive Analysis (NDA) methods (e.g. neutron and gamma spectrometry, gamma tomography, calorimetry, etc.) and Destructive Analysis (DA) are also considered. Other non-conventional techniques (e.g. muon tomography) are also reviewed, the availability of experimental data being extremely important for testing and validation of codes and models. The section is structured into 6 main subsections, which review the following topics: definition of nuclides of interest and observables, nuclide inventory computational methods and tools, sources of bias effects and uncertainties, uncertainty evaluation and sensitivity analysis, experimental determination of source terms and observables, and codes validation.

The second section, Chapter 3, is devoted to out-of-core fuel performance, in particular to the performance of the cladding and fuel integrity in view of the safety criteria for SNF interim storage, transport and canister packaging. Different numerical and experimental approaches and methodologies are discussed. For instance, when considering operational safety cases at the level of surface facilities where the fuel must be encapsulated in special disposal canisters, studies and research activities are required to assess spent fuel performance. Here, conventional techniques for investigating the effect of hydrogen load, hydride distribution and fuel/cladding interaction, mechanical performance of the cladding and cladding integrity, deterioration of the mechanical properties of the cladding material resulting from Delayed Hydride Cracking for high burnup are reviewed, all with the focus on (extended) dry storage conditions. The section is structured into 4 subsections, including key phenomena about spent fuel degradation, experimental characterisation and fuel performance codes.

Finally, a third section, Chapter 4, aims to present the status of knowledge on definition of accident scenarios with respect to pre-disposal activities (storage, transport, encapsulation). The section refers to IAEA general assumptions, being concepts for fuel handling and packaging very specific to country strategies. The section is structured into 4 subsections, beginning with safety standards for predisposal management of SNF, followed by a very general overview of accident scenarios for fuel in interim storage and transportation.

## 2. Characterisation of the fuel, fuel inventory and source term

### 2.1. Observables and nuclides of interest

Due to the number of radionuclides that are present in spent nuclear fuel, spent fuel assemblies need to be characterised for their neutron and  $\gamma$ -ray emission properties and decay heat in view of the safety criteria for casks and canisters for transport, interim storage, and final disposal. Systematic studies in [Hu, 2016; Žerovnik, 2018] reveal that these observables are the result of complex contributions of radionuclides with strongly differing characteristics. This is illustrated in Figure 1 and Figure 2 for a simulated PWR UO<sub>2</sub> fuel sample with an initial <sup>235</sup>U enrichment of 4.8 wt.-% and a burnup of 45 GWd/t. Figure 1 shows the specific total decay heat rate (or thermal power) as a function of cooling time together with the contributions due to the emission of  $\alpha$ - and  $\beta$ -particles and  $\gamma$ -rays [Žerovnik, 2018]. The relative contributions of individual radionuclides are identified in Figure 2. The largest contribution for cooling times in the range of 1 – 10 years is due to relatively short-lived fission products (FPs), mainly the decay chains <sup>144</sup>Ce/<sup>144</sup>Pr and <sup>106</sup>Ru/<sup>106</sup>Rh. For cooling times between 10 and 30 years, contributions from short-lived FPs become negligible and the largest contribution is due to the decay chains of <sup>90</sup>Sr/<sup>90</sup>Y and <sup>137</sup>Cs/<sup>137m</sup>Ba. With increasing cooling time the <sup>241</sup>Am contribution becomes dominant. This is due to the build-up of <sup>241</sup>Am from <sup>241</sup>Pu decay. Other contributions are due to the decay of <sup>238,239,240</sup>Pu. The contributions from light nuclides reduce over time and eventually become negligible for cooling times longer than ~ 300 years.

Similar figures are reported in [Žerovnik, 2018] for the neutron and  $\gamma$ -ray emission properties of the same simulated fuel sample. For cooling times in the range of 1 – 80 years, the spontaneous fission of neutrons by <sup>244</sup>Cm represents the largest contribution to the neutron emission rate, with a relatively small contribution from ( $\alpha$ ,n) reactions due to decay of <sup>238</sup>Pu, <sup>242</sup>Cm and <sup>241</sup>Am. For cooling times longer than 100 years, neutron emission is mainly due to the spontaneous fission of <sup>240,242</sup>Pu and <sup>246</sup>Cm and ( $\alpha$ ,n) reactions due to <sup>241</sup>Am decay. Hence, for cooling times in the range of 1 – 80 years, the observed total neutron emission rate reflects the quantity of <sup>244</sup>Cm. Decay of FPs is the main contributor to spent fuel  $\gamma$ -rays emission for cooling times between 10 and 30 years, with the main contributors being <sup>134</sup>Cs, <sup>137</sup>Cs/<sup>137m</sup>Ba and <sup>154</sup>Eu. For longer cooling times, i.e. 30 – 200 years, the spectrum is dominated by the 661 keV  $\gamma$ -ray due to <sup>137</sup>Cs/<sup>137m</sup>Ba decay. Hence, for such cooling times a measurement of the total  $\gamma$ -ray emission rate provides information on the total amount of <sup>137</sup>Cs, which is directly proportional to the burnup.

In addition to the FPs and actinides, other dose-relevant and safety related radionuclides are generated, mainly by neutron activation of fuel/cladding impurities (e.g. <sup>14</sup>C, <sup>36</sup>Cl, <sup>41</sup>Ca, <sup>59</sup>Ni, <sup>63</sup>Ni, <sup>93</sup>Mo and <sup>94</sup>Nb). These nuclides are of importance for long-term safety assessments in waste disposal conditions up to about one million years. The different production roots are discussed below:

- The primary source is the cladding and related structural components; Modern cladding material is generally Zr-based, with minor amounts of alloying elements (Sn, Fe, Cr, Ni, Nb, O). Structural components (such as the spring material, guide thimbles, grids, hold down springs, etc.) are manufactured from stainless steel, Ni-based alloys, and Zr-based alloys.
- At the outer surface of the cladding (and possibly the inner surface of the shroud), surface deposits generally coming from corrosion products (e.g. (Ni, Fe)OH<sup>+</sup>) from out-of-core regions may deposit as solid particles (e.g. ferrous hydroxide (Fe,M)(OH)<sub>2</sub> or ferrite M<sup>n</sup>Fe<sub>2</sub>O<sub>4</sub> with M = Fe, Ni, Co, Mn...). Various compounds may be formed and are collectively referred to as "crud" or "crud deposits".
- A further source of activation products stems from impurities in either the fuel or the cladding, such as N, Mg, Al, Si, Cl, Ca, Cr, Fe, Ni and Th.

Activation products of the above elements are mainly  $\beta$ -active and, with the exception of <sup>60</sup>Co (estimated to be of the order of 1 %), their contribution to the spent fuel assembly decay heat is negligible (< 0.01 %) over the period of interest.

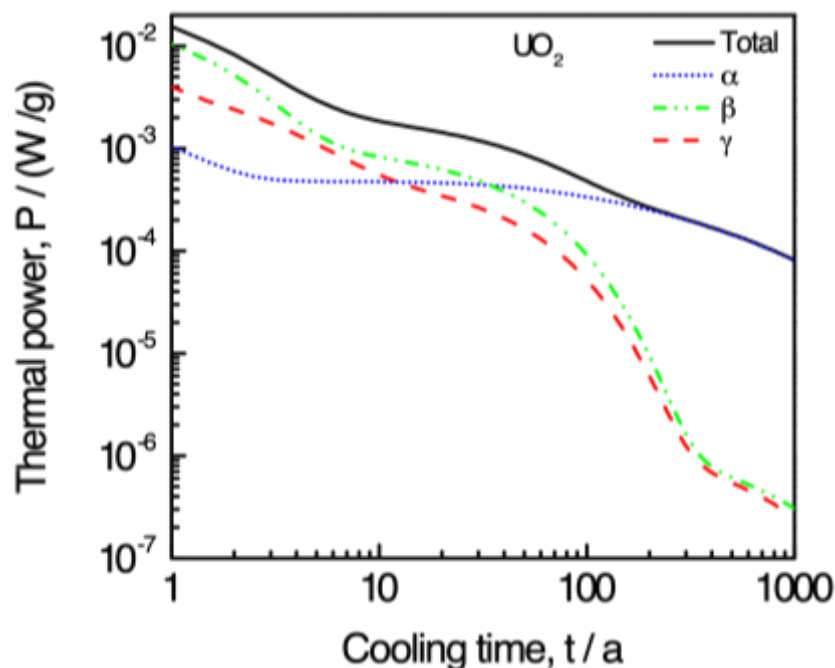


Figure 1 – Specific thermal power (or decay heat rate) of an irradiated fuel sample as a function of cooling time

The total thermal power per unit mass together with the contribution due to  $\alpha$ ,  $\beta$  and  $\gamma$ -ray emission is given for a  $UO_2$  sample with initial enrichment of 4.8 wt.-% irradiated in a PWR to a burnup of 45 GWd/t [Žerovnik, 2018].

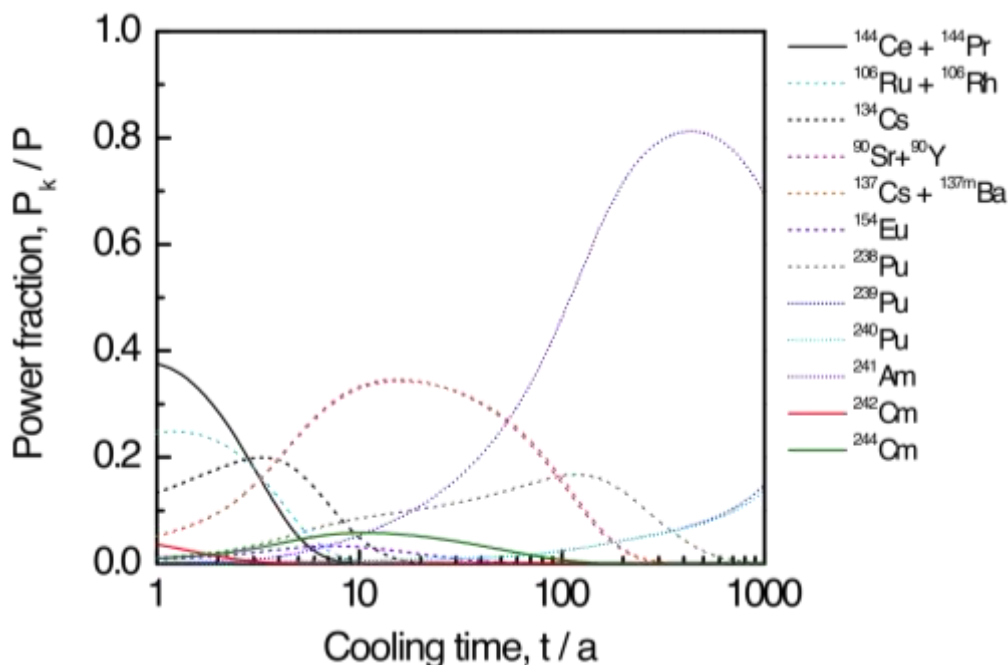


Figure 2 – Relative contribution of radionuclides to the thermal power of an irradiated fuel sample as a function of cooling time

The data are for a  $UO_2$  sample with initial enrichment of 4.8 wt.-% irradiated in a PWR to a burnup of 45 GWd/t [Žerovnik, 2018].

After a cooling time of several thousands of years, the total activity of spent nuclear fuel is dominated by long-lived actinides, in particular  $^{235}\text{U}$ ,  $^{238}\text{U}$ ,  $^{237}\text{Np}$  and  $^{239}\text{Pu}$ . Since plutonium and uranium species are immobile under the reducing conditions of a deep geological repository, they are less important with respect to the long-term safety of spent nuclear fuel disposal. However, the mobility of gaseous or readily soluble and negatively charged species, such as  $^{36}\text{Cl}^-$ ,  $^{129}\text{I}^-$  or gaseous  $^{14}\text{C}$  compounds, are not expected to be limited by the (geo-)technical barriers and will move relatively easily through the surrounding rock of the disposal system [Ewing, 2015]. To assess the radiologically relevant inventory, the amount of long-lived activation/fission/decay products, i.e.  $^{14}\text{C}$ ,  $^{36}\text{Cl}$ ,  $^{79}\text{Se}$ ,  $^{94}\text{Nb}$ ,  $^{99}\text{Tc}$ ,  $^{129}\text{I}$ ,  $^{135}\text{Cs}$  and  $^{226}\text{Ra}$ , as well as the  $^{237}\text{Np}$  inventory have to be estimated.

Safe transport, storage or disposal of spent fuel assemblies also requires a (sub-)criticality safety analysis. To avoid unnecessarily over-engineered and expensive transport and storage casks, the loading scheme should account for the reduction in nuclear reactivity of the assemblies. This effect is due to the net reduction of fissile nuclides (fuel depletion) and the production of non-fissile, strongly absorbing actinides and fission products. The concept of taking credit for the reduction in reactivity is referred to as BurnUp Credit (BUC) [Sanders, 1990]. Hence, criticality safety assessments for spent nuclear fuel management based on a BUC approach require a nuclide inventory prediction involving far more nuclides than in a conservative approach based on the inventory of fresh fuel. Nuclides which strongly affect the reactivity of a spent fuel assembly, are:  $^{235,236,238}\text{U}$ ,  $^{239,240,241}\text{Pu}$ ,  $^{95}\text{Mo}$ ,  $^{99}\text{Tc}$ ,  $^{101}\text{Ru}$ ,  $^{103}\text{Rh}$ ,  $^{109}\text{Ag}$ ,  $^{133}\text{Cs}$ ,  $^{147,149,150,151,152}\text{Sm}$  [Hicks, 2018; Gauld, 2005]. Other discussions on BUC approaches can be found in e.g. Refs. [Agrenius, 2002; Gauld, 2003; Tardy, 2017; Scaglione, 2009; Herrero, 2015; Vasiliev, 2019].

Spent nuclear fuel is subject to nuclear safeguards to ensure the peaceful use of nuclear materials. It requires a final accounting of special nuclear materials that will be removed from the nuclear fuel cycle for ultimate disposal in a geological repository [Hautamäki, 2000; Mongiello, 2013; IAEA, 2018; Niemeyer, 2016; Lindgren, 2019]. The IAEA will verify the inventory of nuclear material that is declared for disposal. The main nuclear materials of interest are the amount of  $^{233,235}\text{U}$  and the total amount of plutonium and thorium. In addition, secure transport and storage of spent fuel assemblies implies the prevention of theft, or other malicious acts involving nuclear material. The IAEA lists the development of safeguards equipment to establish and maintain knowledge of spent fuel in shielding/storage/transport containers at all points in their life cycle as a top priority in their R&D needs [IAEA, 2018a]. Evidently, nuclear safety, security and safeguards require similar or complementary measures for documenting, measuring and monitoring spent fuel characteristics. Therefore, synergies inherent in overlapping methods or techniques should be identified to avoid redundancy or duplication of work and equipment [Niemeyer, 2016; Lindgren, 2019].

## 2.2. Theoretical calculation of the nuclide inventory and observables

The main parameters of interest for the safe, secure, ecological and economical transport, storage and disposal of spent fuel are the decay heat, neutron and  $\gamma$ -ray emission properties and the inventory of some specific actinides, FPs and activation products. Alpha decay of actinides affects the microstructure of the cladding, which is connected to the integrity of the fuel (see section 3). To determine these source terms, the inventory of a large number of nuclides is required. A list of nuclides for which the inventory in spent fuel has to be determined can be found in [Ewing, 2015; Broadhead, 1995; NEA, 2011; Gauld, 2001] and Appendix A [Govers, 2019]. The latter contains radionuclides identified from safety studies of a long-term storage installation for Belgian waste performed by NIRAS/ONDRAF [Vandoorne, 2018].

Due to the complex contributions of radionuclides with different characteristics, estimates of the decay heat, neutron and  $\gamma$ -ray emission properties at any cooling time cannot accurately be derived by simply extrapolating from estimations at shorter cooling times. In addition, the complete nuclide vector of a spent fuel assembly cannot be measured directly; it can only be obtained from theoretical calculations. Such calculations require validated codes that determine the time evolution of the nuclide inventory

during reactor operation. This can be done by coupling a neutron transport and a nuclide production and depletion code.

When the nuclide vector at a cooling time  $t_0$  is known, the nuclide vector at a cooling time  $t > t_0$  can be derived by solving the set of linear differential Bateman equations [Bateman, 1910]:

$$\frac{dN_k(t)}{dt} = \sum_{ik} b_{ki} N_i - l_k N_k(t) \quad (1)$$

with  $N_k$  the number of nuclei of nuclide  $k$ ,  $l_k$  its decay constant and  $b_{ki}$  the probability that nuclide  $i$  decays to nuclide  $k$ . Once the nuclide vector is known, the thermal power  $P(t)$ , neutron emission rate  $S_n(t)$  and  $\gamma$ -ray emission energy distribution  $S_g(E_g, t)$  as a function of cooling time  $t$  can be obtained from:

$$P(t) = \sum_k N_k(t) \lambda_k E_{r,k} \quad (2)$$

$$S_g(E_g, t) = \sum_k N_k(t) \lambda_k S_g(E_g) \quad (3)$$

$$S_n(t) = \sum_k N_k(t) (s_{sf,k} + s_{,k}) \quad (4)$$

with  $E_{r,k}$  the recoverable energy per decay of nuclide  $k$  and  $S_g(E_g)$  the energy distribution of the  $\gamma$ -rays emitted per decay of nuclide  $k$ . The specific neutron emission rates, or neutron rate per nuclide, due to spontaneous fission and  $\alpha$ -decay of nuclide  $k$  are denoted by  $s_{sf,k}$  and  $s_{,k}$ , respectively. The specific spontaneous fission rate is defined by:

$$s_{sf,k} = \lambda_{sf,k} \bar{n}_k \quad (5)$$

with  $\lambda_{sf,k}$  the decay constant for spontaneous fission of nuclide  $k$ , and  $\bar{n}_k$  the corresponding average number of neutrons per fission. The specific emission rate of neutrons due to  $(\alpha, n)$  reactions in mainly light nuclides can be derived from:

$$s_{,k} = \lambda_{\alpha,k} \sum_{ij} P_k(E_{\alpha,i}) Y_j(E_{\alpha,i}) \quad (6)$$

where  $\lambda_{\alpha,k}$  is the decay constant for  $\alpha$ -decay of nuclide  $k$ ,  $P_k(E_{\alpha,i})$  the probability that this decay leads to the emission of an  $\alpha$ -particle with an energy  $E_{\alpha,i}$  and  $Y_j(E_{\alpha,i})$  the probability that the emitted  $\alpha$ -particle creates a neutron by an  $(\alpha, n)$  reaction with material  $j$ .

### 2.2.1. Principles

Neutron transport calculations can be performed in a deterministic way by solving the Boltzmann transport equation, or in a stochastic way by performing Monte Carlo (MC) simulations using codes such as MCNP [Briesmeister, 2000], SERPENT [Leppänen, 2015] and TRIPOLI [Petit, 2008; Brun, 2015]. In principle, MC transport calculations can be performed with less approximations than by a deterministic approach. However, up to now MC simulations are often applied to systems involving one or a few assemblies. In the case of a full core (with burnup calculations), deterministic transport methods are still the only practical way for routine applications and within a reasonable calculation time.

From the neutron transport calculation, the spatial and energy distributions of the neutron fluence are derived. These distributions are used to calculate energy averaged neutron-induced reaction cross-sections, which are required to deplete and produce nuclides by solving a set of Ordinary Linear Differential Equations (ODEs). Since the energy and spatial distributions depend on the nuclide inventory an iterative procedure is required.

In the case of Light Water Reactors (LWRs), the production and depletion of nuclides by nuclear reactions and radioactive decay in a homogenised material as a function of time form a set of ODEs. These equations can be expressed in matrix notation by:

$$\frac{d\mathbf{N}(t)}{dt} = \mathbf{A}\mathbf{N}(t) \quad (7)$$

with  $\mathbf{n}(t)$  the number density vector of the nuclides presents in the fuel and  $\mathbf{A}$  the transition or burnup matrix. The diagonal elements  $a_{kk}$  of this matrix are the removal rates of each nuclide:

$$a_{kk} = - (f \bar{s}_k + l_k) \quad (8)$$

and the off-diagonal elements  $a_{kl}$  are the production rates by other nuclides:

$$a_{kl} = b_{kl}l_l + f b_{kl,r}\bar{s}_{l,r} \quad (9)$$

The decay constant of nuclide  $k$  is  $l_k$ . Its removal rate due to neutron interactions is the product of the total neutron fluence rate and the spectrum-averaged Doppler broadened removal cross-section denoted by  $f$  and  $\bar{s}_k$ , respectively. The matrix element defining the production of nuclide  $k$  from nuclide  $l$  is due to a decay contribution, defined by the decay constant  $l_l$  and branching probability  $b_{kl}$ , and a contribution due to neutron-induced interactions with nuclide  $l$  resulting in the production of nuclide  $k$ . The latter is the product of the total neutron fluence rate  $f$ , the spectrum averaged Doppler broadened neutron-induced interaction cross-section  $\bar{s}_{l,r}$  and the probability  $b_{kl,r}$  that this interaction produces nuclide  $k$ .

The most probable nuclide production interactions are neutron-induced fission and capture reactions. In the case of neutron-induced fission reactions, fission products are produced and the probability  $b_{kl,r}$  is the independent fission yield of the fission product  $k$ . Examples of such production chains for fission products are given in [Nichols, 2002]. Most of the fission products are neutron-rich and decay mostly by  $\beta^-$ . Other nuclides are generated via a combination of different decay processes and neutron-induced reactions, e.g. a combination of neutron-induced capture reactions and  $\beta^-$  decays are the main processes producing actinides such as Pu, Am and Cm starting from  $^{238}\text{U}$ . Several analytical/numerical solutions have been proposed [Moler, 2003; Isotalo, 2011; Hykes, 2013], but only a few are applicable to estimate the nuclide inventory of spent nuclear fuel. A comparison of some of the methods that are implemented in nuclear depletion codes can be found in [Moler, 2003; Isotalo, 2011; Hykes, 2013].

Applying the Transmutation Trajectory Analysis (TTA) method [Cetnar, 2006], also referred to as the linear chain method, the complex nuclide transmutation scheme is considered as a set of individual linear sub-chains that can be solved analytically, following the original work of [Bateman, 1910]. The final result is the sum of the solutions for the individual chains. It involves an enormous network of complex chains that often generate cyclic chains that cannot be linearized. Assumptions are made to terminate unimportant chains based on multiple criteria, e.g. ignoring cyclic chains or terminating them after a few loops. The choice of the termination criterion plays a role in the trade-off between computation speed and accuracy. This method is implemented in the BISON [Cetnar, 2000], CINDER [Wilson, 2007] and VCINDER [Kum, 2018] codes and included as an option in SERPENT [Leppänen, 2015a; Leppänen, 2015b].

The set of first order differential equations can be solved by numerical integration methods such as the Runge-Kutta type of methods [Hairer, 1996; Hairer, 1999]. The primary disadvantage is the relatively high computing time. The 4<sup>th</sup> order Runge-Kutta scheme was implemented in earlier versions of the MENDEL [Tsilanizara, 2016] and DARWIN/PEPIN2 [Tsilanizara, 2000] systems. The ALEPH2 code [Stankovskiy, 2012] is based on the RADAU IIA implicit Runge-Kutta method of order 5.

The solution of the ODEs can be found by the matrix exponential method, resulting in [Pusa, 2010; Pusa 2011]:

$$\mathbf{N}(t) = e^{\mathbf{A}t} \mathbf{N}_0 \quad (10)$$

where the exponential of the matrix is defined as a series expansion

$$e^{At} = \sum_{k=0}^{\infty} \frac{1}{k!} (At)^k \quad (11)$$

with  $I = A^0$  the identity matrix and the initial nuclide vector denoted by  $N_0$ . There are numerous algorithms to compute the matrix exponential, but many of them are computationally expensive and of dubious numerical quality [Moler, 2003]. Given the complexity of the process, the burnup matrix has a wide spectrum of eigenvalues. The presence of short-lived nuclides is problematic since they produce eigenvalues of large magnitude, creating a matrix norm of up to  $10^{27}$  [Pusa, 2010; Pusa, 2011].

The matrix exponential in Eq. 11 can be approximated by a truncated Taylor expansion [Bell, 1973] or a rational Padé approximation [Nigham, 2005], both combined with scaling and squaring. These approximations can only work well when the matrix norm  $\|At\|$  is sufficiently small. This problem can be solved by excluding the short-lived nuclides from the burnup matrix and treating them separately. This results in a kind of hybrid linear chain-matrix exponential method that is used in ORIGEN2 [Croff, 1983]. It is also used in the MOCUP [Moore, 1995] and MONTEBURNS [Poston, 1999] codes which couple MCNP and ORIGEN2 [Croff, 1983]. The latest version of the PHOENIX burnup module solves the ODEs either with a 4<sup>th</sup> order Runge-Kutta method, a Taylor series development of the matrix exponential, or a Krylov subspace-based algorithm [Haeck, 2012]. The latter is also applied in the AEGIS code [Yamamoto, 2007].

One of the most advanced matrix exponential methods is the Chebyshev Rational Approximation Method (CRAM) [Pusa, 2010; Pusa, 2011; Pusa, 2013; Pusa, 2016; Isotalo, 2016]. It is based on a ratio of polynomials using complex coefficients and provides very accurate solutions without excluding nuclides. The main difficulty in using CRAM is to determine the coefficients of the rational approximant for a given order. [Pusa, 2016] provides CRAM coefficients for approximation of orders 4, 8, 12, ..., 48. It is shown that the higher-order CRAM can be used to solve the burnup equations accurately for large time steps. CRAM is implemented as an option in SERPENT [Leppänen, 2015a; Leppänen, 2015b] and in the latest versions of ORIGEN [Gauld, 2011b; Rearden, 2016] and MENDEL [Lahaye, 2017].

## 2.2.2. Burnup codes

A variety of codes/systems are available to determine the nuclide inventory and decay heat and neutron and  $\gamma$ -ray emission properties of SNF assemblies. Only the codes/systems that will be used within the activities of the spent fuel characterisation work package of the EURAD project will be discussed here in detail.

### ALEPH2/MCNP

ALEPH2 is a depletion code developed at SCK•CEN [Stankovskiy, 2012] that makes use of any version of the general Monte Carlo N-Particle Transport Code MCNP [Briesmeister, 2000; Werner, 2017] for MC transport calculations to obtain particle spectra. The reaction rates are handled outside MCNP by ALEPH2 using the same continuous energy nuclear data as MCNP. This ensures consistent use of nuclear data by transport and depletion modules. The depletion module is based on the solver RADAU5 [Hairer, 1996; Hairer, 1999], which uses an implicit 5<sup>th</sup> order Runge-Kutta method. The power-to-fluence rate conversion takes into account the energy deposited by fission and neutron capture reactions, making it possible to accurately model systems containing burnable absorbers. The code is able to reflect in a single run the time evolution of many parameters, such as fuel expansion, fuel reshuffling, changes in material temperature and density, control rod movement and changes in boundary conditions. Besides the nuclide inventory evolution, various radiation source terms such as decay heat, delayed radiation sources and dose rates can be derived.

### CASMO/SIMULATE/SNF

The CMS/SNF methodology is based on the coupled CASMO/SIMULATE/SNF code sequence and used for evaluating the nuclide composition of spent nuclear fuel. It inherently applies a 3D core model

to any assembly irradiated in the core, accounting for realistic irradiation conditions [Bahadir, 2009]. The nuclide library, generated by the lattice physics code CASMO5 [Rhodes, 2006], provides nuclide concentrations, cross-sections and reaction rates, tabulated via exposure, moderator density, control blade and fuel temperature histories. The nodewise exposure and accumulated history parameters, obtained from qualified operational reactor data and core simulation using the nodal reactor code SIMULATE [Grandi, 2011], are used as entry points in the interpolation routines and, together with the power history model in SNF [Børresen, 2004], are used to compute the nuclide concentrations at the time of assembly discharge. CMS5/SNF computes the nuclide concentrations and all relevant spent fuel parameters such as decay heat rate, activity, neutron and photon sources on a nodal basis following the axial nodalisation of the reactor core model.

SIMULATE and SNF share the same cross-section library, generated by CASMO5 and based on ENDF/B-VII.1. The basic decay data in SNF are also based on ENDF/B-VII.R1. The SNF decay library includes basic data such as decay constants and nuclide transmutation chains; radiation emission spectra for photons from radioactive decay, ( $\alpha,n$ ) reactions, bremsstrahlung, and spontaneous fission; electrons and  $\alpha$  particles from radioactive decay; neutrons from radioactive decay, spontaneous fission, and ( $\alpha,n$ ) reactions; decay heat production; and others. These data are compiled from data libraries (e.g. ENDF/B-VII.1 [Chadwick 2011], ENSDF [Tuli, 2001], TENDL-2012 [Koning, 2012]) and processed sources (ESTAR and ASTAR [Berger, 2015]) for 890 nuclides. The evaluation and validation of the decay data in SNF is reported in [Simeonov, 2017].

## DRAGON

DRAGON [Hébert, 2006] is a lattice deterministic code developed at École Polytechnique de Montréal. It uses different models and algorithms to solve the neutron transport equation. In order to find the best trade-off between accuracy and calculation speed, the Collision Probability method (CP) using the DRAGON formatted library is recommended. For self-shielding, the interface current method (SYBILT) can be used to perform the geometry tracking together with a subgroup method (USS module) with physical probability tables. In the subgroup or multiband method, the detailed energy-dependent cross-section behaviour in each coarse energy group is replaced by its probability density representation. An accurate discretisation of each probability density can be obtained, which leads to probability tables which are subsequently used within the fluence rate solution algorithm of the subgroup method. The SYBILT module can also be used for the fluence rate calculation using the fixed Laplacian option and without leakage model. The default option for solving the depletion equations is the 4<sup>th</sup> order Kaps-Rentrop algorithm of the Runge-Kutta family. The power-to-fluence rate conversion is done taking into account a constant power with the total energy released in the complete geometry (GLOB option), by accounting for ( $n,\gamma$ ) reactions outside the fuel. In this case, the power released per initial heavy element at the beginning and at the end of each time step can be set to a constant.

## EVOLCODE

EVOLCODE 2.0 is a combined neutron transport and depletion evolution simulation code to describe the burnup evolution of either critical or subcritical reactors operating in any neutron spectrum [Álvarez-Velarde, 2014]. The code has been focused on the estimation of a large variety of nuclear reactor parameters, with a particular interest in the nuclide composition evolution of the fuel in a nuclear reactor. The evolution with burnup of any material present in the design can be followed for activation purposes. Burnup problems are solved by using a time interval method consisting of the successive calculation of first the neutron fluence rate for fixed material densities at a given time and later the depletion of these densities, using the hypothesis of constant neutron fluence rate. These hypotheses are considered valid only for relatively short irradiation times. Hence, several iterative calculations are needed to solve the system for the whole irradiation period. Each iteration, corresponding to a partial irradiation period, is called an EVOLCODE cycle.

In the present version of the code, the neutron transport calculations are performed by any version of the general MC transport code MCNP/X [Werner, 2017], which is able to model complex 3D geometries. The depletion of the geometry zones, requested by the user, is carried out by the activation code ACAB [Sanz, 2008]. This code is implemented in the EVOLCODE 2.0 system to provide best estimates together with their uncertainties resulting from a propagation of uncertainties of cross-sections, decay data and fission yields, and to enlarge the number of nuclear reactions taken into account by the irradiation calculations. ACAB is a point-depletion and radioactive decay computer code that solves the ODEs using a method similar to the one implemented in ORIGEN2 [Croff, 1983]. The depletion code ORIGEN can be used instead of ACAB. The user chooses which depletion code or version of MCNP/X is used in the simulations.

The spatial dependence of the neutron fluence rate is determined by the MCNP cell definition, which, together with the entire geometry definition, allows for an important degree of the heterogeneity description in the reactor core model. The energy dependence is obtained by means of the energy distribution of the neutron fluence rate for each of these cells. On the one hand, the neutron fluence rate is normalised by means of a predictor/corrector method, so that the depletion is simulated using the proper value of the system thermal power. Finally, the neutron fluence energy distributions are used for creating (outside MCNP) spectrum averaged cross-section libraries for depletion.

EVOLCODE 2.0 uses the same basic libraries as MCNP to ensure consistency in the use of the data. From these basic libraries, the information on those reactions suitable for ACAB and available in the database is selected, disregarding the information about elastic collisions. Additionally, since isomers may have very different half-lives and reaction cross-sections compared with the ground state nuclide (leading to different transmutation chains), the information on the isomer producing reactions is provided to the code by a separate file containing the information on the branching ratios. Finally, the fission yields library is supplied to the code as an external sub-library. Currently, sub-libraries are defined for neutron-induced fission product yields and for yields from spontaneous fission. Besides, independent and cumulative yields are also included in the sub-library. EVOLCODE 2.0 only considers neutron-induced independent fission product yields since these are the data required by the depletion code.

## MCNP-CINDER

The MCNP code in general, and in particular the recent version MCNP6, is widely used for neutron transport calculations from which the neutron fluence energy distribution is obtained and reaction rates can be generated. As far as burnup codes are concerned the depletion part can be disintegrated from the neutron transport code, that is, the reaction rates are calculated separately and several systems operate in this way, e.g. ALEPH2 [Stankovskiy, 2012] and EVOLCODE [Álvarez-Velarde, 2014].

The depletion code that was coupled to earlier versions of MCNP is the MONTEBURNS module [Poston, 1999]. The recent MCNP6 versions integrate the depletion part CINDER [Wilson, 2007] within the transport solution. Hence, the reaction rates are based on the nuclear input data of the MCNP code itself. As a weak point, CINDER uses a pre-calculated 63-group cross-section library obtained externally. CINDER belongs to the group of codes which use the so-called linear chains approach based on the Markov method, i.e. TTA method described in Section 2.2.1. The linearization considerably simplifies the complexity of the exponential matrix but in return, one should be careful with the burnup time steps to maintain the accuracy of the nuclide inventory. On the other hand, it offers the possibility of handling many nuclides with longer depletion chains.

## SCALE

One of the most widely used computer codes for the prediction of spent fuel source terms (nuclide composition, neutron and  $\gamma$ -ray emission and decay heat) is the SCALE code package developed at the Oak Ridge National Laboratory (ORNL). The latest available version, as of September 2019, is SCALE

6.2.3 [Rearden, 2016; Grandi, 2011]. It is described in detail in [Gauld, 2011]. Most of the geometrical systems studied with the SCALE package are related to a limited number of assemblies.

SCALE is a multi-purpose code package offering a range of options for performing source term calculations: starting with pre-packaged LWR libraries in the ORIGEN-ARP module or alternatively determining simplified but assembly-specific cross-sections with the SAS2H control sequence in combination with the one-dimensional discrete ordinate code XSDRNPM-S or computing nuclide vectors with the T6-DEPL control sequence and the KENO lattice physics solver.

The package includes built-in cross-section libraries (e.g. ENDF/B-VII.0 and ENDF/B-VII.1) in Multi Group (MG) approximation (56 or 252 groups) and in pointwise Continuous Energy (CE) detail. These are recommended for general-purpose reactor physics and LWR analysis [Rearden, 2016], along with complementary data from the JEFF-3.0/A library. The latest covariance data are based on the covariance evaluations of ENDF/B-VII.1 and other sources. These covariances, along with perturbation factors, can be used to generate perturbed MG libraries for the cross-sections, decay and fission yield data (see Section 2.4). For nuclide data not covered by ENDF/B-VII.1, "low-fidelity" covariances were estimated using simple procedures in a collaborative project by nuclear data experts of the Brookhaven National Laboratory (BNL), Los Alamos National Laboratory (LANL) and ORNL.

SCALE offers several modules for depletion calculations:

- TRITON couples one of the neutron transport modules to the ORIGEN depletion module in an iterative time-stepping sequence. One can choose between a deterministic 2D approach (NEWT) and a 3D MC simulation (KENO). The latter runs in multi-group or continuous-energy mode. TRITON is also used to generate problem-specific cross-sections that are used by the ORIGEN-ARP module for transmutation and decay calculations [Caruso, 2014b].
- POLARIS is a 2D lattice physics module that is used for the analysis of LWR fuel assemblies [Rearden, 2016]. POLARIS uses the Embedded Self Shielding Method [Williams, 2012a] for evaluating the self-shielded, multi-group cross-sections based on the Bondarenko interpolation, and a Method of Characteristics (MoC)-based transport solver [Williams, 2012a]. The outputs of POLARIS are the critical spectrum, few-group homogenised and condensed cross-sections, and one group condensed microscopic cross-sections.
- ORIGEN – Oak Ridge Isotope GENeration (ORIGEN) code is coupled to TRITON and POLARIS to perform the depletion and decay calculations, and therefore to simultaneously generate the time-dependent nuclide concentrations. POLARIS and TRITON are coupled to ORIGEN by one-group, zone-averaged fluence rates and one-group fluence-weighted cross-sections and reaction yields to compute the stepwise change in the problem-dependent nuclide vector. The coupling is done at the end of each depletion step using the predictor-corrector method, which is then used to update the depleted materials composition for the next self-shielding and transport calculation. ORIGEN can also be used stand-alone for activation, depletion and/or decay calculations using the pre-developed macroscopic cross-section libraries [Caruso, 2016].
- ORIGEN-ARP uses pre-packaged LWR libraries available in the SCALE package. It also allows user-defined libraries to be imported which can be developed with the TRITON module.
- SAMPLER is a module for uncertainty analysis. It is a stochastic sampling super-sequence that was developed for the SCALE system by ORNL in collaboration with GRS on the basis of the XSUSA code [Williams, 2013b]. SAMPLER can be used to perform uncertainty analysis for POLARIS. SAMPLER works by stochastically sampling input parameters (MG nuclear data, depletion data, decay data as well as model parameters such as nuclide concentrations, geometric specifications, operational history). Afterwards, SAMPLER will repeat numerous passes through the employed module (or sequence of modules), output distributed response parameters (or their uncertainties), and finally analyses these distributions to evaluate the correlations between different response parameters (e.g. different radionuclides) or the correlations between simultaneously modelled systems (similarity studies).

## SERPENT

SERPENT [Leppänen, 2015a; Leppänen, 2015b] is a multi-purpose three-dimensional continuous energy MC particle transport code developed at the VTT, Technical Research Centre of Finland since 2004. The latest version, as of September 2019, is SERPENT 2, Version 2.1.31. SERPENT can be used for various reactor physics analyses and decay heat, activity and nuclide inventory calculations. In addition, SERPENT is capable of performing multi-physics simulations and neutron, photon and coupled neutron-photon transport calculations.

The geometry description in SERPENT is handled by a universe-based constructive solid geometry (CSG) model. Different elementary and derived surface types can be used in combination with Boolean operators (intersections, unions and complements) to define homogeneous material cells of practically any shape desired. Special surface types are defined for several lattice structures. In addition to CSG-type universes, SERPENT has the option to import CAD and unstructured mesh based geometries.

Particle transport in SERPENT is based on the combination of conventional ray-tracing based surface tracking and the Woodcock delta-tracking method [Woodcock, 1965] – the rejection sampling based delta-tracking method [Morgan, 2015]. Surface-tracking is used when necessary, e.g. in the presence of localised heavy absorbers which may cause efficiency problems for the delta-tracking method [Leppänen, 2010].

SERPENT has built-in state-of-the-art routines for depletion calculations and no coupling to external solvers is needed. The primary method used for solving the Bateman depletion equations is based on the CRAM method, an advanced matrix exponential solution developed for SERPENT at VTT [Pusa, 2010; Pusa, 2011, Pusa, 2013; Pusa, 2016; Isotalo, 2016].

The main capabilities of the code are:

- **Geometry:** SERPENT is capable of calculating nuclide inventories on assembly level in two (2D) and three (3D) dimensions. Whole core depletion calculations are also possible for small cores, such as research reactors. Serpent includes 2D lattice structures for square (PWR, BWR), hexagonal (VVER) and circular (AGR, CANDU, MAGNOX, RBMK, TRIGA) lattices. There is also a structure for a 1D vertical stack and 3D cuboidal and hexagonal lattices. Other structures are also possible to create by the user. Reflective, periodic and vacuum boundary conditions can be used. Support for spatial domain-decomposition for very large burnup calculations is currently in development.
- **Physics options:** SERPENT includes several modelling options affecting the physics of the modelled problem. One of them is the Doppler-broadening preprocessor routine [Viitanen, 2009] that allows for adjustment of the temperatures of ACE format cross-sections. This results in a more accurate description of the interaction physics in temperature-sensitive applications, as the data in the cross-section libraries are typically available in 300 K intervals. The Doppler-Broadening Rejection Correction (DBRC) method (see Section 2.3.1) is available.
- **Irradiation history:** The irradiation history is defined in units of time or burnup. Reaction rates are normalised to total power, specific power density, neutron fluence rate, fission or source rate, and the normalisation can be changed by dividing the irradiation cycle into a number of separate depletion intervals. Other parameters such as fuel temperature, moderator temperature and density, boron concentration, etc. must apply constant values during a single depletion calculation. However, these parameters can be changed, and fuel shuffling is possible by writing different inputs for each change in the parameters and using SERPENT's restart feature. The effect of the uncertainty of different irradiation history parameters on the source terms can be investigated e.g. by refining the accuracy of which irradiation history is defined in the calculation. Boron history can be modelled using first one average value and then changing the boron concentration during the calculation with increased precision.

- Depletion calculation: SERPENT handles every material as an individual depletion zone and provides nuclide inventories separately for each material. In addition, burnable materials in lattices can be automatically sub-divided into depletion zones, e.g. a lattice comprising one fuel material can be automatically sub-divided into depletion zones separately for each fuel pin. A fuel pin can also be automatically sub-divided into further depletion zones to better account for effects such as Gd burning. The depletion calculation can be followed by a decay calculation of any desired length. All nuclides included in the nuclear data libraries are available in the depletion and decay calculations. The output of the depletion calculation includes total and material-wise volume and burnup. Nuclide-wise output for every depleted material includes: atom and mass density, activity, decay heat, spontaneous fission rate, photon emission rate, ingestion toxicity, and inhalation toxicity.
- Activation analysis: in addition to fuel burnup calculations, SERPENT is capable of calculating the activation of any material defined in the geometry. Materials of interest are the fuel cladding and structural materials such as the spacer grid.
- Nuclear data: SERPENT reads continuous-energy cross-sections from ACE format data libraries based on JEFF-2.2, JEFF-3.1, JEFF-3.1.1, JEFF-3.2, ENDF/B-VI.8, ENDFB/B-VII.1 and JENDL-4.0. In addition, any other continuous-energy ACE format data library generated for MCNP can be added to SERPENT. Radioactive decay data and incident-neutron energy-dependent fission yields and isomeric branching ratios for neutron-induced reactions are read from data libraries in ENDF-6 format. The nuclear data used can be easily changed between different runs.
- Shielding calculations: SERPENT provides a radioactive decay source mode to perform shielding calculations for spent fuel and other irradiated materials. The source term is formed automatically by combining the nuclide composition from a previous burnup or activation calculation and the emission spectra from ENDF decay data. The methodology includes photons and neutrons emitted in radioactive decay, as well as secondary photons produced by  $\beta$ -decay by applying the thick-target bremsstrahlung (TTB) approximation.

Various other codes/systems have been developed such as FISPACT [Sublet, 2017], MENDEL [Lahaye, 2017], MOCUP [Moore, 1995], MONTEBURNS [Poston, 1999], STREAM [Ebiwonjumi, 2019], SWAT [Kashima, 2015], and VESTA [Haeck, 2012]. Information on these codes is available from the quoted references.

### 2.2.3. Code comparison

Recently, the performance of ALEPH2, SCALE, DRAGON and SERPENT were compared using the same nuclear data, fuel design and composition and irradiation history parameters. The code versions used in the exercise are specified in Table 1. All codes were used in combination with the ENDF/BVII.1 library. Details about the exercise are given in [Žerovnik, 2019].

Code	Neutron transport	Solver	Version
ALEPH2	MC	Runge-Kutta (RADAU IIA)	ALEPH2/MCNP6.2
SERPENT	MC	CRAM	V2.1.29
DRAGON	Deterministic	Runge-Kutta (4 <sup>th</sup> order Kaps-Rentrop)	Version 5
SCALE	Deterministic	CRAM	TRITON/NEWT

Table 1 – Burnup codes used in the comparison exercise reported by Žerovnik et al.

A reference 2D model representing a typical 17x17 PWR fuel assembly with reflective boundary conditions was considered. The fuel pins consisted of a stack of 4wt.-% enriched UO<sub>2</sub> pellets in a Zircaloy-4 cladding. The fuel was irradiated for 4 cycles of 300 days each, with interim cooling periods of 30 days. Simplified operating conditions were considered, with:

- constant power levels of 50, 50, 40 and 30 MW/t during each cycle
- coolant density of 0.655 kg/cm<sup>3</sup> with a constant boron level of 800 ppm
- fuel smeared density (95 % of the theoretical density): 10.4 g/cm<sup>3</sup>
- constant material temperatures: fuel and gap at 900 K and coolant and cladding at 600 K

The following approximations were adopted in all codes:

- the neutron transport calculations for each fuel cycle were rerun at time steps of: 1 day, 10 days, 14 days, 3 × 25 days and 4 × 50 days,
- to account for neutron self-shielding effects the fuel pins were divided into 4 radial regions.

The abundance of key nuclides at a cooling time of 5 years is compared in Table 2. Uncertainties due to MC counting statistics are given for the results obtained with SERPENT. The results obtained with the MC codes ALEPH2 and SERPENT are very similar. The largest difference, about 3 %, is observed for the abundance of <sup>149</sup>Sm and the second largest, about 1.2 %, for <sup>246</sup>Cm. The good agreement between ALEPH2 and SERPENT confirms the good performance of the RADAU IIA Runge-Kutta type of ODE solver used in ALEPH2.

Differences between SERPENT (& ALEPH2) and DRAGON, and SERPENT (& ALEPH2) and SCALE are larger. In general, the differences between DRAGON and SERPENT are smaller for the fission products than for the actinides, with the exception of <sup>149</sup>Sm. Substantial differences are observed for <sup>243m</sup>Am and <sup>244,245,246</sup>Cm isotopes. Differences between results from SCALE and SERPENT (& ALEPH2) are even more pronounced. There are no clear similarities between the differences observed with DRAGON and SCALE, except for <sup>149</sup>Sm and <sup>245,246</sup>Cm. Similar observations were made by comparing SCALE and SERPENT in [Kromar, 2019]. To clarify these differences, more systematic studies including results from calculations with the KENO module of SCALE are required.

Nuclide	SERPENT	ALEPH2		DRAGON		SCALE	
	$c_1$ / g/t	$c_2$ / g/t	$100x\Delta c/c_1$	$c_3$ / g/t	$100x\Delta c/c_1$	$c_4$ / g/t	$100x\Delta c/c_1$
<sup>90</sup> Sr	678.56 (2)	678.86	0.04	679.08	0.08	675.43	-0.46
<sup>106</sup> Ru	7.357 (<1)	7.294	-0.86	7.286	-0.96	7.321	-0.49
<sup>133</sup> Cs	1621.7 (2)	1624.2	0.15	1624.3	0.16	1637.9	1.00
<sup>134</sup> Cs	43.86 (2)	43.68	-0.43	43.64	-0.51	41.11	-6.28
<sup>137</sup> Cs	1638.0 (<1)	1640.2	0.13	1639.8	0.11	1643.2	0.32
<sup>144</sup> Ce	4.386 (<1)	4.364	-0.51	4.363	-0.53	4.356	-0.68
<sup>148</sup> Nd	567.92 (1)	569.51	0.28	569.29	0.24	567.45	-0.08
<sup>149</sup> Sm	3.536 (2)	3.645	3.08	3.703	4.72	4.080	15.36
<sup>234</sup> U	178.69 (8)	178.02	-0.37	180.54	1.04	190.23	6.46
<sup>235</sup> U	7109.9 (14)	7064.5	-0.64	7119.6	0.14	7283.3	2.44
<sup>236</sup> U	5620.5 (6)	5612.7	-0.14	5560.7	-1.07	5627.0	0.12
<sup>238</sup> U	920116 (33)	920234	0.01	920143	0.00	919950	-0.02
<sup>237</sup> Np	765.76 (37)	766.47	0.09	795.13	3.84	741.58	-3.16
<sup>238</sup> Pu	426.44 (18)	426.55	0.03	434.35	1.85	429.22	0.65
<sup>239</sup> Pu	6747.4 (18)	6786.5	0.58	6825.4	1.16	6947.2	2.96
<sup>240</sup> Pu	3065.2 (13)	3044.1	-0.69	3056.1	-0.30	2976.3	-2.90
<sup>241</sup> Pu	1556.7 (6)	1561.8	0.33	1570.8	0.91	1608.5	3.33
<sup>242</sup> Pu	970.92 (30)	967.77	-0.32	963.26	-0.79	990.42	2.01
<sup>241</sup> Am	499.66 (17)	499.79	0.03	503.06	0.68	516.77	3.43
<sup>242m</sup> Am	1.253 (<1)	1.261	0.68	1.389	10.85	1.346	7.43
<sup>243</sup> Am	242.95 (24)	242.87	-0.03	238.63	-1.78	225.35	-7.24
<sup>242</sup> Cm	0.015 (<1)	0.015	-0.21	0.015	0.71	0.016	2.00
<sup>243</sup> Cm	0.912 (1)	0.909	-0.37	0.878	-3.74	0.905	-0.83
<sup>244</sup> Cm	109.38 (8)	108.80	-0.52	106.84	-2.32	102.37	-6.41
<sup>245</sup> Cm	11.73 (2)	11.71	-0.19	10.820	-7.79	11.145	-5.02
<sup>246</sup> Cm	1.302 (2)	1.286	-1.18	1.199	-7.91	1.208	-7.18

Table 2 – Comparison of the abundance of key nuclides present in a spent nuclear fuel sample of after a cooling time of 5 years

The irradiation conditions are summarised in the text. To illustrate the observed differences between codes the relative difference with respect to the valued obtained with SERPENT are given. They are given in the column:  $100 \times \Delta c/c_1 = 100 \times (c_x - c_1)/c_1$ . The results are taken from [Žerovnik, 2019]

## 2.3. Sources of bias effects and uncertainties

The discussion in Section 2.2 reveals that various codes/systems are available to calculate source terms of spent nuclear fuel. Bias effects can be due to the methodology that is applied to solve the neutron transport and nuclide production and depletion processes. Independent of the methodology that is applied the final accuracy depends on input data which can be classified into nuclear data and fuel history data. The latter include the initial fuel composition and design and reactor operation and irradiation conditions.

### 2.3.1. Methodology

A detailed model of the irradiation conditions of a fuel assembly is not always possible. One of the reasons is that the full core information is mostly not publicly available and only limited information is provided by the plant operator or fuel vendor. Another reason concerns the tools used to perform the calculations. As mentioned earlier, Monte Carlo transport simulations, which are generally preferred to simulate irradiations, can hardly be applied to a large number of assemblies. Therefore, depending on the method used and depending on the degree of detail known from reactor operation, a simplified description of the irradiation history of a fuel assembly is necessary. For example, the effect of neighbouring fuel assemblies often cannot easily be described. In-core reactor measurements are typically made only for relatively few fuel assembly positions. Moreover, the fuel temperature, the moderator temperature or the moderator boron concentration history are often condensed into a few average values per cycle. In the case of 1D or 2D calculations, the axial profile is typically ignored in favour of a given node average burnup value provided by the power plant's in-core fuel management. This approach ignores shielding effects due to control rod position changes or the neutron fluence suppression at spacer or mixing grid positions. The impact of these factors on the nuclide inventory has been addressed for example in [NEA, 2011]. However, more quantitative studies of possible bias effects due to these assumptions are still needed.

The Doppler effect seems to be well understood, as far as its impact on the broadening of resonance structures is concerned. The broadening of  $^{238}\text{U}$  resonance profiles has a strong influence on the self-shielding effect and the production of  $^{239}\text{Pu}$ . Hence, it is important for reactor licensing and for spent fuel characterisation. Both the scattering and absorption cross-section are Doppler broadened. Until a decade ago, the scattering kernel, that is, the change in energy and angle of the scattered neutron, was simulated for a target nucleus at rest, namely at a temperature of 0K. Temperature-dependent scattering kernel theories which started by Wigner and Wilkins [Wigner, 1944], were further developed by [Rothenstein, 1998]. On the practical side, [Rothenstein, 2004] and later [Becker, 2009] found a technique to include the energy-dependent scattering kernel in stochastic transport calculations. This technique, known as Doppler-Broadening Rejection Correction (DBRC), was validated by a dedicated experiment in [Becker, 2009] and was implemented in MCNP, SERPENT and TRIPOLI [Zoia, 2013]. In the KENO code of SCALE, the angular part is missing. It can be shown that the inventory of  $^{239}\text{Pu}$  in a thermal LWR is underestimated by 1.5 % when the impact of the Doppler effect on the scattering kernel is not properly taken into account [Dagan, 2005]. Evidently this bias of 1.5 % will affect the inventory of all other actinides that are produced in the chains following the  $^{239}\text{Pu}$  production and the source terms depending on this inventory. More efforts should be made to study possible bias effects due to the use of spectrum-averaged cross-sections in the ODEs and in particular, the present assumptions made regarding the energy and angle differential scattering cross-sections for energies above the resolved resonance region.

Different approaches can be applied to account for resonance self-shielding in case of deterministic transport calculations [Williams, 2011]. Two different methods implemented in SCALE were compared in [Illas, 2012]. The results show a substantial difference in the inventory of Sm-isotopes and  $^{245,246}\text{Cm}$  obtained with the two different methods. The effect increases with increasing burnup. For a burnup of 50 GWd/t, the inventory of  $^{239,240,241}\text{Pu}$  can be biased by more than 3 %. Methods to account for self-shielding in the unresolved resonance region are discussed and compared in [Sublet, 2009]. At present

a detailed systematic study assessing the methods used in the different codes is not reported in the literature.

### 2.3.2. Nuclear data

Different types of nuclear data are required to calculate the spent nuclear fuel source terms: neutron interaction cross-sections, fission product yields, decay data and neutron and  $\gamma$ -ray emission properties. Most of these data are available in the main general purpose Evaluated Nuclear Data Files (ENDF) such as the ENDF/B, JEFF and JENDL libraries. The decay data in these files are mostly adopted from the ENSDF library or result from international collaborative efforts such as the Decay Data Evaluation Project (DDEP) [Kellett, 2017]. The general purpose libraries can be complemented by data from special purpose libraries that are dedicated to specific applications, such as the International Reactor Dosimetry and Fusion File (IRDF) file for neutron dosimeter reactions or activation cross-sections in the European Activation File (EAF). The TENDL library can be used to fill the remaining gaps. An overview of evaluated nuclear data libraries can be found on the website of the Nuclear Energy Agency of the OECD (OECDNEA) and the Nuclear Data Section of the IAEA (IAEA-NDS).

The general purpose libraries contain mainly calculated data resulting from an evaluation process that is based on nuclear reaction formalisms or theories involving model parameters which are adjusted to experimental data. Calculated cross-sections are required to ensure consistency and to account for the Doppler effect. The term "general purpose library" is not always appropriate. Some of the cross-sections are adjusted based on results of integral benchmark experiments. Such data are often biased due to compensating effects and can only be used for specific applications. An example of a biased cross-section due to a compensating effect is given in [Sirakov, 2017].

Nuclear data in general purpose libraries are stored in the internationally adopted ENDF-6 format. This format is not adequate for neutron transport or inventory calculations. Therefore, data processing codes are used to transfer the data into a format that is suitable for use in transport and burnup codes. The NJOY nuclear data processing system [MacFarlane, 2010] is widely used to convert evaluated data from the ENDF-6 format into a format useful for practical applications. One of these formats is the ACE format which is the most used format for MC transport codes. The AMPX code is a modular system for processing ENDF-6 formatted data into data that are ready for use in the SCALE system.

The primary goals of projects supporting to the production of evaluated nuclear data were not to fulfil requirements for a spent fuel characterisation. For example, various projects to improve decay heat predictions have been organised or coordinated by both the IAEA-NDS [Dimitrou, 2014] and the [NEA, 2007]. However, they concentrated on decay heat predictions at short cooling times and resulted in a substantial improvement of specific decay heat data for short-lived radionuclides. Measurements to produce such data are very complex. Unfortunately, the results are not relevant for the prediction of the thermal power of a SNF assembly at cooling times longer than one year.

The status and need for nuclear data for spent fuel characterisation is best illustrated by some specific examples. Key nuclides to determine the source terms are e.g.  $^{137}\text{Cs}$  and  $^{90}\text{Sr}$ . These nuclides are predominantly produced in a single mass chain through neutron-induced fission and  $\beta^-$  decay. The total number of nuclides  $N_X$  that are produced during an irradiation period can be approximated by summing the product of the cumulative fission yield  $Y_{c,k}$  and total number of fission reactions  $N_{f,k}$  due to neutron-induced fission of nuclide  $k$ :

$$N_X \approx \sum_k Y_{c,k} N_{f,k} \quad (12)$$

The total number of fission reactions for each nuclide  $k$  is given by:

$$N_{f,k} \approx s_{f,k} j T \quad (13)$$

with  $T$  the total irradiation time, the total fluence rate and  $s_{f,k}$  the fission cross-section of nuclide  $k$ . The main contribution to fission events starting from fresh  $\text{UO}_2$  fuel in a LWR is due to  $^{235}\text{U}(n,f)$ . With

increasing irradiation time, the burnup of the initial fuel and production of  $^{239}\text{Pu}$  progresses. This results in an increased contribution of fission events due to  $^{239}\text{Pu}(n,f)$ . At high burnup the latter can even dominate. Evidently, in the case of MOX the relative contribution of  $^{235}\text{U}(n,f)$  and  $^{239}\text{Pu}(n,f)$  depends on the composition of the initial fuel.

The approximation in Eq. (12) can be made due to the relatively long half-life and small capture cross-section of  $^{137}\text{Cs}$  and  $^{90}\text{Sr}$ . Hence, the nuclear data required to derive their inventory are the cumulative fission yields and fission cross-sections. They are reported in Table 3 and Table 4 for thermal neutron-induced fission of  $^{235}\text{U}$  and  $^{239}\text{Pu}$ . These data suggest that there is a rather good consensus on the fission cross-sections and their uncertainties. However, for the cumulative fission yields there are larger differences. For  $^{235}\text{U}(n,f)$  the difference between the yields recommended in JEFF-3.3 and ENDF/B-VIII.0 is almost 2 % and their uncertainties differ by a Factor 2. The inventory of these nuclides, as such, is not a key source term. However,  $^{137}\text{Cs}$  has a substantial contribution to the  $\gamma$ -ray emission and decay heat. The data used to derive the  $\gamma$ -ray emission spectrum due to the decay of  $^{137}\text{Cs}$  are well known and they can be taken from the ENSDF data base [Tuli, 2001]. The total energy that can be transformed into heat, which is also referred to as recoverable energy, is summarised in Table 5. These values are deduced from a combination of decay data. The uncertainty of the recoverable energy due to the decay data is less than 1 % for both  $^{90}\text{Sr}$  and  $^{137}\text{Cs}$ . It is remarkable that all recommended values differ from the value  $E_r = 1'147$  (9) keV that was derived by Ramthun from a direct calorimetric measurement [Ramthun, 1967]. The results in Table 5 suggest that the recommended values might be underestimated with a bias between 1.5 % and 3.5 %. New measurements are required to resolve these discrepancies.

Library	$\sigma(n,f)$ at 2'200 m/s		$\langle \sigma(n,f) \rangle$ : spectrum-averaged	
	$^{235}\text{U}(n,f)$	$^{239}\text{Pu}(n,f)$	$^{235}\text{U}(n,f)$	$^{239}\text{Pu}(n,f)$
ENDF/B-VIII.0	586.7 (29) b	747.4 (69) b	33.99 (14)	77.62 (107)
JEFF-3.3	584.5 (38) b	749.3 (65) b	33.49 (23)	78.02 (95)
JENDL-4.0	585.0 (20) b	747.3 (84) b	34.06 (11)	78.53 (59)

Table 3 – Cross-section for neutron-induced fission of  $^{235}\text{U}$  and  $^{239}\text{Pu}$  recommended in the latest versions of the main data libraries

The cross-section at thermal energy (or at 2200 m/s) is given together with a spectrum-averaged cross-section based on a typical neutron energy distribution in a PWR. Uncertainties are at the 68 % confidence limit.

Library	$^{90}\text{Sr}$	$^{90}\text{Sr}$	$^{137}\text{Cs}$	$^{137}\text{Cs}$	$^{148}\text{Nd}$	$^{148}\text{Nd}$
	$^{235}\text{U}(n,f)$	$^{239}\text{Pu}(n,f)$	$^{235}\text{U}(n,f)$	$^{239}\text{Pu}(n,f)$	$^{235}\text{U}(n,f)$	$^{239}\text{Pu}(n,f)$
ENDF/B-VIII.0	0.0578 (5)	0.0210 (4)	0.0619 (3)	0.0661 (3)	0.01674 (6)	0.01662 (8)
JEFF-3.1.1	0.0573 (13)	0.0201 (5)	0.0622 (7)	0.0659 (8)	0.01681 (12)	0.01658 (17)

JEFF-3.3	0.0568 (13)	0.0208 (6)	0.0609 (6)	0.0673 (8)	0.01693 (12)	0.01685 (15)
JENDL-4.0	0.0577 (6)	0.0210 (4)	0.0618 (3)	0.0660 (3)	0.01671 (7)	0.01642 (8)

Table 4 – Cumulative fission yields of  $^{90}\text{Sr}$ ,  $^{137}\text{Cs}$  and  $^{148}\text{Nd}$  for neutron-induced fission of  $^{235}\text{U}$  and  $^{239}\text{Pu}$  at thermal energy (or 2'200 m/s)

The cross-sections recommended in evaluated data libraries are compared. Uncertainties are at the 68 % confidence limit.

Library	$^{90}\text{Sr}/^{90}\text{Y}$			$^{137}\text{Cs}/^{137\text{m}}\text{Ba}$		
	$E_r$ / keV	$E_{r,cp}$ / keV	$E_{r,\gamma}$	$E_r$ / keV	$E_{r,cp}$ / keV	$E_{r,\gamma}$ / keV
DDEP [Kellett, 2017]	1'129.4 (14)			813.3 (18)	247.9 (12)	813.3 (18)
ENDF/B-VIII.0	1'128.8	1'128.8	0	805.7	240.1	565.6
JEFF-3.3	1'128.5	1'128.5	0	804.1	237.4	566.7
JENDL/FPD-2011	1'129.6	1'129.6	0	811.2	247.9	563.3

Table 5 – Total recoverable energy ( $E_r$ ) together with that resulting from charged particle ( $E_{r,cp}$ ) and  $\gamma$ -ray ( $E_{r,\gamma}$ ) emission due to the decay of the  $^{90}\text{Sr}/^{90}\text{Y}$  and  $^{137}\text{Cs}/^{137\text{m}}\text{Ba}$  chains

The energies recommended in nuclear data libraries are compared with the ones derived from the data in the DDEP [Kellett, 2017]. Uncertainties are at the 68 % confidence limit.

The capture cross-section of  $^{134}\text{Cs}$  is relatively large and cannot be ignored when estimating the abundance of  $^{134}\text{Cs}$ . Figure 3 compares the capture cross-section that is recommended in the ENDF/B-V and ENDF/B-VII.0 libraries. It is shown in [Ilas, 2012] that the difference between the cross-sections in ENDF/B-V and ENDF/B-VII.0 results in a 7.5 % difference in the  $^{134}\text{Cs}$  abundance in case of a 50 GWd/t burnup. Even larger differences of up to 30 % are observed for  $^{149-152}\text{Sm}$ ,  $^{155}\text{Eu}$  and  $^{155}\text{Gd}$  [93]. This shows the importance of estimating the cross-section in the resolved resonance region based on resolved resonance parameters, which can only be derived from a resonance shape analysis of experimental data (see [Fröhner, 2000; Schillebeeckx, 2012]).

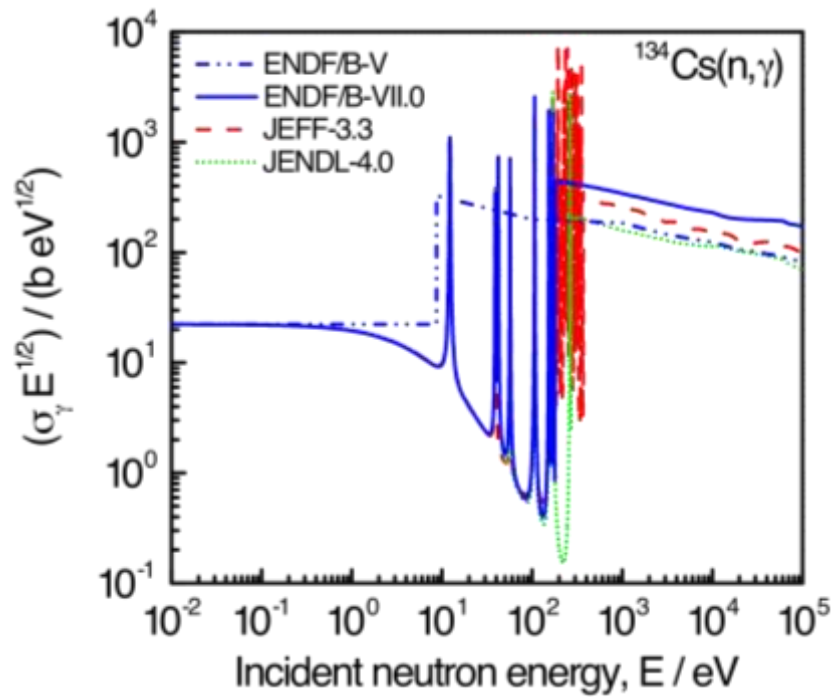


Figure 3 – Comparison of the  $^{134}\text{Cs}(n,\gamma)$  cross-sections as a function of neutron energy which are recommended in the ENDF/B-V, ENDF/B-VII.0, JEFF-3.3 and JENDL-4.0 libraries

The capture cross-section  $\sigma_\gamma$  is multiplied with the square root of the energy.

One of the important contributors to the neutron emission rate of spent fuel is  $^{244}\text{Cm}$ . Starting from  $\text{UO}_2$  based fuel, this curium isotope is produced through a sequence of neutron capture reactions and  $\beta^-$  decay starting from the  $^{238}\text{U}(n,\gamma)$  reaction. The main production chain involves six neutron-induced capture reactions. Several studies [Hu, 2014; Zu, 2016; Leray, 2016; Borella, 2017; Rochman, 2018b] show that the uncertainty of the predicted  $^{244}\text{Cm}$  abundance is in the order of 10 %. This is mainly due to the uncertainty of the  $^{242}\text{Pu}(n,\gamma)$  and  $^{243}\text{Am}(n,\gamma)$  cross-sections [Hu, 2014; Leray, 2016]. To derive the neutron emission rate, the  $^{244}\text{Cm}$  abundance has to be combined with the specific neutron emission per decay, which is  $3.74 (11) \times 10^{-6}$  based on data in the JEFF-3.3 library. Hence, at present the total uncertainty of the predicted neutron emission rate due to  $^{244}\text{Cm}(\text{sf})$  is dominated by the one of the  $^{244}\text{Cm}$  production. This uncertainty can only be reduced by performing new experiments to improve the capture cross-section data for  $^{242}\text{Pu}(n,\gamma)$  and  $^{243}\text{Am}(n,\gamma)$ . In the case where the neutron emission is dominated by the production of  $(\alpha,n)$  neutrons, there is a substantial contribution to the uncertainty due to the specific  $(\alpha,n)$  neutron production which is in the order of 8 % [Simakov, 2017]. This uncertainty component is difficult to reduce and requires both improved experimental data and theoretical modelling.

For a criticality safety assessment based on a BUC approach, the concentrations of nuclides with a relatively large absorption cross-section are required together with reliable estimates of the cross-sections. Oscillator experiments [Gruel, 2011] were performed at the MINERVE reactor of CEA Cadarache (FR) to validate the capture cross-section of fission products that are important for such a criticality safety analysis. For most of them, substantial differences were observed between the measured and calculated reactivity-worth. Based on these differences, correction factors are proposed to define criticality safety margins [Tardy, 2015]. However, results derived from such oscillator experiments might be biased due to poor knowledge of the sample properties as discussed in [Šalamon, 2019; Ma, 2019]. Problems with the sample properties could explain the reactivity-worth difference in the order of 10 % observed for  $^{103}\text{Rh}$  in Ref. [Gruel, 2011]. Since natural rhodium is mono-isotopic and metallic homogeneous samples are easy to produce, its capture cross-section can be determined with an uncertainty of less than 2 % [Schillebeeckx, 2012]. Therefore, the use of correction factors is not recommended and reliable safety margins should be derived starting from accurate microscopic absorption cross-sections resulting from an evaluation process that is based on a resonance analysis of experimental data reported in the literature. Unfortunately, the present status of the evaluated libraries does not always reflect the quality of the available experimental data. Table 6 compares the capture cross-section for  $^{103}\text{Rh}$  at thermal energy as recommended in the main general purpose libraries. The values are consistent within the quoted uncertainties, except for the one in JENDL-4.0. Nevertheless, it seems that none of the evaluation procedures included the value  $\sigma_\gamma = 144.9 (7)$  b derived by [Dilg, 1974], even though this value was derived by the same method that was used to derive the value for  $^{197}\text{Au}(n,\gamma)$  [Dilg, 1973], which is still the basis of the present neutron standard [Carlson, 2018].

Library	$^{103}\text{Rh}$		
	$\sigma (n,\text{tot}) / \text{b}$	$\sigma (n,n) / \text{b}$	$\sigma (n, \gamma) / \text{b}$
ENDF/B-VIII.0	146.5	4.34 (87)	142.1 (15)
JEFF-3.3	146.6 (38)	3.88 (92)	142.7 (37)
JENDL-4.0	136.4	3.27	133.1

Table 6 – Total cross-section and cross-section for neutron elastic scattering and capture of  $^{103}\text{Rh}$  at thermal energy

The data in recommended data libraries are compared.

### 2.3.3. Fuel history

The importance of the fuel history, i.e. fuel composition and design, reactor operation and fuel irradiation conditions, is discussed in a state-of-the art report that was issued by the NEA/OECD. This report was the result of an Expert Group on Assay Data of Spent Nuclear Fuel (EGADSNF) [NEA, 2011]. In this report, the impact of modelling approximations due to missing or uncertain fuel history data is discussed based on calculations done using the Takahama PWR 17x17 assembly as a reference. The report discusses how various parameters such as power history, moderator temperature (density), moderator soluble boron, fuel temperature, sample burnup, assembly pitch and surrounding assemblies affect the nuclide inventory.

Assigning an uncertainty to these parameters to propagate them to the uncertainty on the source terms is not evident. It will depend on the quality of the documentation provided by the fuel manufacturer, operators and engineering companies. In the OECD-NEA state-of-the-art report, estimates of representative uncertainties at a 68 % confidence limit are given for the initial enrichment (0.05 wt.-%), fuel temperature (50 °C), moderator temperature (2 °C) and fuel sample (local) burnup (2 %, relative). The impact of the uncertainty of the initial enrichment and burnup on the inventory of some key nuclides is illustrated in Figure 4 [Schillebeeckx, 2018]. This figure gives the sensitivity of the nuclide inventory to a change in IE and BU for a PWR assembly with an initial enrichment of 4.8 wt.-% and burnup of 45 GWd/t. The results illustrate that the inventory of <sup>137</sup>Cs and <sup>148</sup>Nd is not sensitive to the initial enrichment and a 1 % uncertainty of the burnup results in a 1 % uncertainty of the inventory. For a relative variation of 1 % of the initial enrichment and burnup, the inventory of <sup>244</sup>Cm changes by 2 % and 4 %, respectively. The impact of burnup increases due to the number of neutron-induced reactions involved in the production process.

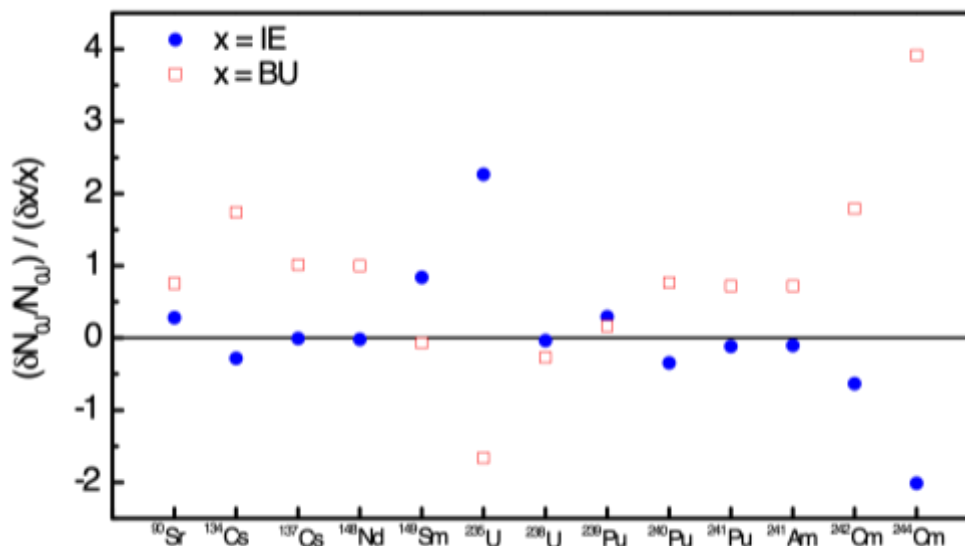


Figure 4 – Relative sensitivity of the nuclide inventory to the initial enrichment (IE) and burnup (BU)  
The data are for a UO<sub>2</sub> sample with initial enrichment of 4.8 wt.-% irradiated in a PWR to a burnup of 45 GWd/t.

Burnup is an essential parameter for the calculations. It is related to time integrated the thermal power that is extracted from the nuclear fuel. The thermal power of a system is used to determine the neutron fluence which is required to normalise the theoretical calculations. The relation between thermal power  $P$  and neutron fluence rate is [Gauld, 2011]:

$$= \frac{P}{\sum_k N_k (N_{f,k} E_{f,k} + \sum_a N_{a,k} E_{a,k})} \quad (14)$$

with  $N_{f,k}$  and  $N_{a,k}$  the total number of fission and other absorption reactions with nuclide  $k$ , respectively, and  $E_{f,k}$  and  $E_{a,k}$  the corresponding recoverable energies for these reactions. The inventory of nuclide  $k$  is denoted by  $N_k$ . Table 7 lists the recoverable energy per fission and capture event for  $^{235}\text{U}$  and  $^{239}\text{Pu}$ , which are recommended in the main data libraries. There is almost no difference between the adopted values. The recoverable energy for some nuclides with a relatively large absorption cross-section are given in Table 8. These energies are the same in the main data libraries and are used in SERPENT and ALEPH2. They are also used in SCALE, except for  $^{155}\text{Gd}$  and  $^{157}\text{Gd}$ , for which a default energy of 5 MeV is adopted. This can create bias effects in the case of Gd-loaded fuel.

	$^{235}\text{U}$			$^{239}\text{Pu}$		
	$E_r$ / MeV	$E_{r,f}$ / MeV	$E_{r,\gamma}$ / MeV	$E_r$ / MeV	$E_{r,f}$ / MeV	$E_{r,\gamma}$ / MeV
ENDF/B-VIII.0	200.645	194.1	6.545	205.134	198.6	6.534
JEFF-3.3	200.415	193.87	6.545	205.234	198.7	6.534
JENDL-4.0	200.345	193.8	6.545	206.434	199.9	6.534

Table 7 – Recoverable energy due to neutron-induced interaction with  $^{235}\text{U}$  and  $^{239}\text{Pu}$   
The energies recommended in evaluated data libraries are compared.

Library	Recoverable energy, $E_r$ / MeV				
	$^1\text{H}(n,\gamma)$	$^{16}\text{O}(n,\gamma)$	$^{10}\text{B}(n,\alpha)$	$^{155}\text{Gd}(n,\gamma)$	$^{157}\text{Gd}(n,\gamma)$
ENSDF [Tuli, 2001]	2.225	4.143	2.790	8.536	7.937

Table 8 – Recoverable energy for some important neutron absorption reactions  
The energies in the decay libraries are adopted in the main evaluated data libraries. They are also used in SCALE, except for  $^{155,157}\text{Gd}(n,\gamma)$ .

The burnup is mostly defined as time integrated thermal power per unit initial actinide mass in the fuel and often expressed in gigawatt-days per ton (GWd/t) or megawatt-days per kg (MWd/kg). In the case where samples of irradiated fuel are analysed, the burnup is mostly derived from the total number of Fission reactions per Initial number of heavy Metal Atoms (FIMA). It is often assumed that the burnup defined by the total thermal power is directly proportional to the total number of fissions, with a constant conversion factor. Evidently, this assumption is not always valid and might introduce bias effects [Kępisty, 2007; Kenya, 2006]. The recoverable energy depends on the fissioning nuclide such that the average energy released per fission event will change with burnup. A more detailed discussion on the relation between burnup and FIMA is given in [Kępisty, 2007].

The number of fission events of an irradiated sample can be derived by determining the amount of a specific fission product. An ideal fission product to determine the number of fissions should have a cumulative fission yield that is independent from the fissioning nuclide, a low yield from neutron capture, a low neutron absorption cross-section and a relatively long half-life. Under these conditions, the amount of this fission product is directly proportional to the total number of fission reactions, even independent of the initial enrichment. In addition, it should not be volatile and not be produced through volatile precursors. The use of the stable fission product  $^{148}\text{Nd}$  as a FIMA monitor or indicator is generally accepted as a standard method since the issue of the ASTM method E 321-96 [ASTM, 1969; ASTM, 2012]. However, in spite of the short half-life of  $^{147}\text{Nd}$  and the small  $^{148}\text{Nd}(n,\gamma)$  cross-section, the production of  $^{148}\text{Nd}$  is affected by the  $^{147,148}\text{Nd}(n,\gamma)$  cross-sections [Suyama, 2005]. These capture reactions will have an opposite effect on the  $^{148}\text{Nd}$  production. The results in Ref. [Kenya, 2006] show that ignoring the contributions due to the  $^{147,148}\text{Nd}(n,\gamma)$  reactions and the dependence of the recoverable energy, the burnup derived from the amount of  $^{148}\text{Nd}$  can be biased by 3 %. To reduce bias effects, it is recommended to derive the burnup by theoretical calculations by adjusting the theoretical  $^{148}\text{Nd}$  inventory to the experimental value as in Refs. [Zwicky, 2010; Gauld, 2016]. Applying such a procedure, the total number of fission reactions can be determined with an uncertainty of 1.5 % (68 % confidence limit) [Gauld, 2016].

Evidently, the  $^{147}\text{Nd}(n,\gamma)$  cross-section enters into such a calculation. Although, this reaction contributes less than 2 % to the  $^{148}\text{Nd}$  production, the results in Figure 5 illustrate the need for a re-evaluation of this cross-section. This figure compares the cross-section recommended in the ENDF/B-VIII.0, JEFF3.3, JENDL-4.0 and TENDL-2017 libraries. The cross-section in TENDL-2017 relies on a re-evaluation of the cross-section at thermal energy in [Rochman, 2016a]. This evaluation is based on the value reported in [Heck, 1974] combined with results of optical model calculations. Unfortunately, the value in [Heck, 1974] is the only experimental value for this reaction at thermal energy that is reported in the literature. Hence, the experimental data available for performing an evaluation are rather scarce.

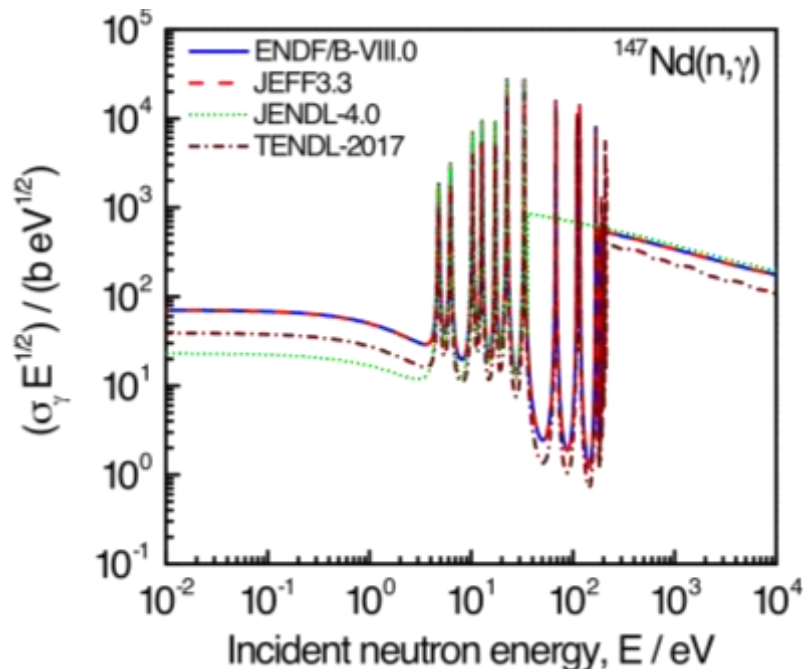


Figure 5 – Comparison of the  $^{147}\text{Nd}(n,\gamma)$  cross-sections as a function of neutron energy that are recommended in the ENDF/B-VIII.0, JEFF-3.3, JENDL-4.0 and TENDL-2017 libraries

*The cross-section  $\sigma_\gamma$  is multiplied with the square root of the energy.*

Alternative methods to determine the number of fission events are based on measurements of other Nd isotopes, fission products such as  $^{133,137}\text{Cs}$  and  $^{235}\text{U}$  or  $^{239}\text{Pu}$  [Zwicky, 2010; Gauld, 2016; Kim, 2007; Kim, 2015]. Different methods to be compared in [Zwicky, 2010]. The results are consistent within 3 %. The advantage of using  $\gamma$ -ray emitting indicators such as  $^{137}\text{Cs}$  is that their inventory can be determined by non-destructive  $\gamma$ -ray spectroscopic methods and used to verify the burnup of an assembly. All these methods use the inventory of a specific nuclide to normalise the local burnup of the sample being investigated and to compare measured and calculated inventories of other nuclides. However, for final applications, the burnup information provided by the operator has to be used. Unfortunately, no detailed study is available in the open literature that provides an uncertainty assessment to link FIMA to the burnup information of the operator.

## 2.4. Uncertainty evaluation and sensitivity analysis

A reliable characterisation of spent fuel requires best estimates of the observables together with their uncertainties and covariance matrix. They will finally define the confidence limits and safety margins and influence the decision-making. Hence, a careful evaluation of the covariance matrix of the calculated nuclide vector is required. Unfortunately, the relationship between the nuclide vector and the input data is rather complex. Since the neutron and  $\gamma$ -ray emission rates and thermal power are linear functions of the nuclide vector, their uncertainties can be derived by conventional first order uncertainty propagation, also considering the uncertainty of decay constants, specific emission properties and recoverable energy.

### 2.4.1. Methods

Propagation of uncertainties can be performed by deterministic or probabilistic methods [Rochman, 2011; Wieselquist, 2013]. Deterministic methods are based on the first order uncertainty propagation formula:

$$\mathbf{V}_Y = \mathbf{S}\mathbf{V}_X\mathbf{S}^T \quad (15)$$

with  $\mathbf{V}_Y$  the covariance matrix of the output,  $\mathbf{V}_X$  the covariance matrix of the input data and  $\mathbf{S}$  the sensitivity matrix. The latter is defined by the partial derivatives of the output with respect to the input. Most of the deterministic sensitivity and uncertainty analysis codes used for reactor applications rely on perturbation theory [Kodeli, 2001; Rearden, 2011]. For neutron transport problems, the sensitivity matrix is directly obtained from the forward and adjoint transport equation [Wieselquist, 2013; Kodeli, 2001]. Adjoint equations for depletion calculations were implemented in ORIGEN [Rearden, 2011] based on the work of [Gandini, 1975]. The present version of ORIGEN includes adjoint calculations based on the CRAM method for sensitivity and uncertainty analysis [Isotalo, 2015; Gauld, 2017].

The direct perturbation approach works well for smooth relationships between input and output and when the uncertainties are relatively small. When non-linearity effects are important this approach is not applicable and can be replaced by stochastic sampling-based uncertainty propagation [Rochman, 2011]. This consists of repeating the nominal calculation a large number of times, each time with different input data. The input data are sampled from independent or multivariate probability distributions. These distributions reflect the covariance  $\mathbf{V}_X$  of the input data. In most cases they are based on multivariate normal distributions. However, this is not a restriction, for example inherently positive data can be sampled from a log-normal or rectangular distribution. The choice of the distributions depends on the available information about the input data and can be based on the Maximum Entropy Principle [Jaynes, 1968]: when only a best estimate of an inherently positive observable is known the data should be sampled from a decreasing exponential distribution; however, when an estimate of the covariance matrix is also available the optimum probability distribution for further inference is a multivariate normal distribution [Fröhner, 2000]. Stochastic sampling offers the advantage that uncertainties of all input data can be propagated, independently of their relationship with

the output of interest and of the magnitude of the uncertainty. In addition, it provides the final probability distributions of output quantities from which the uncertainties can be derived.

Various codes and platforms have been developed to propagate uncertainties by stochastic sampling, e.g. SHARK-X [Wieselquist, 2013; Aures, 2017], XSUSA [Aures, 2017; Zwermann, 2014], NUSS [Zhu, 2015], NUDUNA [Diez, 2015], SAMPLER [Williams, 2013b; Rearden, 2015] and SANDY [Fiorito, 2017]. The development and testing of these codes have been motivated by the Benchmark for Uncertainty Analysis in Modelling (UAM) for design, operation and safety analysis of LWRs organised by the OECDNEA [Ivanov, 2013].

The SHARK-X platform has been developed at the Paul Scherer Institute for sensitivity analysis and uncertainty propagation based on a deterministic perturbation and stochastic sampling approach [Wieselquist, 2013; Aures, 2017]. It is a set of Perl-based tools build around the lattice code CASMO-5. It allows perturbation to nuclear data, i.e. cross-sections for  $(n,n)$ ,  $(n,n'\gamma)$ ,  $(n,2n)$ ,  $(n,f)$  and  $(n,\gamma)$  reactions, the average number of neutrons per fission and the prompt fission neutron energy distribution. In addition, any parameter contained in the input file, e.g. cladding thickness, fuel enrichment, can be perturbed.

The XSUSA Cross-section Uncertainty and Sensitivity Analysis (XSUSA) method [Zwermann, 2014] is based on the random sampling method implemented in the code package Software for Uncertainty and Sensitivity Analysis (SUSA) Krzykacz, 1994]. It enables simultaneous correlated sampling of  $(n,n)$ ,  $(n,n')$ ,  $(n,2n)$ ,  $(n,f)$ ,  $(n,\gamma)$  cross-sections, fission neutron multiplicities and fission neutron spectra. As a basis for generating the data variations, the SCALE 6.1 covariance data library is used and processed in a multi-group structure with 44 energy groups. Normal distributions are assumed as default distributions. In addition to neutron cross-section uncertainties, uncertainties of data relevant for the production of nuclides and their decay chains can be propagated, i.e. uncertainties of fission yields, decay constants and branching. These uncertainty data are extracted from the ENDF/B-VII library. The XSUSA method is also integrated into the SAMPLER module [Williams, 2013b; Rearden, 2015] of the SCALE code system, where it can be used in combination with the POLARIS sequence. The SAMPLER module uses the XSUSA method to repetitively sample nuclear data in multi-group approximation, execute the sequence and analyse the distributions of e.g. decay heat rate or nuclide vector.

The Nuclear data Uncertainty Stochastic Sampling (NUSS) random sampling tool [Zhu, 2015] combines multi-group uncertainties and pointwise/continuous energy nuclear data. This tool is implemented for the continuous energy ACE format, facilitating direct use by MC codes such as MCNP and SERPENT. It is capable of introducing perturbations to  $(n,n)$ ,  $(n,n')$ ,  $(n,2n)$ ,  $(n,f)$ ,  $(n,\gamma)$  cross-sections, fission neutron multiplicities and fission neutron energy distribution data using multivariate normal distribution. Caution has to be taken that associated total quantities are updated accordingly, i.e. summation rules are not applied automatically.

The Nuclear Data Uncertainty Analysis (NUDUNA) package [Díez, 2015] provides full random sampling of nuclear data inputs for transport and depletion calculations. NUDUNA takes the information provided by nuclear data evaluations in the standardised ENDF-6 format as input, taking into account best estimates and covariances of neutron-induced cross-sections, resonance parameters, fission neutron multiplicities, angular distributions of outgoing particles and decay data, assuming normal or log-normal distribution. The NUDUNA output files can be used as input for different neutron transport and fuel depletion codes, such as SCALE, SERPENT or MCNP.

The random sampling code SANDY [Fiorito, 2017] enables sampling of nuclear data for which covariance data are available: resonance parameters, cross-sections, angular and energy distributions, fission neutron multiplicities, fission yields and decay data. The code includes capabilities for verification of mathematical correctness of the covariance data and automated correction methods to make the covariance matrix positive semi-definite [Higham, 2011]. It uses multivariate normal or log-normal distribution for sampling of correlated parameters. Apart from the basic option of uncertainty propagation, it also includes capabilities for sensitivity analysis using linear regression. This method is analogous to the first order deterministic sensitivity analysis since it is accurate for small uncertainties

or (close to) linear functions. It enables simultaneous determination of the entire sensitivity matrix using one set of samples with all input parameters perturbed. Due to the nature of random sampling, this method works for any functional relationship. The SANDY code is freely available and works with nuclear data files in ENDF-6 format.

## 2.4.2.Examples

The codes presented in Section 2.4.1 have been used for sensitivity and uncertainty analysis of the source terms of spent nuclear fuel, see [Leray, 2016; Borella, 2017; Rochman, 2018b; Zwermann, 2014; Cabellos, 2011; Fiorito, 2015; Rochman, 2013; Leray, 2017; Rochman, 2020a]. They focus on nuclear data uncertainties with the emphasis on cross-sections and fission yields.

### Nuclear data

The results in [Cabellos, 2011; Fiorito, 2015] reveal that uncertainties due to decay constants have a negligible contribution to the total uncertainty of the nuclide inventory, except for the production of  $^{151}\text{Eu}$ . The results in [Cabellos, 2001; Fiorito, 2015] are based on a recommended half-life of  $T_{1/2} = 90$  (8) for  $^{151}\text{Sm}$ . The present recommendation by DDEP is  $T_{1/2} = 94.7$  (6) a. This value is based primarily on results of measurements reported in Ref. [Bé, 2015] and has been adopted in JEFF-3.3 but not in ENDF/B-VIII.0.

Most of the studies verifying the impact of nuclear cross-section data report only final uncertainties. Sensitivity studies to identify the main reactions contributing to the uncertainty of the nuclide inventory are rather scarce. However, such studies are needed to define nuclear data that need to be improved. A study of reaction cross-section data that are important for the production of  $^{244}\text{Cm}$  and  $^{238}\text{Pu}$  is presented in [Tiehun, 2016] and [Gauld, 2017], respectively. These studies show the convenience of the adjoint equations for the depletion calculations for such a sensitivity study.

Efforts are made to propagate uncertainties of fission yields. Table 9 compares reported uncertainties for the predicted  $^{137}\text{Cs}$  and  $^{148}\text{Nd}$  inventory due to the propagation of fission yields covariance data for  $\text{UO}_2$  in a PWR [Leray, 2016; Rochman, 2018b; Rochman, 2013; Leray, 2017b]. The results reveal strong differences, e.g. for  $^{137}\text{Cs}$  the uncertainty varies between 0.3 % and 7.0 % and for  $^{148}\text{Nd}$  between 0.4 % and 14 %. Part of these differences is due to the use of independent fission yields which are needed for a complete consistent burnup calculation. Unfortunately, independent fission yields are generally more complicated to measure compared to cumulative yields. Therefore, they have larger uncertainties. Methods have been proposed and developed to produce covariance data for independent fission yields that are consistent with cumulative yields, that is, to maintain the cumulative yields together with their uncertainties [Fiorito, 2014; Fiorito, 2016; Rochman, 2016b]. However, given the difference between the evaluated data discussed in Section 2.3, a difference of a Factor 2 will remain. Hence, a consensus on the evaluated cumulative yields and their uncertainties is required.

Ref.	Library	Con- straint	Reactor	Fuel	BU (GWd/t)	IE (wt.-%)	$^{90}\text{Sr}$	$^{137}\text{Cs}$	$^{148}\text{Nd}$
[Zwermann, 2014]	SCALE-6.1		PWR	$\text{UO}_2$	40	4.1	5.0 %	1.7 %	14 %
[Fiorito, 2016]	ENDF/B-VII.0		PWR	$\text{UO}_2$	40	4.1	5.6 %	2.0 %	12 %
[Leray, 2016]	ENDF/B-VII.1	Y	PWR	$\text{UO}_2$	54	3.4	1.5 %	4.0 %	0.4 %
[Rochman, 2018b]	ENDF/B-VII.1	Y	PWR	$\text{UO}_2$	54	3.4	0.7 %	6.2 %	0.4 %
[Rochman, 2018b]	ENDF/B-VII.1	Y	PWR	$\text{UO}_2$	40	4.1	0.7 %	7.0 %	0.4 %

[Leray, 2017b]	ENDF/B-VII.1	Y	PWR	UO <sub>2</sub>	60	4.1	3.6 %	0.3 %	0.9 %
[Leray, 2017b]	JEFF-3.1.1	Y	PWR	UO <sub>2</sub>	60	4.1	9.3 %	0.8 %	0.6 %

*Table 9 – Uncertainties of the inventory due to the propagation of nuclear data uncertainties*

*All results are for UO<sub>2</sub> fuel in a PWR. The burnup (BU) and initial enrichment (IE) are specified together with the nuclear data library that is used. The 3rd column specifies whether the covariance of the independent fission product yields was based on boundary conditions (constraints) (see [Fiorito, 2014; Fiorito, 2016; Rochman, 2016]).*

An uncertainty assessment of decay heat predictions for BWR SNF assemblies is reported by Ilas and Liljenfeldt [Ilas, 2017]. The impact of uncertainties due to nuclear data and fuel history parameters were verified using the SAMPLER module of SCALE. The results, which are summarised in Table 10, suggest that for a cooling time of about 15 years, the total uncertainty of the predicted heat is about 1.3 %. The contribution of the uncertainties due to both nuclear data and fuel history is about 0.9 %. 70% of the decay heat at such cooling times derives from the decay chains of <sup>137</sup>Cs and <sup>90</sup>Y. The discussion on the fission yields and recoverable energy in Section 2.3.2 suggests that an uncertainty of less than 1 % is questionable. Using the data in Table 4 and Table 5, a difference of about 2.5 % in estimated thermal power only due to nuclear data can be expected for the conditions considered in [Ilas, 2017]. A study in [Rochman, 2016] reports for similar conditions an uncertainty of at least 3 % by propagating only cross-section and fission yield uncertainties. In addition, the discussion in Section 2.3 suggests that an absolute prediction of the burnup with an uncertainty of less than 1 % is questionable. Hence, a more detailed uncertainty assessment of decay predictions is required to define realistic confidence limits that can be presented to licensing authorities.

Uncertainty component		Relative uncertainty (68 % confidence limit)
Fuel history	Fuel design	0.20 %
	Operation history	0.85 %
	Total	0.87 %
Nuclear data	Cross-sections	0.88 %
	Fission yields	0.26 %
	Total	0.92 %
<b>Total</b>		<b>1.27 %</b>

*Table 10 – Uncertainty evaluation of the decay heat estimated by theoretical calculations*

*Reported in [Ilas, 2017]. The uncertainties are for a UO<sub>2</sub> assembly with an initial enrichment of 2.9 wt.-% that was irradiated in a BWR to a burnup of 36.9 GWd/t. The results are for a cooling time of 15.6 years.*

## Fuel history

The impact of fuel history data on the inventory of a PWR spent fuel assembly is discussed in the state-of-the-art report issued by OECD-NEA [NEA, 2011]. The OECD-NEA started a new initiative to produce a guidance report on "Code validation for decay heat application". This report will include a section discussing the impact of fuel history data on the calculated decay heat [Fiorito].

Kromar and Kurinčič performed a sensitivity analysis for UO<sub>2</sub> spent fuel from the Krško nuclear power plant using SERPENT [Kromar, 2015; Komar, 2017]. They verified the influence of several factors, such as initial enrichment, burnup, fuel temperature, moderator temperature and density, soluble boron concentration, average power density and burnable absorbers on the decay heat and neutron and  $\gamma$ -ray emission. The main conclusions drawn from this analysis are valid for any PWR fuel in the form of low-enriched UO<sub>2</sub>.

Change the burnup of 50 GWd/t by 20 % changes the thermal power and  $\gamma$ -ray emission rate by ~ 20 % and the neutron emission rate by ~ 35 % at the end of irradiation. Hence, around a burnup of 50 GWd/t the thermal power and  $\gamma$ -ray emission rate are almost linearly dependent on burnup (i.e. the relative sensitivity ~ 1), whereas the neutron emission rate has a stronger dependence on burnup (i.e. absolute relative sensitivity ~ 2). This is expected since, at the end of irradiation, the dominant contributions to the thermal power and  $\gamma$ -ray emission is due to the decay of fission products whose build-up depends almost linearly on the number of fissions, whereas the neutron emission comes entirely from actinides whose build-up as a function of burnup can typically be approximated as a higher order polynomial dependence.

Changing the initial enrichment of 3.525 wt.-% by 20 % changes the thermal power by ~ 5 %, the  $\gamma$ -ray emission rate by ~ 3.5 % and the neutron emission rate by 25 % at the end of irradiation. The relative sensitivities of the decay heat and  $\gamma$ -ray emission to the initial <sup>235</sup>U enrichment at short cooling times are small. The sensitivity of the neutron emission rate from spent fuel on initial enrichment is higher ~ - 1.3 due to the build-up of higher actinides.

The effects of other operational parameters on decay heat, neutron and  $\gamma$ -ray emission were smaller. Moderator density (due to thermal expansion) and the presence of boron in the moderator and burnable absorbers are important, while the sensitivity of the observables to the fuel temperature and the specific power is smaller and needs to be considered only in very detailed cases.

In addition to the sensitivity study itself, non-linearity (departure from the first-order sensitivity approximation) was examined. Such analyses are important, since they indicate the errors produced in the averaging process, which is usually applied in practical applications. Results show that simple averaging of the enrichment and burnup domains can induce errors of several %. To avoid this, a sufficiently heterogeneous problem decomposition (several axial and perhaps even radial regions) is required.

## 2.5. Experimental determination of SNF source terms and observables

As discussed in Section 2.1, the ability to calculate the nuclide inventory of spent nuclear fuel is essential for many licensing aspects of the back-end of the fuel cycle, such as spent nuclear fuel transport, interim storage and final disposal. The accuracy in the radionuclide inventory that is required cannot be determined directly from measurements; it can only be derived from theoretical calculations using codes as described in Section 2.2. Independently of the progress made to improve the calculation methodologies and capabilities, a code validation and assessment of the accuracy based on a comparison with experimental data is required. This is essential for having procedures relying on such calculations accepted by licensing and nuclear safeguards authorities.

Due to the importance of having experimental data for code validation, the Expert Group on Burnup Credit Criticality (EGBUC) formed by the NEA/OECD supported the development of the SFCOMPO-2.0 database [Michel-Sendis, 2017]. It includes experimental data for 750 spent nuclear fuel samples resulting from material that was irradiated in a wide variety of reactors. The data are supplemented with

reviewed fuel design information, irradiation conditions and characteristics of the host reactors. At present, the data-base contains only results of Destructive Analyses (DA), which are mostly part of complex Post Irradiation Examination (PIE) studies [Degueldre, 2016]. However, the possibility to include results of Non-Destructive Assay (NDA) methods is considered, in particular, results of direct decay heat measurements by calorimetry, such as those produced in [SKB, 2006; Maeda, 2004; Jaboulay, 2012].

Promising NDA data result from the SKB-50 campaign organised at the interim storage facility CLAB in Sweden [Tobin, 2016]. In this campaign, characterisation of 50 PWR and BWR fuel assemblies using a calorimeter [SKB, 2006], a  $\gamma$ -ray spectroscopic scanning device [Vacaro, 2016] and two advanced neutron based systems, a Differential Die Away (DDA) [Martini, 2016] and Differential Die Away Self-Interrogation (DDSI) system [Trahan, 2020], have been performed. An integrated NDA system [Tobin, 2018b] that combines the capabilities of a Passive Gamma-ray Emission Tomography (PGET) [White, 2018], a Passive Neutron Albedo Reactivity (PNAR) instrument [Tobin, 2018] and a load cell has been developed in Finland. This system will be used to verify BWR and VVER-440 assemblies in Finland. Results of such NDA characterisation measurements provide useful data for code validation. They will be extremely important for verifying or adjusting fuel design parameters or irradiation history conditions to improve the nuclide inventory calculation prior to the encapsulation of the assemblies. A verification of the burnup of a SNF assembly by NDA is required for criticality safety analysis to avoid criticality safety problems due to misloading of assemblies [Bevard, 2009]. Another field of research is the development of NDA detection systems to verify the presence of fuel assemblies in transport or storage casks.

### 2.5.1. Analysis of fuel rods and segments

Most of the code validation studies reported in the literature are based on nuclide inventories of segments of a spent fuel rod determined by destructive chemical and radiochemical analysis methods (for example in Refs. [Gauld, 2016; Zwicky, 2010; Gauld, 2011; Hu, 2017]). It involves a series of steps including the selection of representative samples, dissolution of the sampled material and chemical separation of elements, followed by a combination of different analysis techniques to determine the elemental and isotopic compositions.

The selection of a representative sample is performed on the basis of a full-rod  $\gamma$ -ray scanning of the axial total activity or activity of specific nuclides, e.g.  $^{134}\text{Cs}$ ,  $^{154}\text{Eu}$  and  $^{137}\text{Cs}$ . Ideally, a large enough sample or segment from the fuel rod is taken that includes both pellets and pellet gaps. For  $\text{UO}_2$  and MOX fuels, digestion of the sampled material is performed in concentrated, boiling  $\text{HNO}_3$  under reflux. Where iodine is to be measured, a dedicated iodine trap is installed to condense the iodine in the off-gas. Often, a residue consisting mostly of hard-to-dissolve metallic fission products (Mo, Ru, Rh, Pd, Tc, Ag) is filtered off and digested in a second step with higher molarity  $\text{HNO}_3$  to which a catalytic amount of HF is added. If full dissolution of the metallic precipitates is desired, a third, alkaline melt based, step is sometimes applied to the residue remaining after the second step. The concentrations of specific nuclides are measured by various analytical techniques. The most common techniques are:

- radiation detection techniques: applying  $\alpha$ - and  $\gamma$ -ray spectroscopy and liquid scintillation counting
- mass spectroscopy: using a thermal ionisation mass spectrometer (TIMS) or inductively coupled plasma mass spectrometer (ICP-MS) combined with the Isotope Dilution technique (IDMS), addition of a standard solution or an external calibration

The state-of-the-art report prepared by the OECD-NEA [NEA, 2011] discusses these techniques and provides recommendations for measurements of some key nuclides. In [Hu, 2017], a table with experimental techniques, measured nuclides and associated uncertainties is given and the problem of determining the inventory of nuclides with low abundance by ICP-MS is discussed. The uncertainties range from 1 % to 5 %, with the smallest uncertainty for data derived by IDMS.

Radiochemical-based analysis methods are time-consuming and expensive to study the characteristics of a full rod or to determine axial and radial distributions of fuel characteristics. For such studies, NDA techniques are preferred. The MOSAIC calorimeter was used in the MERCI experiment to measure the decay heat of PWR fuel rods with a thermal power between 4 W and 200 W with an uncertainty below 2 % (68 % confidence limit) [Jaboulay, 2012]. The results were used to validate burnup calculations performed with TRIPOLI-4 [Petit, 2008] combined with the PEPIN2 solver of the DARWIN system [Tsilanizara, 2000].

The axial distribution of fission products and actinides can be obtained by non-destructive high resolution  $\gamma$ -ray spectroscopic scanning as shown in [Matsson, 1997]. Such axial profiles are used to study fission gas release and to determine the axial burnup and power profiles by analysing full energy peaks of  $\gamma$ -rays emitted by  $^{85}\text{Kr}$ ,  $^{137}\text{Cs}$  and  $^{140}\text{La}$  [Matsson, 1997]. Other radionuclides that provide useful  $\gamma$ -ray spectroscopic signatures are  $^{134}\text{Cs}$ ,  $^{144}\text{Ce}$  and  $^{154}\text{Eu}$  [Berndt, 1988; Caruso, 2007].

Axial and radial spatial information of spent fuel rods can be derived from  $\gamma$ -ray emission tomographic measurements. Details about techniques and methods for imaging can be found in [Parker, 2015]. One of the first two-dimensional  $\gamma$ -ray scanning measurements of spent fuel rods to determine the spatial distribution of radionuclides (fission and activation products) were carried out at LANL by [Barnes, 1970; Barnes, 1982; Philipps, 1979]. Other examples are the ISARD program developed at Grenoble [Ducros, 1985] and the measurement campaign at the VENUS facility of the SCK•CEN [Borms, 1999]. A  $\gamma$ -ray tomographic analysis of fuel cladding to verify its integrity has been performed by [Dobrin, 1997]. Tomographic measurements to determine within-pin distributions of  $^{134}\text{Cs}$ ,  $^{137}\text{Cs}$ , and  $^{106}\text{Ru}$  are reported in [Buurveld, 1993]. A  $\gamma$ -ray tomography cell station has been designed and developed at the Paul Scherrer Institute (PSI) for the investigation of individual LWR spent fuel rod segments at a within-rod level of resolution [Caruso, 2014a]. This computerised tomographic system benefits from an advanced high-resolution  $\gamma$ -ray spectrometry methodology [Caruso, 2008]. Transmission tomography, relying on the absorption of an external source (e.g. neutron,  $\gamma$ -ray or X-ray) crossing an object, is able to assess the internal morphology of an object. It is applied for quality control of radioactive waste packages [Tanke, 1991; Camp, 2002]. The use of  $\gamma$ -ray transmission tomography to determine the within-rod spatial distribution of the fuel density and  $\gamma$ -ray attenuation coefficients was demonstrated on a commercial nuclear fuel rod in [Caruso, 2014a; Caruso, 2009] using a  $^{60}\text{Co}$  source. These spatial properties were used in combination with results of  $\gamma$ -ray spectroscopic emission tomography to determine the radial and axial distribution of  $^{134}\text{Cs}$ ,  $^{137}\text{Cs}$  and  $^{154}\text{Eu}$  in spent fuel rod segments with a burnup between 52 GWd/t and 121 GWd/t [Caruso, 2014a].

The best results for code validation are those from an international programme including an inter-comparison exercise involving different laboratories and techniques to identify potential bias effects and define realistic uncertainties. The different measurements should include all stages of the process starting from the fuel dissolution to the data reduction. Examples of such programmes are: ARIANE [Belgonucléaire, 2000], MALIBU [Boulanger, 2004], REBUS [Baeten, 2003] and REGAL [Govers, 2015]. The aim of the ARIANE (Actinide Research In A Nuclear Element) programme was to improve the knowledge of the inventories of actinides and fission products in  $\text{UO}_2$  and MOX fuels irradiated to various burnups in PWRs and BWRs. Spent fuel samples were analysed using different techniques to determine the inventory of 49 different nuclides [Belgonucléaire, 2000]. The MALIBU programme, a successor of the ARIANE programme, was designed to obtain assay data for high burnup  $\text{UO}_2$  and MOX fuel from both PWR and BWR [Boulanger, 2004]. The REBUS programme was dedicated to the validation of codes for criticality calculations involving BUC. It included DA measurements to determine the nuclide inventory of the irradiated fuel and a measurement of the reactivity in the VENUS critical facility at SCK•CEN [Baeten, 2003]. The objective of the REGAL (Rod-Extremity and Gadolinia Analysis) programme is to investigate rod extremity effects and the study atypical shielding patterns in gadolinia-doped fuel rods [Govers, 2015]. The data of the ARIANE, MALIBU and REBUS programmes were used to validate SCALE and the ENDF/B libraries [Ilas, 2010; Ilas, 2012; Gauld, 2013]. The use of the REBUS data to validate SCALE and MONTEBURNS is reported in [Töre, 2013].

## 2.5.2. Non-destructive assay of spent fuel assemblies

Most of the NDA systems used for quantitative characterisation of SNF assemblies have been developed to verify the amount of fissile material for nuclear materials safeguards applications [Hue, 1978; Tarvainen, 1997; Lebrun, 2013] and to verify burnup for nuclear criticality safety applications applying a BUC approach [Bevard, 2009; Lebrun, 2001a].

### Conventional nuclear safeguards NDA systems

At present NDA systems that are routinely in use are limited to total neutron counting,  $\gamma$ -ray counting and  $\gamma$ -ray spectroscopy. The main detectors are fission and ionisation chambers measuring the total neutron and  $\gamma$ -ray emission rate, respectively, and  $\gamma$ -ray spectrometric detection systems based on HPGe, CdTe and CZT detectors, recording a spectrum of  $\gamma$ -rays emitted by the spent fuel assembly.

The FORK detector type of instrument is one of the main NDA detection systems used by safeguards inspectorates, providing quantitative signatures of the SNF. The first model was designed and constructed at LANL [Phillips, 1983; Rinard, 1988; Bosler, 1991]. The detector consists of two arms that can be positioned around a LWR fuel assembly. Each arm contains three detectors: two fission chambers, one surrounded by a thin sheet of cadmium, and one ionisation chamber. These signals are used through calibration curves to estimate the burnup and cooling time [Rinard, 1988]. The main signature is the total neutron count which is mainly due to spontaneous fission of  $^{244}\text{Cm}$ . The sensitivity of the total neutron count rate to the burnup is illustrated in Figure 6, which shows the  $^{244}\text{Cm}$  inventory as a function of burnup for a  $\text{UO}_2$  sample with an initial enrichment of 4.8 wt.-% irradiated in a PWR to a maximum burnup of 60 GWd/t. The strong sensitivity to the burnup is due to the total number of neutron-induced capture reactions in the production of  $^{244}\text{Cm}$ . Evidently, the results strongly depend on the declaration of the operator. The importance of having fuel history data to use the FORK detector for partial defect verification of LWR spent fuel assemblies is demonstrated in [Tiitta, 2002].

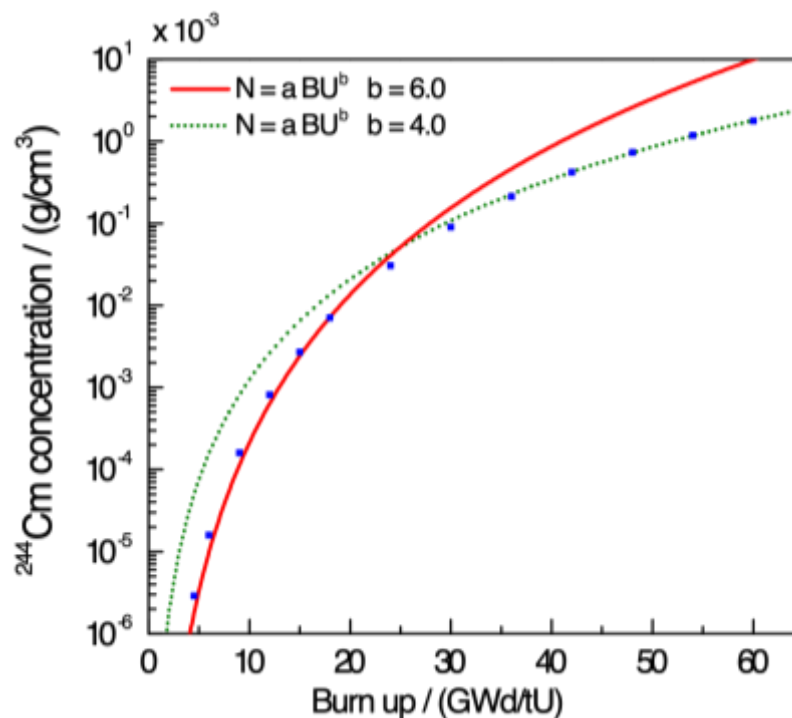


Figure 6 – Concentration of  $^{244}\text{Cm}$  as a function of burnup for a  $\text{UO}_2$  sample with initial enrichment of 4.8 wt.-% irradiated in a PWR to a burnup of 45 GWd/t

The potential to predict the output of the FORK detector by burnup codes is demonstrated in [Gauld, 2015; Gauld, 2006; Vaccaro, 2018] based on measurements of 15 PWR and 15 BWR assemblies as part of the SKB-50 exercise at CLAB. The experimental response is compared with the one obtained using the Integrated Review and Analysis Program (iRAP). This program, which is developed jointly by EURATOM and IAEA in collaboration with ORNL, is based on the ORIGEN module [Gauld, 2011] of SCALE [Bowman, 2011]. To account for the experimental details such as the absolute detection efficiency a normalisation was applied based on the average ratio between calculated and measured data [Vaccaro, 2018]. For PWR assemblies, the ratios of the observed and calculated neutron emission and  $\gamma$ -ray emission have a standard deviation of 4.6 % and 2.4 %, respectively. For BWR assemblies, the standard deviations for the neutron and  $\gamma$ -ray emission rates become 5.7 % and 5.2 %, respectively. The results in [Gauld, 2015; Gauld, 2006; Vaccaro, 2018] show the importance of accounting for neutron multiplication in the assembly and for the non-linear response of the ionisation chamber to the  $\gamma$ -ray intensity. The FORK detector is also suitable to determine the axial profile of the total neutron and  $\gamma$ -ray emission rate with limited special resolution. This provides additional information on burnup profiles.

Variants of the original LANL design are reported by [Lee, 2015; Tiitta, 2001]. The fission chambers in the system of Lee et al. [Lee, 2015] are replaced by  $^{10}\text{B}$  proportional counters. The use of  $^{10}\text{B}$  counters avoids logistic problems related to transport and use of fission chambers containing fissile material. However, due to their higher sensitivity to  $\gamma$ -rays, they require additional shielding against the  $\gamma$ -rays emitted by the spent fuel assembly. In the system proposed by [Tiitta, 2001], a CZT detector is included that offers the possibility to perform  $\gamma$ -ray spectroscopic analysis and separate the contribution due to  $^{134}\text{Cs}$ ,  $^{137}\text{Cs}$  and  $^{154}\text{Eu}$ . The Safeguards MOx PYthon (SMOPY) system was developed by the French Support Program to IAEA Safeguards. It includes fission chambers to determine the total neutron emission rate and a CZT detector to perform  $\gamma$ -ray spectroscopic measurements.

The added value of  $\gamma$ -ray spectroscopic data for a more quantitative assessment of the SNF is demonstrated in [Vaccaro, 2016; William, 2006a; William 2006b]. At CLAB a  $\gamma$ -ray spectroscopic scanning system using an HPGe detector is installed that measures the  $\gamma$ -ray spectrum from a SNF assembly with an axial resolution of about 15 mm. From these measurements, the total  $\gamma$ -ray emission rate of  $^{137}\text{Cs}$  together with the abundance ratios  $^{106}\text{Ru}/^{137}\text{Cs}$ ,  $^{134}\text{Cs}/^{137}\text{Cs}$ ,  $^{144}\text{Ce}/^{137}\text{Cs}$  and  $^{154}\text{Eu}/^{137}\text{Cs}$  were derived and combined with model calculations to provide information about the initial enrichment, burnup and cooling time [Vaccaro, 2016].

## Tomographic systems

A  $\gamma$ -ray emission tomographic system, referred to as Passive Gamma Emission Tomography (PGET), was developed by the IAEA for partial defect verification of spent fuel assemblies [Tobin, 2018]. The development started in the early nineties as part of the Finnish support programme to the IAEA [Lévy, 1993; Honkamaa, 2014]. It consists of an array of collimated CdTe  $\gamma$ -ray detectors and two neutron detectors, which are rotated in the horizontal plane. Measurements are performed with a spent fuel assembly placed in the centre of the toroidal shaped detector platform. The PGET system was used at spent fuel ponds in Finland and Sweden to verify VVER-440, BWR, and PWR spent fuel assemblies with burnups ranging from 5.7 GWd/t to 57.8 GWd/t and cooling times between 1.9 years and 26.6 years. These tests confirm that missing rods inside an assembly can be identified. The IAEA is studying new reconstruction processing techniques that should result in a more accurate localisation of missing rods and calculation of the relative  $\gamma$ -ray activities of individual rods.

With a tomographic device such as PGET, it is difficult to produce activity levels of specific radionuclides in individual rods due to the limited energy resolution of the  $\gamma$ -ray detectors. Using high-resolution Ge-detectors rod-wise activity distributions of specific radionuclides, i.e. actinides, fission and activation products, can be obtained. Such distributions can be used to study fuel properties, e.g. burnup and power profiles of individual rods [Svärd, 2005], fission gas release [Holcombe, 2016] and fuel behaviour under loss-of-coolant accident conditions [Andersson, 2016], from a measurement of an entire fuel

assembly. This avoids the need for dismantling the fuel to measure each rod separately. An example of such a tomographic system is described by [Holcombe, 2015]. This system was used to characterise an assembly consisting of rods that were irradiated at the Halden Boiling Water Reactor. The assembly contained four rods with a burnup of 26 GWd/t and five rods with a burnup of 50 GWd/t. The system of Holcombe et al. [Holcombe, 2015] is based on a single detector, which limits the spatial resolution due to time constraints. Using a segmented HPGe detector increases the efficiency such that a better spatial resolution can be reached in the same measurement time [Andersson, 2020].

### Advanced neutron based detection systems

The Next Generation Safeguards Initiative – Spent Fuel (NGSI-SF) established by the Department Of Energy (DOE) of the United States triggered the development and testing of new NDA techniques to characterise spent nuclear fuel assemblies [Tobin, 2009; Tobin 2011]. A total of 14 promising detection techniques, covering passive and active measurements including both  $\gamma$ -ray and neutron detection, were identified within NGSI-SF. A review of these systems is given in [Bolind, 2015]. A first assessment of the techniques was based on results of simulations using a spent nuclear fuel library which was established as part of the NGSI-SF [Trellue, 2013]. Three neutron-based detection systems, i.e. Partial DEfect Tester (PDET) [Ham, 2011; Henzl, 2013], Differential Die-Away (DDA) [Martinik, 2016; Henzl, 2013; Martinik, 2015] and Differential Die-away Self-Interrogation (DDSI) [Trahan, 2020; Menlove, 2009; Kapkhan, 2014], were constructed and used at the CLAB facility as part of the SKB-50 project [Tobin, 2016]. The performance of a Passive Neutron Albedo Reactivity (PNAR) system was tested at the Fugen power plant in Japan [Eigenbrodt, 2014, Eigenbrodt, 2016] and at the spent fuel interim storage facility at the Olkiluoto power plant in Finland [Tobin, 2019]. At present, the analysis procedures of these systems concentrate on nuclear safeguards applications. The main objective is the detection of partial defects (missing fuel rods) and the determination of the plutonium content. However, results from these measurements can be used to validate depletion calculations and are extremely important for defining procedures to verify and improve the fuel history of an assembly based on NDA measurements during industrial operation. This will require dedicated analysis methods.

PDET is a passive NDA device that relies on the detection of neutrons spontaneously emitted by a spent fuel assembly [Ham, 2011; Ham, 2015]. It is designed for the detection of missing fuel rods in an assembly. The present version has been prototyped for a PWR 17x17 spent fuel assemblies [Ham, 2011]. It consists of a set of fission chambers and ionisation chambers to measure the total neutron and  $\gamma$ -ray emission rate. The detectors are placed in a construction that can be inserted in the guide tubes of a PWR assembly that are used for the insertion of the control rods. Results of measurements at the CLAB facility in Sweden show that the instrument can be used to verify average burnup levels and to detect partial defects [Ham, 2015].

The PNAR concept was first proposed by [Lee, 1982] and demonstrated by measurements of fresh fuel by [Menlove, 1997]. It is a passive NDA technique that relies on the emission of neutrons spontaneously emitted by the assembly. The neutrons are measured in two configurations. One configuration is designed to enhance the multiplication of primary neutrons due to mainly spontaneous fission of  $^{244}\text{Cm}$ . In the second configuration this multiplication is suppressed. In other words, in one configuration the albedo is maximised while in the other it is minimised. The amount of fissile material present in the assembly is estimated from the ratio of the count rates obtained from measurements with the two configurations [Bolind, 2014]. Two prototype detection systems have been developed to test the PNAR concept. The first prototype was used for measurements of seven irradiated MOX assemblies at the Fugen power plant in Tsuruga, Japan [Eigenbrodt, 2014; Eigenbrodt, 2016]. The second was designed as part of an integrated system that includes a PGET device [Tobin, 2018; Tobin, 2018; Tobin, 2019; Tupasela, 2009; Tobin, 2018c]. This system is optimised for measurements of BWR fuel irradiated in the Olkiluoto power plant. Results of measurements on 23 BWR spent fuel assemblies are reported in [Tobin, 2019].

The DDA technique is an active NDA technique that uses a pulsed external neutron source that interrogates the assembly by neutron-induced fission. The prompt fission neutrons from the fission chain reactions initiated by the source neutrons are detected by a set of neutron detectors surrounding the assembly. DDA is a well-known technique that is used for characterisation of nuclear waste drums [Caldwell, 1985] and cargos [Jordan, 2008]. It mostly uses a D-T neutron generator producing a 14 MeV pulsed neutron source. The detected neutrons are registered as a function of the difference between the time of detection and of the creation of the neutron pulse. This distribution in time is analysed to determine the rate of fission events induced by thermal neutrons, which is proportional to the fissile content of the assembly. The results of an active measurement are combined with a passive measurement providing an estimate of the total number of neutrons spontaneously emitted by the assembly. The NGSF spent nuclear fuel library was used to simulate the response for PWR assemblies for a broad range of initial enrichments, burnups and cooling times [Henzl, 2013, Martinik, 2015]. The results of these studies confirm that DDA is a suitable instrument for verifying the fissile content of spent fuel assemblies with a limited number of calibration constants depending on the fuel history [Henzl, 2013]. A prototype DDA device was designed for measurements at the CLAB facility taking into account the requirements of the Swedish regulator and constraints given by the industrial environment of the facility [Martinik, 2016]. Experiments with this device have been finalised and the data analysis is in progress.

The DDSI technique is a passive NDA technique that uses the neutrons spontaneously emitted by the assembly as an internal interrogating neutron source [Menlove, 2009]. These neutrons are thermalised in the water of the storage pool and induce fission in the fissile material present in the assembly, which results in the emission of prompt fission neutrons. The neutrons emitted by the assembly are detected by an array of  $^3\text{He}$  proportional counters surrounding the assembly and the time correlation technique is applied to construct a Rossi- $\alpha$  distribution. The resulting time distribution consists of a sum of two main components which "die away" as a function of time. The two components have different time constants. This feature is used to separate the contribution of spontaneous fission neutrons and neutrons from neutron-induced fission. The former is related to the amount of  $^{244}\text{Cm}$  and the latter provide information about the fissile content in the assembly. The NGSF library was used in [Menlove, 2009] to simulate the response of a DDSI system for a variety of PWR assemblies. An analysis of these data reveals that the neutron multiplication, which is related to the fissile content in the assembly, can be derived from the observed Rossi- $\alpha$  distribution [Kaplan, 2014]. A system based on the design of [Kaplan, 2014] was constructed and used for measurements of 50 PWR and BWR spent fuel assemblies at the CLAB facility in Sweden [Trahan, 2020]. The results of this measurement campaign, which are reported in [Trahan, 2020], confirm that the DDSI instrument is an NDA instrument that meets the safeguards requirements for the characterisation of spent nuclear fuel assemblies.

The calorimeter installed at the CLAB facility [SKB, 2006] is at present one of the most valuable instruments for determining the thermal power of an entire fuel assembly. It is based on the design of the calorimeter that was constructed and tested by General Electric's Morris Operation [McKinnon, 1986]. Results of decay heat measurements of BWR assemblies with this calorimeter are reported Ref. [McKinnon, 1986]. The procedure applied at CLAB is similar to the one described in [McKinnon, 1986]. It relies on a measurement of the temperature increase as a function of time. The gradient of the temperature increase is translated into the thermal power produced by a fuel assembly through a calibration curve that is obtained from measurements with an electrical heater. Two corrections are required: a correction to account for the difference in heat capacity of the electrical heater and the fuel assembly and a correction to account for heat losses due to  $\gamma$ -rays that escape from the calorimeter. The CLAB calorimeter was used to determine the decay heat of 34 PWR and 22 BWR assemblies covering a burnup range of 14 – 51 GWd/t, cooling times between 12 years and 27 years and initial enrichments between 2.2 wt.-% and 3.4 wt.-%  $^{235}\text{U}$ . Details about the fuel design and composition and irradiation history are given in Refs. [SKB, 2006; Murphy, 2009]. The results of the measurements at CLAB are summarised in [SKB, 2006; Ilas, 2008; Ilas, 2014]. A blind test was organised by SKB Sweden to assess the quality of decay heat predictions by burnup codes. For these tests five 17x17 PWR

assemblies were measured. Details of the measurements are described in [Jansson, 2020]. The results of this blind test will be published once all the data has been processed.

The experiments at CLAB provide important benchmark data for decay heat calculations. Unfortunately, no detailed uncertainty evaluation has been carried out for the calorimeter at CLAB. A study to improve the analysis procedures together with a performance assessment and uncertainty evaluation has started as part of the EURAD project. The result of this study should make from the calorimeter at CLAB a reference instrument for decay heat measurements of spent fuel assemblies.

### 2.5.3. Verification of transport and storage casks

At present only Finland and Sweden have taken a final decision to open a deep underground geological repository for final disposal of spent fuel assemblies. Due to a lack of well-defined strategies by other countries, there is an accumulation of dry storage casks at temporary/interim storage facilities. Current safeguards approaches for dry storage casks rely heavily on containment and surveillance to maintain Continuity of Knowledge (CoK). However, failures of the seals cannot be excluded. The growing number of casks increases the probability of loss of CoK. A reverification of the contents by opening the cask is an extremely costly and time consuming procedure. Therefore, there is a strong interest in NDA techniques to verify casks. It is one of the top priority R&D needs of the [IAEA, 2018]. The minimum requirement is the possibility to detect the removal or missing of one Significant Quantity, which is approximately equivalent with one PWR and four BWR spent fuel assemblies.

Application of conventional NDA techniques based on the detection of radiation emitted by the spent fuel is not trivial, if not impossible, since the casks are designed to limit radiation exposure outside the cask. Nevertheless studies have been made to use the neutrons and  $\gamma$ -rays emitted by the fuel as fingerprints [Ziock, 2005; Peerani, 2007; Santi, 2010; Harkness, 2018; Ham, 2019]. Other complications are the neutron and  $\gamma$ -ray emission rates which change with cooling time and the background from neighboring casks. To account for the change in neutron emission characteristics, i.e. change in contributions of spontaneous fission and ( $\alpha$ ,n) neutrons, the use of a spectroscopic system is proposed [Harkness, 2018]. A fast neutron counting detection system with limited spatial resolution is proposed in [Ham, 2019]. All these methods suffer from the low intensity of the radiation escaping from the casks. [Peerani, 2007] concluded from simulation studies that it is not evident to detect the removal of a PWR assembly from a CASTOR V21/A based on neutron intensities outside the cask. Conventional neutron detection spectroscopy systems such as Bonner spheres remain useful instrumentations to monitor the neutron exposure of the personnel during transportation and storage of the casks [Rimpler, 2002].

The use of cosmic muons as an external source to verify the contents of spent fuel casks is very promising [Chatzidakis, 2016; Checchia, 2017; Kaiser, 2018; Poulson, 2018; Durham, 2018; Checchia, 2018; Ancius, 2019]. Cosmic muons can penetrate meters of dense material and therefore can be used to image the contents of spent fuel held in heavily-shielded containers. In addition, they are an external probe which do not suffer from background from other casks and do not require any prior knowledge. The use of muons to verify the contents of a cask is discussed in [Chatzidakis, 2016; Checchia, 2017; Poulson, 2018]. Most of these studies are based on results of Monte Carlo simulations. Experimental verification of the potential of imaging with muons are reported in Refs. [Durham, 2018; Checchia, 2018]. Further work to quantify the sensitivity of the technique to complicated diversion scenarios is still required.

## 2.6. Code validation

### 2.6.1. ALEPH2

ALEPH2 [Stankovskiy, 2012] has been validated using various sets of experimental data. The REBUS programme [Baeten, 2003] provides nuclide concentrations from a radiochemical analysis of samples from UO<sub>2</sub> spent fuel that was irradiated for four full cycles in a PWR nuclear power plant at

Neckarwestheim in Germany. The data were compared with predictions based on calculations with the previous version of ALEPH2 and the ORIGEN 2.2 and WIMS codes. The best results were obtained with ALEPH2. Nevertheless, an overall overestimation of fission product abundances was observed. This overestimation is most probably due to the limitations of the fission product yield data [Stankovskiy, 2010].

The nuclide inventories of two samples from a spent fuel rod which was irradiated in the Gösigen nuclear power plant in Switzerland were predicted using ALEPH2, MONTEBURNS and SCALE in [Massinon, 2018]. The results were compared with results of a destructive analysis carried out at the JRC-Karlsruhe and SCK•CEN. Calculations with ALEPH2 were repeated using different nuclear data libraries, i.e. ENDF/B-VII.1, JEFF-3.2 and JEFF-3.3T. The libraries used with MONTEBURNS and SCALE were JEFF-3.1 and ENDF/B-VII.1, respectively. The overall best agreement between calculated and measured inventory was obtained for the calculations with ALEPH2 using the JEFF-3.2 and ENDF/BVII.1 libraries.

The potential of ALEPH2 for prediction spent fuel decay heat was demonstrated in [Gérard, 2018] by the results of decay heat measurements of 25 PWR and 34 BWR spent fuel assemblies at CLAB [SKB, 2006]. ALEPH2 combined with the JEFF-3.2, JEFF-3.3, ENDF/B-VII.1 and ENDF/B-VIII.0 libraries was used to predict the decay heat. A clear distinction between the average ratio of calculated and experimental decay heat for BWR and PWR assemblies was observed. The calculated values obtained for the BWR assemblies are on average higher compared to experimental data, and for the PWR assemblies they are lower. This trend was observed for all nuclear data libraries and was confirmed by independent calculations using the TRITON and SAS2H modules of SCALE. It is not clear if this difference is due to a systematic effect of the experimental data or of the theoretical estimates.

A similar exercise was carried out in [Broustaut, 2012] based on the results of decay heat measurements for fast reactor spent fuel from the JOYO MK-II core experimental program [Maeda, 2004]. An ALEPH2 simplified model was used which was based on open data for the average neutron fluence rate and burnup. The experimental and theoretical estimated decay heat were compared as a function of cooling time for a period of about 800 days. The predicted and experimental value were normalised at the first measurement point (almost zero cooling time). Even after this normalisation the predicted values are on average about 4 % lower compared to the measured ones. This systematic difference was observed for the calculations using the JEFF-3.1.2 and ENDF/B-VII.1 libraries [Broustaut, 2012].

## 2.6.2.CASMO and SIMULATE

The code system consisting of CASMO and SIMULATE [Bahadir, 2009; Rhodes, 2006] is regularly used at PSI to support the Swiss safety authority ENSI for cycle reloading licenses [Rochman, 2019a; Rochman, 2019b]. Over the years, a large database of validated models for the five Swiss reactors has been developed [Ferroukhi, 2008], containing CASMO and SIMULATE models, and experimental data (in-core measurements such as boron concentrations and aerobic data) for various code versions. This represents a tremendous source of validation, spanning over hundreds of reactor cycles and many decades of operations, for both PWR and BWR. Such an automated and validated chain of calculations opens up the possibilities for core calculations with uncertainties due to nuclear data [Rochman, 2018b; Leray, 2017a] and transient calculations with uncertainties [Dokhane, 2018]. Additionally, it is relatively straightforward to extend such a validation chain for spent nuclear fuel calculations with the addition of the SNF code [Borresen, 2014]. With the validated chain CASMO-SIMULATE-SNF, the information (source term, decay heat...) for all Swiss spent fuel can be calculated at once (with uncertainties and biases due to code versions). With the addition of Monte Carlo calculations for canister criticality [Rochman, 2018a], the complete lifetime of spent fuel can be estimated, with information at the pin-by-pin and segment level. Such general and validated approach represents the state-of-the-art for the calculation of spent fuel source terms.

Additional validations of CASMO are routinely performed based on specific PIE samples from the Swiss nuclear power plants. As a detailed fuel history of the assemblies concerned is known (with surrounding

assemblies, and full 3D characteristics), such validations generally go beyond the traditional approach used to calculate PIE data such as from the SF-COMPO database. In the present case, the 13 samples from the LWR-PROTEUS programme, as well as a number of samples from the ARIANE and MALIBU programmes are used for validations, using the core simulator (SIMULATE), avoiding any normalisation to the sample burnup or specific burnup indicator (e.g.  $^{148}\text{Nd}$ ) [Rochman, 2020b]. A detailed validation exercise based on PIE data of samples from a rod irradiated to an average burnup of 70 GWd/t in a Spanish PWR reactor is reported in [Zwicky, 2010].

Finally, such extensive validations allow for application of the present approach to burnup credit calculations with a high degree of confidence. This is performed for the calculations of loading curves for the waste disposal canisters, together with the Swiss waste management organisation Nagra [Vasiliev, 2019; Herrero, 2017].

### 2.6.3.DRAGON

DRAGON has been widely employed both by academic institutions and research centres around the world. Due to the fact that DRAGON is able to solve the deterministic multi-group neutron transport equation both in 2D and 3D based in different Eulerian (i.e. collision probability, discrete ordinates) or Lagrangian (i.e. Method of characteristics) methods of solution, some validation test cases have been carried out. For example in [Donnelly, 2000] a code-to-code verification and an experimental validation for a 3D model of a CANDU device is reported. However, most of the validation cases have been carried out at the scale of a 2D lattice representation. Examples are presented in [Hong, 2002; Zain, 2018; Choi, 2018; Yaakoubi, 2019]). Some of them include new core CANDU designs for which DRAGON have already built-in modules for neutron transport studies. Others include PWR type of assemblies as part of a collaborative effort with CEA to test the APOLLO deterministic lattice code. The validation exercise included results obtained with MCNP calculations [Choi, 2018; Ortensi, 2010] and benchmark data of the International Handbook of Evaluated Criticality Safety Benchmark Experiments [Martin, 2011].

### 2.6.4.EVOLCODE

The EVOLCODE system has been used extensively at CIEMAT for the simulation of both current and advanced nuclear power plants. Given that in Spain only LWRs have been commissioned, CIEMAT has focused on validating EVOLCODE with published data from such reactors. This effort led to the validation of EVOLCODE [Álvarez-Velarde, 2014] with the Isotope Correlation Experiment (ICE) [Koch, 1981], now available at the SF-COMPO database as Obrigheim-1. This experiment was developed by a working group of the European Safeguards Research and Development Association (ESARDA) to check the feasibility of the isotopic correlation technique. The samples were irradiated to a burnup of about 30 GWd/t. The amount of some actinides and inventory ratios of fission products of irradiated samples were derived by radiochemical analysis at the reprocessing plant WAK at Karlsruhe. The agreement between experiment and theoretical estimate was very good for uranium and plutonium isotopes, with the exception of  $^{235}\text{U}$ ,  $^{236}\text{U}$  and  $^{238}\text{Pu}$ . The difference between the calculated and measured inventory was less than 3 %, which is smaller than the experimental uncertainties. The calculated fission product ratios were in good agreement with the experimental ones, in particular for the Kr, Xe, Nd and Cs isotopic ratios. A sensitivity/uncertainty method was developed to verify whether the differences between experimental and calculation data were compatible with the uncertainties in the nuclear data. This exercise showed that the uncertainty of the theoretical estimates due to reported uncertainties in cross-sections is in general smaller than the experimental uncertainty. For some nuclides such as  $^{239}\text{Pu}$  and  $^{240}\text{Pu}$ , the uncertainty due to the cross-section data is similar to or larger than the differences between experimental and simulated values. For  $^{235}\text{U}$ ,  $^{236}\text{U}$  and  $^{238}\text{Pu}$ , the differences between the results obtained with EVOLCODE and the experimental data cannot be explained by the experimental or nuclear data uncertainties.

### 2.6.5.SCALE

The SCALE code system has been extensively validated in Refs. [Gauld, 2016; Gauld, 2011a; Hu, 2017; Ilas, 2010; Ilas, 2012; Gauld, 2013; Ilas, 2008; Ilas, 2014; Gauld, 2010, Ilas, 2011; Smith, 2013]. Most of the calculation–experiment comparisons for decay heat and nuclide concentrations have been undertaken with samples from commercially irradiated nuclear fuel. In a few cases, single effect tests were used. For example, predicted total energy release rates following the fission of  $^{233}\text{U}$ ,  $^{235}\text{U}$ ,  $^{238}\text{U}$ ,  $^{239}\text{Pu}$ ,  $^{241}\text{Pu}$ , and  $^{232}\text{Th}$  during very short cooling times have been compared with results of SCALE in [Gauld, 2010].

Calorimetric measurements of at CLAB were used to validate the decay heat predictions of SCALE using the ENDF/B-VII.0 library [Ilas, 2008; Ilas, 2014; 247, Gauld, 2010]. A comparison of the calculated and measured decay heat shows in general a very good agreement. The average ratio between calculated and measured heat (C/E) is 1.002 for PWR and 0.997 for BWR assemblies, with a corresponding standard deviation of 1.2 % and 2.4 %, respectively [Ilas, 2014]. Considering that the main contribution is due to the decay of  $^{90}\text{Sr}/^{90}\text{Y}$  and  $^{137}\text{Cs}/^{137\text{m}}\text{Ba}$ , the average ratios will change by almost 2 % taking the latest JEFF-3.3 fission yield data. The results in [Ilas, 2014] favour the fission yields used in SCALE which are those adopted in ENDF/B-VIII.0. However, such a conclusion is not straightforward due to possible compensating effects resulting from biases in both the calculations and the experiment. Unfortunately, the uncertainties on nuclide inventories for  $^{90}\text{Sr}$  and  $^{137}\text{Cs}$  obtained from radiochemistry data are mostly larger than 2 % and cannot be used to clarify the situation. This confirms the need of a detailed performance assessment of the calorimeter.

For nuclide inventory validation, more than hundred PWR spent fuel samples were obtained from low-, moderate-, and high-burnup spent fuel assemblies from nine PWRs. Initial enrichments were in the range 2.5 – 4.6 wt.-%  $^{235}\text{U}$  and burnup values were between 7 – 70 GWd/t. Many of the experimental programs, such as ARIANE, MALIBU and REBUS, provided measurement data for up to 50 nuclides, including actinide and fission products mostly relevant to burnup credit. These data were used to validate SCALE. The C/E values show a high variance, with fluctuations as high as  $\pm 125\%$  and more around one. In particular, there can be large fluctuations between C/E values for samples with similar burnup, although no obvious dependence of the C/E bias with increasing burnup could be distinguished. Also, often error estimates from the different experimental programs vary widely even though irradiation conditions must have been very similar during irradiation.

Since samples were taken from commercially irradiated fuel, uncertainties from fuel production and irradiation boundary conditions have to be added on top of the microscopic data and model uncertainties. This makes it difficult to pinpoint the root source of the above-mentioned C/E fluctuations in the validation exercise. It underlines the need for high quality validation data if any improvement in the accuracy is desired: either performing single-effects tests or obtaining samples from a fuel assembly with very well-known irradiation history. While the average energy generation of a single fuel assembly during operation inside a reactor can usually be determined with an accuracy better than 5 %, there are higher uncertainties for pellet-sized samples due to: control rod movements, local void content, fuel assembly bow, axial power offset, fuel assembly neighbour neutron spectrum.

### 2.6.6.SERPENT

SERPENT is currently used in some 220 organisations around the world, and even though several users have performed verification and validation studies for their own purposes, only limited systematic V&V has been carried out by the code developers at VTT. Since SERPENT shares the cross-section library format with MCNP, the physics routines are regularly verified by comparison to reference MCNP5 or MCNP6 calculations. This type of calculation is run, for example, when new features are implemented or new cross-section data is produced using NJOY. This type of code-to-code comparison does not guarantee the accuracy of the results, but it does confirm that the interaction physics is handled properly.

Systematic validation has been carried out at VTT for criticality safety by running benchmarks in the International Handbook of Evaluated Criticality Safety Benchmark Experiments, but the cases have been limited to those relevant for Finnish power reactors (VVER, PWR, BWR). Other benchmark calculations include burnup credit,  $\gamma$ -ray shielding and kinetics.

In addition to the validation of the neutron transport part of the calculation, more efforts will be devoted in the future to burnup calculations. This includes both calculations run at VTT, as well as collecting data from the user community.

## 2.7. Summary and conclusions

The characterisation of spent fuel assemblies in view of transport, intermediate storage and final disposal was discussed. The main source terms of interest were identified. Due to the complex character of the source terms, a theoretical calculation of the inventory of key nuclides is required. The status of theoretical methods and codes to estimate the source terms including their uncertainties was reviewed. The review reveals that the methodologies are well established.

The main problem producing accurate source terms with reliable confidence limits is related to the input data, i.e. nuclear data and fuel irradiation history. To reduce bias effects and provide reliable covariance data, improved nuclear data are needed. This requires a dedicated evaluation programme based on sensitivity studies and dedicated experiments.

Most of code validation exercises rely on experimental data mainly resulting from destructive analysis of segments of samples reported in the SFCOMPO data based. They often result from dedicated international programmes. The SKB-50 campaign will provide additional data to validate theoretical calculations and verify declared uncertainty limits. Part of this campaign includes decay heat measurements of entire fuel assemblies using the calorimeter installed at the CLAB facility. Unfortunately, no detailed uncertainty evaluation for this measurement system exists. However, once the analysis procedures including the evaluation of the measurement uncertainty are reviewed these data can be used to assess the performance of codes for decay heat predictions.

Results of NDA measurements of fuel assemblies can be used to verify and improve fuel history parameters, e.g. burnup, initial enrichment and cooling time. Some of the neutron-based methods and techniques developed within the NGSF-SF are very promising. At present the analysis procedures are focused on nuclear safeguards applications. Improved analysis procedures tailored to the use of the data to improve the fuel history data should be developed. This can be realised using results of the SKB-50 campaign which includes measurements with the DDA and DDSI instruments.

## 3. Performance of spent nuclear fuel during pre-disposal activities and experimental characterisation

### 3.1. Introduction about spent nuclear fuel degradation

The main aim of this chapter is to report current progress regarding spent nuclear fuel (SNF) characterisation and its performance with respect to pre-disposal activities. In particular, the behaviour of irradiated cladding, the phenomena ruling the potential SNF degradation, the fuel/cladding chemical interaction (FCCI), and the ageing effect under conditions of extended interim storage, transport and emplacement in a final disposal system are considered through experimental as well as modelling studies. The chapter gives an overview of SNF experimental characterisation methodologies, from destructive assays to non-destructive assays.

As reported by the IAEA [IAEA, 2019a], the potential degradation mechanisms that may affect the cladding integrity of light water reactor (LWR) fuels during dry storage (and subsequent handling and transport operations) under normal operating conditions are:

1. Air oxidation
2. Thermal creep
3. Stress corrosion cracking (SCC)
4. Delayed hydride cracking (DHC)
5. Hydride reorientation
6. Hydrogen migration and redistribution

Other physico-chemical processes may occur during dry cask storage, such as self-radiation damage and He build-up (due to  $\alpha$  decay of the actinides). Both processes are temperature-dependent and lead to a volume expansion of the  $UO_2$  structure, in addition to the strain from pressure due to gas accumulation in the crystal structure [Ewing, 2015].

There is a broad spectrum of monitoring techniques for spent nuclear fuel [IAEA, 2019a], including basic visual inspections, portable gas analysers (for the presence of gaseous fission products), pressure monitoring of the seals and radiometric systems (gamma detector of the 514 keV  $^{85}Kr$   $\gamma$ -line, whose half-life is 10 years).

### 3.2. Key phenomena

The understanding of spent fuel performance during dry interim storage is indispensable both for the analysis of the failure probability and to characterise the state of the cladding, so that fuel management is conducted with accurate knowledge of the fuel conditions. The main interest is on cladding degradation mechanisms, as it is the first physical barrier between fission products and the environment. A brief description of the key phenomena governing the fuel rod state during dry storage is given here on the basis of the gap analysis carried out by Hanson [Hanson, 2012].

Key phenomena mainly related to the initial conditions of the dry-stored spent fuel are:

- **Hydrogen migration/precipitation:** Hydrogen picked up during irradiation is distributed heterogeneously throughout the zirconium alloy [Feria, 2018] and can precipitate in the form of hydrides according to solubility limits. For burnups greater than 45  $GWd/t_{HM}$ , the concentration of hydrides is much higher close to the cladding waterside; this brittle zone is called the hydride rim. The hydrogen present in the cladding may also affect creep behaviour (hardening or softening effect, depending on the state of hydrogen in the material [Suman, 2018]).
- **Hydride blister formation:** At some point during in-reactor operation, the zirconium oxide layer formed may spall and, as a consequence, a cold spot will form at the outer surface of the cladding. In this situation, the hydrogen will quickly migrate to this spot to form a zone with an extremely high

hydrogen concentration, known as a blister or lens. This brittle morphology may lead to local failure [Martin-Rengel, 2017].

- **Pellet-cladding bonding:** Higher burnup fuels have shown a trend to form tenacious layers between fuel pellets and cladding (bonding) that would condition fuel rod performance during dry storage [Lyon, 2018].

Key phenomena that may occur during dry storage are:

- **Creep:** The main contribution to cladding deformation in dry storage is thermal creep. It is considered self-limiting because hoop stress will decrease when creep occurs (stress relaxation due to creep out) and temperature decreases over time. However, even if it does not result in a cladding failure, the corresponding cladding thinning and the change in the pellet-cladding gap are important aspects for the cladding integrity during subsequent handling or transport. Attention should be paid to the following two aspects: very long-term effects from fuel swelling on local Pellet-Cladding Mechanical Interaction (PCMI) that could give rise to athermal creep, and the hardening effect during irradiation that could be annealed in dry storage and that, consequently, might enhance creep [Ito, 2004].
- **Hydride radial reorientation:** During the drying process in preparation for dry storage, hydrides may dissolve and, under high hoop stress, may reprecipitate in the radial direction as the cladding cools down. If there are sufficient radial hydrides, the cladding could become brittle at higher temperatures; in other words, at an earlier stage of the dry storage period [Billone, 2013b; Billone, 2019].
- **Delayed Hydride Cracking (DHC):** Under long-term dry storage conditions, the potential PCMI mentioned above may cause sufficient stress in the cladding to foster the diffusion of dissolved hydrogen to an incipient crack tip (flaw), followed by nucleation, growth, and fracture of the hydride at the crack tip. This is known as Delayed Hydride Cracking.
- **Oxidation of  $UO_2$ :** If the pellet is exposed to an oxidising environment during dry storage due to fuel management operation issues and an undetected defect in the cladding,  $UO_2$  oxidation can occur. The main concern is that if oxidation develops up to the formation of  $U_3O_8$ , the fuel will swell and can result in the propagation of the cladding defect due to PCMI enhancement [Hanson, 1998]. Additionally, fission gas release and fuel grain decohesion might be fostered. A number of major parameters affecting  $UO_2$  oxidation are detailed in Section 3.2.1.
- **$\alpha$  decay:** Another potential driver for the enhancement of cladding stress during long-term dry storage is the PCMI resulting from pellet swelling and gas content build-up due to  $\alpha$  decay. Additionally, precipitation of helium bubbles at grain boundaries could eventually result in the decohesion of the grains and a reduction of the mechanical strength [Rondinella, 2011].

### 3.2.1. $UO_2$ oxidation

Temperature and oxygen partial pressure are the major quantifiable variables that promote the oxidation of the nuclear fuel matrix [Olsen, 2018; Herranz, 2009; McEachern, 1998; IAEA, 2019a] with time [Olsen, 2018; McEachern, 1998; Anderson, 1955a; Anderson, 1955b; Bae, 1994; Leinders, 2016b; Leinders, 2016a; Hoekstra, 1961; Taylor, 1980; Elorrieta, 2018a]. From a safety perspective, the loss of inert conditions due to the replacement of the inert cover gas with air should be considered as a potential scenario during dry storage [IAEA, 2019a]. Moreover, morphometric properties such as the physical form (powders, fragments or pellets) and the grain size have an effect on the rates of oxidation [Herranz, 2009; McEachern, 1998; Anderson, 1955b; Gómez, 2008; Leinders, 2016c; Bannister, 1968; Martin, 1948; Iglesias, 2008; Wood, 1986]. Water in a dry storage container can be found as either bound water (chemically or physically absorbed) or free water (physically trapped or simply unbound) [Patterson, 2015]. Moisture is regarded as a technical issue of concern by several countries in their gap-assessment procedures [Patterson, 2015], as it can lead to Zircaloy cladding

corrosion [IAEA, 2019a; Smith, 2011; Jung, 2013] and UO<sub>2</sub> oxidation [Massih, 2018; Olander, 1999; NSFPOISG, 2006; Espriu-Gascon, 2015].

On the other hand, fuel burnup [McEachern, 1998; IAEA, 2019b; Cobos, 1998; NRC, 2019] and composition have been pointed out to delay fuel matrix oxidation [McEachern, 1998; Massih, 2018; Olander, 1976; Thomas, 1993; Wilson, 1961; Kim, 2001; Hanson, 2003; You, 2000; Elorrieta, 2016; Elorrieta, 2018b; Choi, 1996; Park, 1992; Fujino, 1992; Kim, 1995; Kvashnina, 2013; Kleykamp, 1979; Eloirdi, 2018; Norris, 1983; Suresh, 2004; Talip, 2018; Elorrieta, 2017]. Fission reactions during reactor operation produce oxygen and other elements: some of them (i.e. metallic FPs: Y, Zr, Nb, lanthanides and actinides) can react with oxygen to form oxides [Massih, 2018]. The excess oxygen dissolves in the fuel matrix, thus oxidising uranium. At first, the net effect of burnup is to generate more hyperstoichiometric UO<sub>2</sub> fuel than fresh UO<sub>2</sub> and to increase the oxygen potential of the fuel [Massih, 2018; Olander, 1976]. In general, for doped UO<sub>2</sub>, the kinetic stability of the cubic U<sub>4</sub>O<sub>9+y</sub> fluorite type structure is then enhanced with respect to U<sub>3</sub>O<sub>8</sub> formation [McEachern, 1998] for longer time periods than the undoped UO<sub>2</sub> material [Thomas, 1993].

Other source of impact on fuel matrix oxidation is the aging process, which consists of the alteration of the fuel due to the effect of long-term ambient-air storage. Early studies on unirradiated UO<sub>2</sub> pellets, as the one performed by [Campbell et al., 1989], have proved that for storage periods up to two years and temperatures of 250°C, the oxidation kinetics experiment significant changes. However, an increasing of the aging time delays both, the weight gain and the oxidation rate, hindering the solid sample spallation and pulverization and, in a later stage, the oxidation reaction. It is suggested that these slower rates could be due to the formation of a thin oxidized layer in the sample surface, identified by XPS, that prevents oxygen diffusion inside the pellet. This layer has been also observed on aged CANDU fuel at 150°C (burnup in the range of 7...10 MWd/kg U) [Wasywich et al, 1993].

The intrinsic difficulties associated to get empirical data on long-term aged fuels led [Wiss et al. 2014] to use artificially accelerated aged-materials. They analyzed a set of alpha-doped UO<sub>2</sub> pellets, simulating alpha doses in real spent fuel. With this purpose, they varied the Pu concentration to simulate samples aged from 5 to 30 years, and then, characterized the materials by XRD, thermal desorption spectroscopy and electron microscopy. From their results, a similar behavior on delaying oxidation of aged fuel would be expected. However, it is necessary to broaden the data set in order to extend the conclusions to different scenarios. More studies about ageing effect on oxidation behavior are needed to confirm the aforementioned layer hypothesis.

In summary, irradiated fuel undergoes a series of dynamic physico-chemical changes directly influenced by the irradiation history, including irradiation cycles, power history and burnup. The specific features of SNF (inventory, HBS, distribution of fission gas, heat content and state of the protective cladding) will determine its behavior in case of an incidental event or during predisposal/disposal activities. A detailed picture of the above-mentioned parameters on oxidation behavior is not completely drawn.

### 3.2.2. Pellet-Cladding Interaction

Pellet-Cladding Interaction (PCI) should be considered as a mid-priority process in the investigation of the safety approach for water reactor fuel due to the possibility of cladding failure during a power transient. Cladding integrity (as the first FP containment barrier) must be ensured in all operating conditions.

Pellet-Cladding Interaction and Stress Corrosion Cracking (PCI-SCC) remain one of the causes identified as leading to potential fuel failure. The occurrence of PCI-SCC may be reduced by NPP operators placing restrictions on power variations and by using advanced fuels with increasing resistance to PCI-SCC. The fuels are commonly termed "Accident Tolerant Fuels" (ATF), which consist of UO<sub>2</sub> with additives (Cr, Al, Si and Zr). Another option widely used is the use of a cladding inner liner [NEA, 2018].

Irradiation induces fuel densification, with density increasing from the theoretical density of UO<sub>2</sub> pellets of ~ 95 % (3 – 5 % porosity) to a range of 97 – 98 %. Densification (pellet shrinkage) occurs as a consequence of porosity removal and affects the gap size. According to the literature, the amount of densification depends on burnup, initial density, pore size distribution, grain size, temperature and oxygen-to-metal ratio. Due to the thermal gradient (stress), the pellet transitions to an "hourglass shape" [CEA, 2009], which causes irreversible deformation to the cladding (Figure 7). Pellet-cladding contact takes place because of a decrease in the cladding diameter (creep-down due to pressure from the coolant) and an increase in the pellet diameter (thermal expansion and swelling due to the inclusion of solid FP in the matrix and inter- and intra-granular accumulation of fission gas in pores).

Contact first occurs at the inter-pellet spaces while a continuing rearrangement of pellet fragments takes place simultaneously [CEA, 2009]. Thus, due to pellet swelling, the cladding is subjected to tensile fields, and modifies the diametrical strain via irradiation deformation (creep). The probability of cladding damage is extremely low as the equilibrium hoop stress inside the cladding is lower (< 100 MPa) than the creep rupture strength (> 600 MPa) [CEA, 2009]. In the case of an incident (power increase), the temperature at the pellet centre can increase abruptly, leading to exacerbated hourglassing and/or release of volatile FPs such as iodine (prone to attack the cladding). Cladding rupture, resulting from excessive thermal creep deformation, could likely end in a "pinhole" (or tight crack) rupture, given the loss of the driving force (i.e. rod internal pressure) upon depressurisation together with the very low mechanical energy stored in a fuel rod. Under these potential circumstances, a process of stress corrosion cracking (SCC) is likely to be triggered on the inner surface of the cladding. This may initiate a radial crack and lead to mechanical failure. The edge crack results in a loss of rod tightness, with a potential risk of release of volatile FPs.

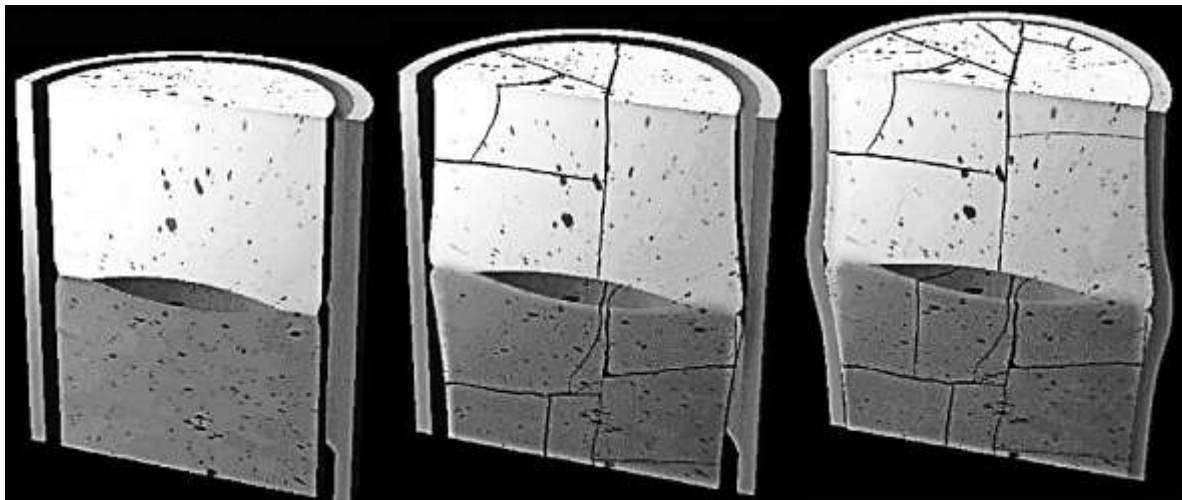


*Figure 7 – Schematic representation of pellet cracking, evolution of the "hourglass" shape, and pellet-cladding gap during operation*

*Figure reproduced from [CEA, 2009]*

The low temperatures presumed in dry storage, especially at extended times, should not promote the FGR. As SNF temperature decreases with time, the driving forces for PCI failure (rod internal pressure and tensile stress) will decrease or, at least, would be expected to be small.

The assessment on the long-term corrosion behavior of SNF and the impact of storage and disposal of radioactive waste should meet safety criteria. However, the lack of an adequate experimental database for SNF oxidation, especially long-term evaluations, due to problems in the handling of irradiated fuel, have led to study some corrosion scenarios by analyzing SNF analogues, i.e. unirradiated materials. A systematic approach to compare surrogates and irradiated fuel behavior still remains as an uncertainty

in some cases. An assessment of the anticipated phenomenon of PCI consequences is essential and requires more studies, especially those that relate to the inner tensile fields, hydride reorientation and creep rupture of the cladding, important to mitigate the effects of the release of volatile FPs or exposition of fuel matrix to an oxidizing ambient.

### 3.3. Experimental characterisation

#### 3.3.1. Radiochemical and chemical analysis of irradiated fuel rod components

The radionuclide inventory present in the components of irradiated fuel rods (spent nuclear fuel, cladding, and structural components) is determined by means of radiochemical and chemical analyses after digestion of the respective samples. Both acid digestion and digestion in alkaline media are applied to completely dissolve the samples. Radionuclides present in the digestion liquor (e.g. actinides, lanthanides, and sparingly soluble fission and activation products) or in gaseous samples (e.g. volatile fission and activation products, fission gases or gaseous radionuclide reaction products such as  $^{14}\text{CO}_2$ ) are measured consecutively after various chemical separation methods.

Concentrations of radionuclides present in the aqueous or gaseous phases are measured by various analytical techniques. Currently, new analytical techniques are being developed for radionuclides that are difficult to measure such as  $^{14}\text{C}$ ,  $^{129}\text{I}$  or  $^{36}\text{Cl}$  present in highly active samples.  $\alpha$ -spectroscopy is applied to quantify  $^{235,238}\text{U}$ ,  $^{237}\text{Np}$ ,  $^{238,239,240,242}\text{Pu}$ ,  $^{241,243}\text{Am}$ , and  $^{243,244}\text{Cm}$  present in aqueous samples. Usually, Pu isotopes are measured after separation from other  $\alpha$ -emitting radionuclides. Fission products and minor actinides with characteristic  $\gamma$ -rays, e.g.  $^{134,137}\text{Cs}$ ,  $^{129}\text{I}$ ,  $^{241,243}\text{Am}$ ,  $^{154}\text{Eu}$ , and  $^{125}\text{Sb}$ , are quantified in digestion liquors using  $\gamma$ -spectroscopy. Minor actinides, activation and fission products such as  $^{14}\text{C}$ ,  $^{55}\text{Fe}$ ,  $^{36}\text{Cl}$ , and  $^{241}\text{Pu}$  are measured in the digestion liquor or gas phase after separation from other radionuclides, using liquid scintillation counting. In addition, isotopes such as  $^{99}\text{Tc}$ ,  $^{233,234,235,236,238}\text{U}$ ,  $^{237}\text{Np}$ ,  $^{239,240,241,242}\text{Pu}$ ,  $^{241,243}\text{Am}$ , and  $^{244,245,246,248}\text{Cm}$  present in digestion liquors can be quantified using high-resolution mass spectrometry (inductively coupled plasma – sector field – mass spectrometry, ICP-SF-MS). Gas phase composition and the concentration of fission gases Kr and Xe released during the digestion of irradiated fuel rod components into the gas phase can be analysed by means of a multipurpose mass spectrometer with a customised gas inlet system.

The experimental uncertainty of the above-mentioned analytical methods is, in most cases, less than 5 %. In accordance with section 2.5.1., the used experimental techniques are suitable for determining the inventory of the mentioned radionuclides. See also [NEA, 2011] and [Hu, 2017] for state-of-the-art measuring techniques of specific radionuclides and the uncertainties associated with these measurements. It should be emphasized, that this is only the experimental uncertainty related to the measurement of the specific radionuclides and should not be mixed up with theoretical uncertainties based on models. Later, the experimental and theoretical data will be compared to each other with its own uncertainty.

#### 3.3.2. Fuel-cladding chemical interaction analysis

During irradiation in a nuclear reactor, the cladding is affected both by interactions with the cooling water, causing some oxidation of the outer cladding surface and hydride precipitation within the Zr alloy, and by corrosion from volatile fission products (e.g. iodine compounds) at the fuel/cladding interface. These chemical reactions lead to embrittlement and weakening of the mechanical properties of the cladding.

Current experimental studies focus on the chemical interactions between Zircaloy and precipitates of volatile fission products at the plenum of an irradiated fuel rod, a location where pellet-cladding interactions cannot occur. Samples of fuel/cladding interfaces and samples from rod plenum sections were taken from fuel rod segments irradiated in pressurised water reactors. The composition of agglomerates found on the inner surface of the plenum cladding and in fuel-cladding interaction layers

were analysed by means of scanning electron microscopy and spectroscopic methods, such as X-ray photoelectron spectroscopy and synchrotron radiation-based techniques.

Preliminary investigations of the plenum cladding inner surfaces show precipitates containing Rb in addition to Zr, Ba, Cs, and U. The analysis of fuel-cladding interaction layers of the UO<sub>2</sub> and MOX fuels show the presence of Cs-U-O-Zr-Cl-bearing compounds in these layers, in addition to Te, Ba and U. So far, no Rb was found in the fuel-cladding interaction layers.

### 3.3.3. Thermo-mechanical creep test

Thermo-mechanical creep is the progressive deformation of a material under stresses lower than the yield stress. Creep occurs in three stages (Figure 8). The primary stage shows rapid deformation and a decrease in the creep rate over time, the secondary stage has a constant creep rate and the tertiary stage has a rapidly increasing creep rate over time until fracture occurs. The creep behaviour of unirradiated cladding may be a function of many material parameters including chemical composition, metallurgical structure, and processing conditions. For irradiated cladding, the radiation effects overshadow these fabrication and chemical effects as, during irradiation, the anisotropy disappears and the material texture becomes homogeneous [Nakatsuka, 1987]. The irradiation-assisted creep in the reactor is an order of magnitude greater than thermo-mechanical creep. Most codes calculate the two modes of creep separately [Martin, 2007]. In spent fuel, the irradiation becomes negligible, but the thermo-mechanical creep of the irradiated material continues.

The two principal physical factors affecting the creep behaviour of the cladding in interim storage are the hoop stress and the temperature. The hoop stress results from the rod internal pressure, a combination of the original fill gas and the fission gas released during operation, and the temperature results from the decay heat of the fuel assemblies [ASTM1562, 2010]. The creep strain rate and the strain upon failure of the spent nuclear fuel cladding are affected by material parameters such as alloy composition, fabrication steps (for example, cold work, solution annealing, recrystallisation annealing), and radiation fluence [ASTM1562, 2010].

The spent fuel, which has undergone some corrosion during operation, may contain some dissolved hydrogen or precipitated hydrides. It is important to quantify the effect of the hydrogen content on the creep properties. Previous studies [Kamimura, 2003; Kamimura, 2004] have shown that hydrogen does not have the same effect on BWR and PWR cladding. As hydrogen concentration above the solid solubility limit under high stress tends to suppress creep of BWR cladding, while a hydrogen concentration below the solubility limit under high stress tends to accelerate creep. For PWR cladding, while no creep-accelerating effect has been observed for hydrogen concentrations below the solid solubility limit, the remarkable creep-suppressing effect has been observed with hydrogen concentrations above the solid solubility limit. Irradiated materials have shown some creep-suppressing effects compared to unirradiated material, but the degree of suppression depends on temperature and stress conditions.

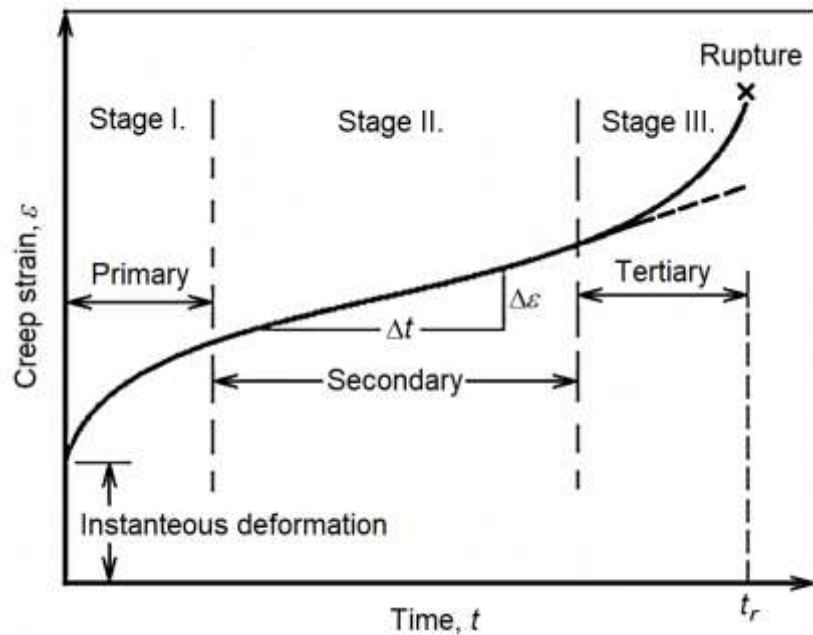


Figure 8 – The three stages of creep

[Faridani, 2011]

For creep test sample preparation, hydrogen gas is dissolved in cladding samples in a vacuum furnace. The absorbed hydrogen content can be verified by observing a pressure decrease in the furnace or by a mass increase of the sample, and the distribution of hydrogen can be measured by neutron-induced prompt gamma-ray spectroscopy. At the end of the measurement, destructive analysis can also be performed by hot extraction. Before (on a parallel sample) and after the creep test, the structure and orientation of the hydrides can be inspected using metallography. As the heat treatment during sample preparation may also have an effect, a heat-treated control sample (subjected to the same preparation process, but in a pure Ar atmosphere) should also be measured.

The samples are mechanically loaded in a furnace. One method is to pressurise the samples through steel pipes and capillaries connected by hydraulic fittings. The samples are periodically removed from the furnace, and the outer diameter is scanned (e.g. by laser micrometer) at a given azimuthal orientation; this requires high-precision measurement. The measurements should include the heat-treated and hydrogenated samples as well as the non-pressurised samples and as-received (untreated) samples to quantify the diameter change due to oxidation by air or water vapour entering the furnace.

### 3.3.4. Mandrel ductility test

During normal reactor operation, the gap between the fuel pellet and the cladding tube closes, and in the case of an incident or a sudden increase in power, the thermal expansion of the pellet could rupture the cladding wall. Another case of volumetric expansion of the pellet is due to air ingress during the high-temperature phase of dry storage, as higher uranium oxides have a lower density; this could also result in cladding rupture. The ductility of the cladding is an important parameter under both transport and storage conditions.

Historically, pellet-cladding mechanical interaction (PCMI) tests were often conducted using multi-element tools to determine the plasticity limits of fuel cladding tubes or rings. These tearing tools are referred to as segmented expanding mandrels. Their role is to distribute the radial load evenly along the perimeter of the tubes. The advantage of the test is that it is relatively easy to perform and does not require lengthy preparation and irradiation to obtain a properly fragmented pellet and cladding. The initial heat treatment, corrosion, amount of hydrogen and iodine absorbed by the specimens can be controlled

and the specimen can be inactive or irradiated. These tests can be performed both at room temperature and near the operating temperature (350 °C).

The design of the mandrel tools and the measuring arrangement may differ. In the simplest case, 4-12 mandrels can be used for the tests, with more segments providing a more even stress distribution. Their number is limited only by their manufacturability. Because they have to fit in a cladding tube, the mandrels are quite small and have low manufacturing tolerances. The tool material may be steel or hard ceramic (such as tungsten carbide) and may come into direct or indirect contact with the cladding samples. To simulate the fragmentation of the fuel pellets, an aluminium-oxide ceramic ring may be placed between the mandrels and the sample. The sample breaks at several points during the test, resulting in a stress concentration on the cladding wall that may induce cracks. If the mandrel is also made of alumina, it may also crack and break during measurement, meaning that new mandrels are required for each measurement.

There are several methods for generating radial stress. In one case, a soft metal cylinder (zirconium or aluminium) is pressed inside the cladding [Nobrega, 1985; Foster, 1987; Jiang, 2014] and deformed to increase its diameter, thereby transferring radial load. Alternatively [Nilsson, 2011; Catherine, 2006], a cone or spike is pressed into the center of the tool. The main disadvantage of this method is that the tool design is much more complicated. The advantage is that the cone or spike is not deformed, i.e. the measured force depends only on the bank angle of the cone and the friction between the cone and the mandrels, so that the radial force applied to the sample can be more precisely determined.

Standard mandrel experiments are usually carried out until failure occurs. An important parameter can be the rate of deformation. In the case of soft metal cylinder compression, the compression is very slow, typically 0.01 mm/min, which is significantly lower than the tensile rate of 5-50 mm/min commonly used in tangential tensile tests. The slow loading, especially the so-called "ramp-and-hold" (sustained load over a longer period of time) can more effectively investigate crack propagation. The higher stretch speed (above 10 %/h) simulates the cladding elongation during a power increase due to thermal expansion caused by the temperature increase. Lower (below 0.5 %/h) speed simulates the subsequent prolonged swelling of the fuel pellet due to slow swelling and increased internal pressure. In the case of RIA or sudden power increase, the deformation may be orders of magnitude faster.

The mandrel experiment conducted by the OECD/NEA-coordinated Studsvik Cladding Integrity Project (SCIP III phase [SCIP]) differs slightly from the measurement methods described above. While those aim to distribute the peripheral load as evenly as possible, in SCIP the effect of the slowly expanding pellet on fuel corrosion is investigated, especially the stress-corrosion effect of the iodine and the mechanisms [Nagai, 1983]. The SCIP mandrel test can be used to investigate the effects of the aggressive chemical environment of the fission products, the temperature, elongation rate, local stresses in the cladding, different pellet cracks or missing pellet surfaces, changing one parameter while all other parameters are kept constant. So far, experiments have been conducted with western-type cladding, typically with a burnup of 50 – 70 GWd/t<sub>HM</sub>, in PWR (Zry-4) and BWR (Zry-2) environments.

Based on data obtained from finite element analysis of the SCIP mandrel experiments, there is a clear difference between the previous studies listed above and those carried out under SCIP III [Dostal, 2015]. In these tests, the tension is concentrated at the rim of the ceramic ring as the piston and mandrels press the ceramic at an angle, causing uneven loads at the cladding tube wall. In modelling mandrel experiments and ramp tests, the comparable tensile stresses in the inner wall of the cladding were calculated. The failure time for ramp tests was typically about 10–20 minutes, whereas it was somewhat longer for mandrel tests. Based on the results obtained, mandrel experiments were found to be suitable for reproducing and simulating some previous tests and for evaluating the resistance of the cladding to PCI failure.



Figure 9 – The mandrel test performed with a ductile (left) and a brittle sample (right)

Courtesy of MTA-EK

The mandrel test setup at MTA-EK can simulate the pellet-cladding mechanical interaction by expanding segmented dies (mandrels) inside cladding samples (Figure 9). This setup represents the actual mechanical conditions of the cladding better than the ring compression tests that are widely used to investigate cladding ductility. The mandrels are driven apart by a pyramidal taper connected to the crosshead of a universal testing machine, and the force is measured under the mandrels. The friction coefficient between the mandrels, and the base plate they move on is kept constant by applying graphite-based high-temperature-bearing grease. The temperature can also be varied up to 300 °C using a small furnace around the mandrels. The results of the tests define the maximum force, the force-displacement curve integral, the maximum diameter reached and the mode of failure (shape of fracture and crack propagation). These all give important information about the ductility of the sample. The effect of treatments such as hydrogenation and high-temperature heat treatment on the ductility of the cladding can also be investigated. These mandrel tests are performed on unirradiated cladding, but the technique is applicable for hot cells in a destructive analysis of defueled cladding samples. The comparison between irradiated and unirradiated cladding must be made as there are significant differences in the state of the material (e.g. irradiation hardening).

### 3.3.5. Three-point bending and impact tests

Several attempts, mostly consisting of modelling approaches and rather limited experimental studies, have been conducted by the international research community to enrich the knowledge of the underpinning mechanisms affecting the mechanical properties of SNF rods. The majority of the experimental studies focus on irradiated cladding properties by performing tests on defueled cladding ring specimens (i.e. ring compression tests). However, results from experiments on the composite fuel-cladding configuration, i.e. real SNF rods, are extremely rare. Direct tests on irradiated fuel rods require technologically sophisticated facilities and apparatus (hot cells, specific remotely-operated equipment, etc.), significantly sized highly radioactive samples, produce a lot of spent fuel waste and are therefore quite expensive and technically difficult to perform.

At JRC – Karlsruhe, a simple free-falling hammer device inducing fuel rupture events was developed and installed in a hot cell in 2008. The impact tests were performed on irradiated commercial LWR UO<sub>2</sub> fuel segments with burnups between ~ 19 and ~ 74 GWd/t<sub>HM</sub>. Although the rigidly fixed SNF rod specimens ruptured at three points, 3.9–5.6 g coarse fuel fragments were released in total, i.e. 1.3 – 1.9 g per breakage. Details of these pilot tests can be found as part of the IAEA Coordinated Research Project SPAR III [IAEA, 2015], as well as in [Papaioannou, 2009b; Papaioannou, 2009c; Dallongeville, 2010].

The results of bending tests, using fresh and spent fuel rods with an average burnup of 50 GWd/t<sub>HM</sub>, were presented in 2010 [Dallongeville, 2010]. The objective of the joint project was to assess the response of LWR fuel assemblies (FA) during the 9-m drop test as specified in the IAEA transport regulations. The bending test span corresponded to roughly the fuel pin inter-grid distance. Fuel rod failures were observed at about 35 mm net lateral deflection. Ring compression tests or, as the authors called them, hull-lateral compaction tests, were also performed for modelling purposes.

In 2016, a new experimental campaign was initiated at JRC – Karlsruhe to establish a basis for reference data and provide reliable conclusions by performing tests on SNF rod segments with specially developed equipment. The equipment is described in [Vlassopoulos, 2018b] and includes the capability to undertake 3-point bending and gravitational impact tests on fuelled, pressurised SNF rod segments. The new campaign aims to determine the fuel rod response to external loads until failure. Segments with different properties (burnup, fuel composition, history, cladding, etc.) are pressurised to the original rod pressure and subjected to quasi-static bending or dynamic (impact) mechanical loading experiments, determining the critical fracture load (or energy) and the fuel mass released. A thorough characterisation of the fuel rod and concomitant specimens is carried out before and after each experiment for a comprehensive evaluation of the SNF rod behaviour.

The force (or energy) required for a fuel rod to fail is determined under the experimental boundary conditions. As the accident scenarios are limitless, it has been decided to study the SNF mechanical integrity under two reference conditions by applying quasi-static or dynamic loads. The acquired data are correlated to properties and processes that potentially affect the SNF mechanical stability. In addition to post-irradiation examinations performed on the fuel rod at previous stages (including many non- or destructive hot cell techniques), the fuel and cladding of the tested specimen are extensively examined after the experiment. Metallography of the failure location is undertaken to investigate the hydride morphologies, population and orientation, while the local H<sub>2</sub> content is determined by means of the hot-gas extraction method. After dynamic impact, the released fuel particles are observed by scanning electron microscopy (SEM), and corresponding size distributions are determined by image analysis.

The employed experimental setups are shown schematically in Figure 10. The 3-point bending apparatus consists of a force transmitter fixed on a loading column, which is driven perpendicular to the sample axis by a step-motor at a constant slow speed between 4 and 17 μm/s. The force transmitter, termed "deflector", has a concave, round contact surface (see details in the insert scheme in Figure 10a) adjusted to the cladding shape, so that no other side- or edge-load is applied on the fuel rod segment during the experiment. The flexible modular design of the device allows the use of different loading transmitters, or, due to removable supports, different specimen lengths. The geometrical configuration of the device follows the prerequisites of a standard bending test as specified in the ISO standard 7438 [ISO7438, 2016]. The device is equipped with sensors for simultaneous acquisition of the applied load and the sample deflection and internal pressure of the segment. The raw data are in the form of load-displacement curves. The loads are used to evaluate the stresses in the sample. The uncertainty associated with the reported flexural strength is derived based on the method described in [Vlassopoulos, 2018a].

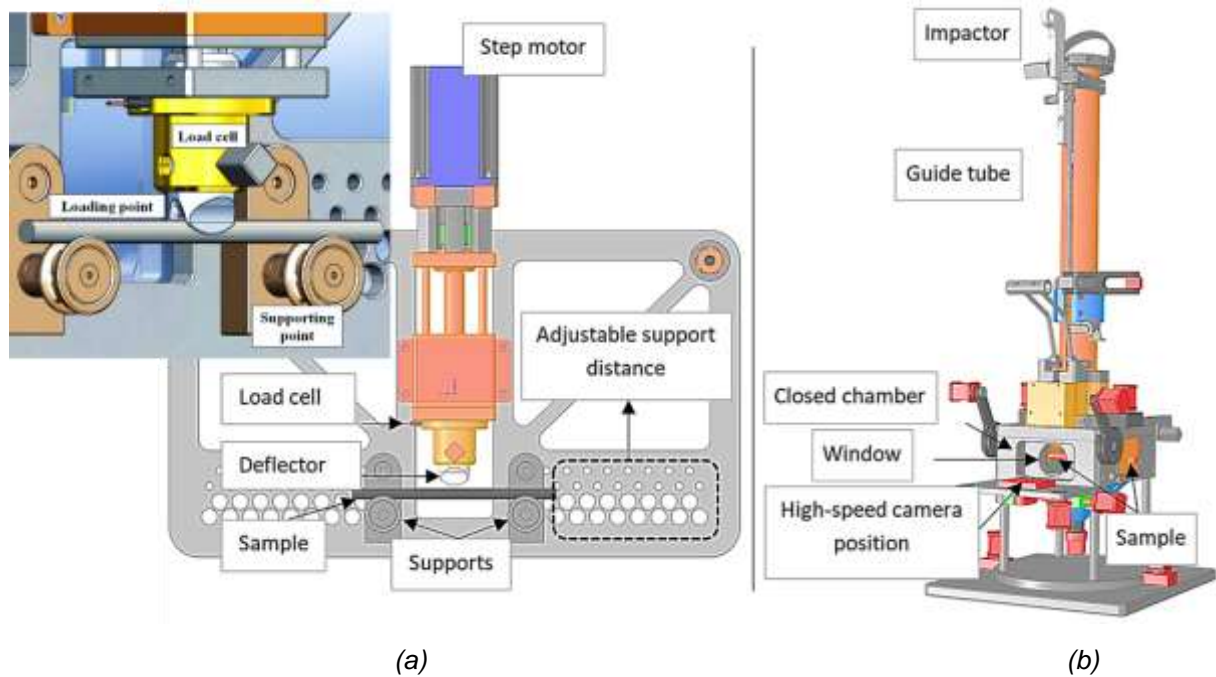


Figure 10 – Overview of the 3-point bending apparatus (a) and impact tower (b)

The new apparatus for impact tests, shown in Figure 10b, is based on the same principles as the older one used to perform the experiments reported in [Papaioannou, 2009b; Papaioannou, 2009c]. The specimen is impacted by a falling body (hammer), or 'impactor', through a vertical guiding column. The impacting occurs in a closed chamber, where the released material (mainly fuel with some pieces of the outer-cladding oxide layer) is completely captured. The coarse fragments are collected at the bottom due to the funnel shape of the chamber interior, whereas the fine aerosol particles settle on the internal walls or are caught in the particulate filter of an integrated aspiration system. The impact of the specimen is video-recorded by a high-speed digital camera (2000 frames/s) placed on the window of the chamber and provided with its own illumination.

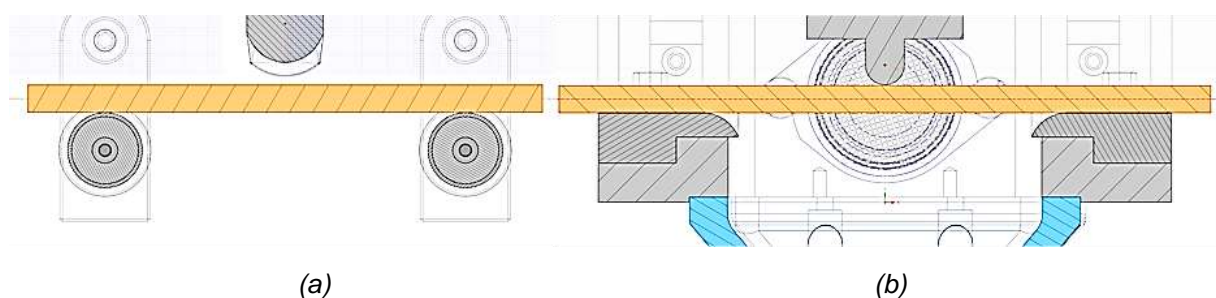


Figure 11 – Scheme of the specimen positioning in the bending (a) and impact (b) device

Rounded supports of the same radius and the same specimen lengths are used for both experiments.

As far as possible, the design of the two devices is mutually consistent. In both experiments, the specimens are bent or impacted by rounded compactors, as shown in Figure 11. The main difference between the two experiments is related to the velocity of the impactor and the bending deflector, enabling a direct comparison of the results in both configurations. The velocity of the falling hammer at point of impact is 3.5 m/s, i.e. at least  $2 \times 10^6$  times faster than in the 3-point bending test.

A typical specimen for mechanical testing is presented in Figure 12. Using exact tube fittings to preserve the required tightness, 25 to 27-cm-long segments cut from SNF rods are connected to a helium gas flask, pressurised to the desired pressure and disconnected after closing the attached gas valve. A pressure transducer, fixed on the other end of the segment, provides continuous pressure control and instant detection of the rupture/crack, which is very important for the bending tests.



Figure 12 – A gastight specimen assembly connected to the pressure gauge and with the attached pressure transducer, ready for mechanical testing

The investigations in the hot cells include experiments on commercial SNF rods from light water reactors, pressurised to their corresponding internal pressure as measured at the end of in-pile service. Bending and impact are conducted on sets of carefully selected rod segments, excluding segments close to the spacer grids of the fuel assembly, or, if relevant, close to locations where there is suspicion of cladding or fuel failures. Studies have so far used UO<sub>2</sub> fuel rods covering an extended burnup (BU) range, from 18 to over 100 GWd/t<sub>HM</sub>.

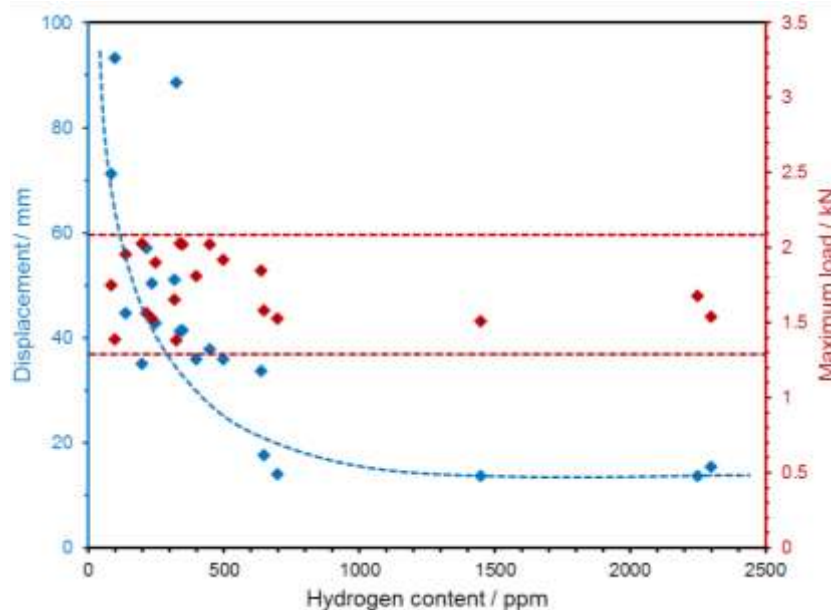


Figure 13 – Measured deflection and maximum fracture load as a function of hydrogen concentration in the cladding during the cold 3-point bending test

Prior to their installation in a hot cell, the two devices presented above were extensively controlled for proper functionality and operation with tele-manipulators. Many cold trials with surrogate specimens were carried out for this purpose. The simulated tests used hydrogenated Zry-4 cladding tubes, filled with Al<sub>2</sub>O<sub>3</sub> pellets and pressurised to 4 MPa. Most of the results obtained from the bending tests have already been reported [Nasyrow, 2016] in the form of displacement vs. hydrogen content (Figure 13).

Despite the enormous changes in the displacement measured, the corresponding maximum loads persist within a very narrow range between 1.3 to 2.1 kN and seem – contrary to the displacement – not to have been affected by the hydrogen concentration in the cladding.

Two load-displacement curves from the 3-point bending experiments on SNF rod segments with low and high average burnup and corresponding hydrogen pickups, respectively, are compared in Figure 14. The data were recently presented and extensively commented in [Vlassopoulos, 2018a; Vlassopoulos, 2018b; Rondinella, 2017]. A remarkable feature of the data is the instant drop in the applied load exactly at the point of specimen fracture, i.e. at the very early stage of crack initiation. Roughly 20 % higher loads were applied to rupture the high BU fuel segments, whereas the total displacement was less than half of that of the low BU rods.

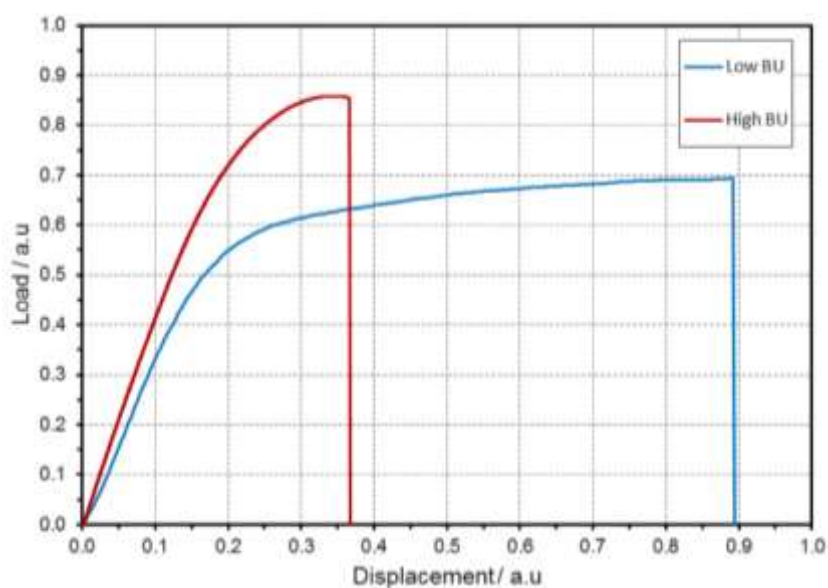


Figure 14 – Load-displacement curves of high and low BU samples during the 3-point bending test

Considering the results from the cold test of Figure 13, the overall behaviour of the SNF rods is fairly consistent. The higher displacement of the low BU specimen was expected, as the material preserves its ductility, but a relatively small change in the maximum critical load to rupture was observed. Nearly three times more energy, as calculated by integrating the area under the curve, must be transmitted to the low BU fuel rod to induce its fracture. The different slopes of the curves in the elastic region denote the higher stiffness of the specimens, which is apparently caused by the higher hydrogenation of the cladding and closure of the gap between fuel and cladding.

The impact device is not equipped with explicit sensors for the acquisition of load-displacement curves. Instead, a high-speed camera attached to the closed chamber of the apparatus records the tests. A sequence of images over a total collection time of only 6.1 ms obtained from the original video file are listed in Figure 15. The visual inspection of the impact provides extremely valuable insight into the various phenomena occurring. Image (a) shows the hammer just before touching the specimen. In the images (b) and (c), several splinters of the cladding's outer oxide layer are clearly propelled from the contact area between hammer and specimen. The crack initiation, morphology and propagation are revealed in image (c). The same photograph illustrates the moment of the "explosive" fuel release in the form of a fine particle cloud. Finally, the subsequent progression and release of coarse fuel fragments at the opening of the crack are observed in images (d) and (e).

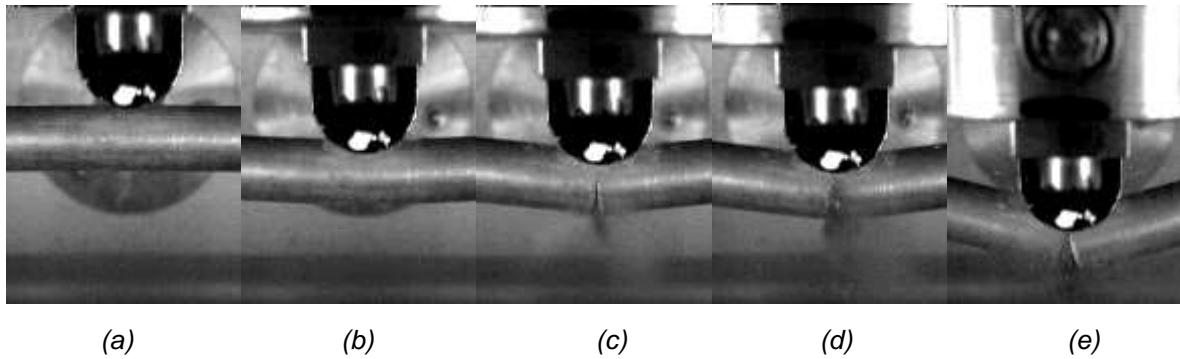


Figure 15 – Representative selected frames of the image sequence during an impact test on a SNF rod

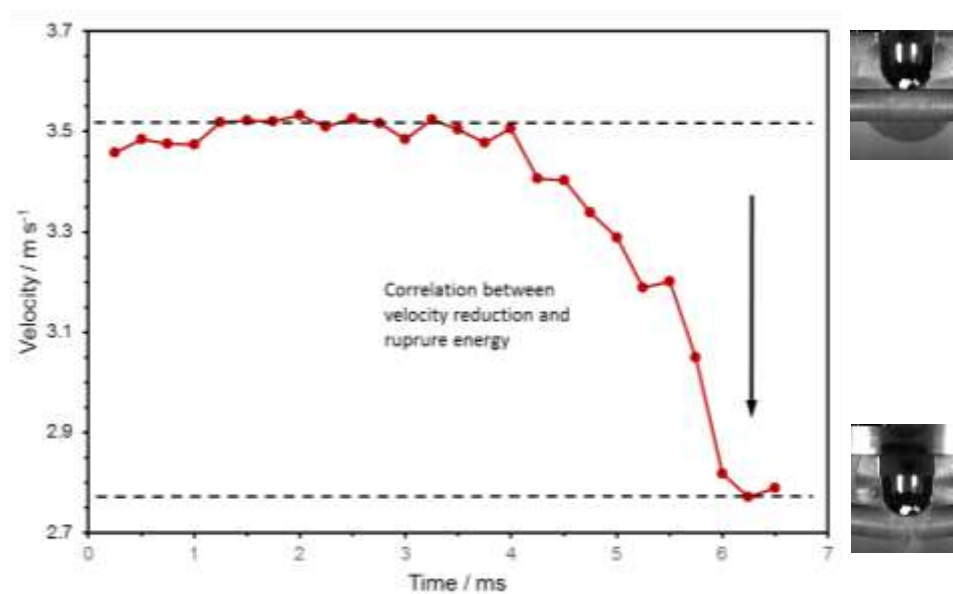


Figure 16 – The hammer velocity change is used to calculate the transmitted energy that caused the specimen rupture

An image analysis (IA) methodology to extract velocity data from the video records has been developed. The process converts the obtained impact sequence images into instantaneous sample deflection and hammer velocity. Thus, the kinetic energy transmitted by the hammer to the specimen can be calculated from the observed velocity reduction upon impacting, as illustrated in Figure 16. The quantification of the uncertainty associated with the derived IA methodology has not yet been evaluated. A direct estimation of this uncertainty is very challenging, since it depends on the minimum detectable displacement and applied object tracking algorithms, which can differ for each case.

### 3.3.6. Ring compression test

Hydrogen embrittlement is known to affect the structural integrity of existing nuclear fuel cladding (zirconium alloys), as has been extensively reported in the literature [e.g. Billone, 2013a; Ruiz, 2015; Billone, 2018; Billone, 2019]. In water-cooled reactors, an oxide layer is formed at the outer side of cladding, and zirconium hydrides (the hydrogen resulting from the reaction of cladding and cooling water) are precipitated in the cladding when the solubility limit is reached. It has been recognised that, depending on their morphology and the hydrogen content, the hydrides are the most important factor influencing the mechanical performance of the cladding. As an example, the hydrides mainly precipitate along the circumferential direction of the cladding when operating in cold-work stress-relieved cladding (typically Zircaloy-4, ZIRLO® and E110). However, during drying operations, hydrides may re-dissolve in the zirconium matrix as the temperature increases and will become available for precipitation when the temperature decreases. If the circumferential stress in the cladding rises above a threshold value (typically around 90 MPa), the hydrides will precipitate along the radial direction when the temperature decreases. This latter hydride morphology, cf. Figure 17, can be very detrimental to cladding behaviour in the case of a "pinch-loading" accident, which involves a diametral compression of the fuel rod due to contact with the grid assembly.

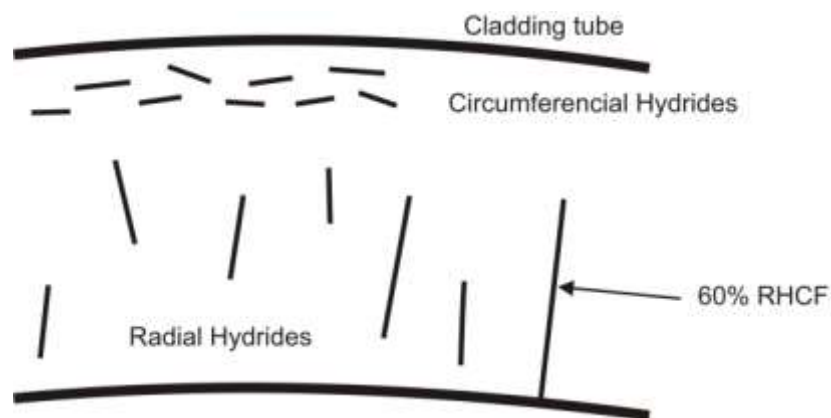


Figure 17 – Typical hydride distribution in a cladding tube

*RHCF means radial hydride continuity factor*

The mechanical integrity of the cladding tubes during handling, transport, or in accident scenarios (e.g. a cask drop) should be ensured after long-term storage, despite possible embrittlement. To assess the risk of failure, assessment methods have to be chosen to gain an understanding of the behaviour of hydrides in a zirconium matrix. A local damage-mechanics approach has been proposed by Le Saux [Le Saux, 2015], using a modified Gurson-Tvergaard-Needleman model with extensions to incorporate plastic anisotropy and viscoplasticity. Ductile failure was reproduced for temperatures of 25, 350 and 480 °C, and a hydrogen content up to 1'200 wppm, with damage initiation induced both through hydride cracking and the debonding between the matrix and the precipitations. The damage evolution is deduced from observations of the microstructure and further parameters obtained from experiments. Implemented in a finite element analysis, the model could predict experimental results with reasonable accuracy. Due to the nature of the damage model, the impact of lower hydrogen contents with high degrees of anisotropy were not taken into consideration and could not be modelled.

Assuming that hydride platelets are considered as cracks inside the cladding material, a fracture-mechanics approach can be used to address microscopic crack growth as the failure mechanism and to consequently investigate fracture behaviour. Compact Tension (CT) specimens are commonly used for research on fracture behaviour. Using cathodic and gaseous charging processes, studies on hydrogen-charged CT specimens show a decrease of the fracture initiation parameter  $J_{IC}$  for increasing

hydrogen contents and low temperatures [Bertolino, 2003]. The macroscopic fracture behaviour was considered as ductile, and therefore a transition from ductile to brittle material response could not be deduced. A negative influence on the fracture toughness of zirconium alloys could be confirmed from 25 °C up to 300 °C, and precipitations along grain boundaries have been determined as a reason for the loss in fracture toughness [Hsu, 2012]. During a pin-loading test performed with hydrogen-charged Zircaloy-4 rings, circumferential hydrides reduced the fracture toughness by 20 %. Combined radially and circumferentially aligned hydrides could reduce the fracture toughness by up to 90 % [Langlade, 2006]. Even in the case where macroscopic failure appears to be brittle, microscopic crack growth was considered to be plastic strain-driven.

Although common fracture-mechanics testing procedures allow the observation of some effects regarding hydride embrittlement, the impact of crack fields remains unanswered. In addition, the result of a CT test with its defined stress state is hardly applicable to the complex structure and geometry of a thin-walled tube. Therefore, the ring compression test (RCT) was established to consider these effects. In this test, a cylindrical sample of the cladding material is deformed within movable plates, and a loading force vs. displacement curve is obtained. Experimental results from RCTs for different hydride contents and temperatures are used to develop numerical models that help to understand and interpret the micromechanical processes inside the cladding. Based on a predictive simulation, failure criteria for the cladding material can be derived. An experimental procedure was developed for the commercially available alloys ZIRLO<sup>®</sup>, M5<sup>®</sup> and Zircaloy-4 by Billone [Billone, 2013a; Billone, 2013b]. Both samples from higher burnup fuel rods and as-fabricated, hydrogen-charged cladding segments were heated up to 400 °C and pressurised to induce peak hoop stresses from 80 MPa up to 140 MPa to simulate drying and storage. Hydrogen contents ranged from 350 wppm to 650 wppm for ZIRLO<sup>®</sup>. Afterwards, the ring segments were cooled with cooling rates of ~ 5 °C/h. RCTs were performed with as-irradiated as well as hydride-reoriented samples at distinct temperatures from room temperature up to 200 °C and with a displacement rate of 5 mm/s. The extent of radial hydrides was quantified by the radial-hydride-continuity factor (RHCF) as the ratio of continuous radial hydride length to wall thickness of the cladding, cf. Figure 17. It could be shown that through-cracks during the tests correlate with the extent of radially-aligned-hydride formation. Furthermore, the re-precipitation of platelets in the radial direction is controlled by the peak hoop stress. The highest testing temperature, at which brittle behaviour occurs, is defined as the ductile-to-brittle transition temperature (DBTT). This temperature depends on the type of material, hydrogen content and reorientation stress. The embrittlement criterion is an "offset strain" of 2 % [Billone, 2013b].

Further RCT procedures were performed by Martin-Rengel [Martin-Rengel, 2012; Martin-Rengel, 2013] and Ruiz-Hervías [Ruiz, 2015]. Ring segments of ZIRLO<sup>®</sup> were charged with hydrogen to achieve contents of up to 2'000 wppm. The heating, reorientating and cooling were performed in a similar way as described above. Two additional failure criteria were proposed based on the strain energy density and the equivalent plastic strain respectively. Furthermore, numerical methods using Finite Element Analysis (FEA) were proposed. A fracture-mechanics approach could re-produce load-displacement curves from RCTs using the cohesive crack model, and further non-linear optimisation could enhance the results [Gomez, 2017]. It could be shown that the cladding material with reoriented hydrides was less susceptible to brittle failure during the three-point bend test in comparison with the RCT. Based on the results of 102 RCTs, a computational model was developed by Herb [Herb, 2014]. The derived failure criterion considers the ratio of burst stress, i.e. the stress at which the first drop in the load-displacement curve occurs, and the yield stress of the material to predict the ductile-to-brittle transition.

An elastic-plastic fracture-mechanics FEA model was proposed by Nilsson [Nilsson, 2010]. A two-dimensional plane-strain tube segment was modelled with a suitable constitutive model for Zry-4. Individual straight cracks of different lengths, locations and angles were added to the model. A stress load was applied as a boundary condition and the J-integral was calculated. It could be confirmed that circumferentially aligned cracks have no impact on fracture initiation because J values for those cracks were essentially zero. The ligament starts yielding at lower stresses for cracks close to the inner or outer surface. Fragmented hydrides were then modelled as kinked cracks with angles from 30° to 30° differing

from the radial direction. Radial cracks with kinks had the same initiation values for  $J$  as straight cracks. The likelihood of crack growth is increased, however, for kinked cracks in comparison with straight cracks. Since cladding tubes can contain many hydrides, the distance between the platelets is often smaller than their individual length. Therefore, the complex interaction between cracks was analysed depending on the distance of the crack tips and the angle between neighboring cracks. For a realistic study, photographs of hydrides were analysed and transferred to an equivalent FEA model of a crack field. It was concluded that cladding failure becomes more unstable if several radial hydrides interact. Failure might be triggered by a critical hydride configuration, even if the configuration is very local. Hydride-induced failure is strongly influenced by the yielding along the ligaments. The size of the hydrides in the radial direction is the most significant parameter for the load necessary to initiate failure.

Hence, the ring compression test is the established experimental method for the investigation and characterisation of the mechanical behaviour of defueled cladding tubes. The test can be carried out in hot cells with irradiated material as well as with unirradiated material under normal laboratory conditions. The effort for hot cell tests is very high, but investigations outside hot cells require unirradiated mock-up cladding tubes with material behaviour representative of the irradiated material state. Real Zircaloy claddings contain circumferential and radial hydrides due to the conditions in water-cooled reactors and subsequent vacuum-drying. Therefore, the influence of these hydrides on the material behaviour must also be reproduced.

Realistic distributions of circumferentially or radially oriented hydrides can be created by hydrogen charging of unirradiated claddings. Ruiz-Hervías [Ruiz, 2015] describes a cathodic charging method for a controlled insertion of hydrogen into an unirradiated sample. In an electrochemical reaction, the sample acts as the cathode, and a platinum wire coiled around the sample as the anode in a KOH-aqueous solution. After hydrogen charging, the sample is exposed to an inert gas atmosphere with constant elevated temperature and then slowly cooled down (approx. 1.2 °C/min). The hydrides are circumferentially oriented at this stage of the procedure. Based on a subsequent thermo-mechanical treatment with applied hoop stress (or reorientation stress), the hydrides can be dissolved and partly reoriented along the radial direction of the cladding. The resulting hydride density and orientation is similar to radial hydrides found in the cladding of irradiated fuel rods after radial-hydride treatment (cf. Figure 17). In the case of Zircaloy M5®, mostly individual long radial hydrides precipitate. For ZIRLO®, typically a mix of radial and circumferential hydrides predominates.

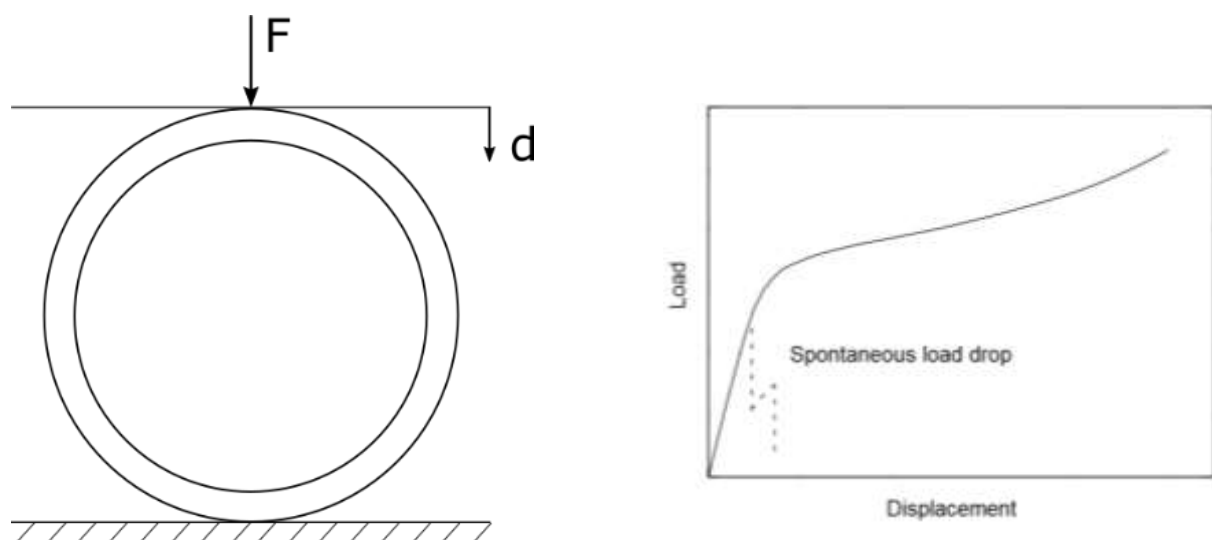


Figure 18– Ring compression test experimental setup (left) and typical load-displacement curves (right)

The experimental setup of the ring compression test is shown schematically in Figure 18. Tests are displacement-controlled by means of two plane and parallel steel plates. The load is measured with a load cell. The upper plate moves with constant velocity, while the lower one is fixed. Maximum tensile hoop stresses occur at the inner surface of the 6 and 12 o'clock positions and at the outer surface of the 3 and 9 o'clock positions. Specimens are ring-shaped with a height of 10 mm. The dimensions of the cladding tube may vary. Typical values are an outer diameter of 9.5 mm and a wall thickness of 0.5 mm.

Figure 18 illustrates the characteristic load-displacement curve of pre-hydrided samples. Cladding samples with circumferentially oriented hydrides typically show ductile behaviour during a RCT. The displacement at maximum load is much larger than the typical gap between tube and fuel. After large deformation, ductile failure is detected and the load decreases gradually (not shown in the figure). By contrast, hydrides oriented in radial direction of the cladding can cause brittle failure associated with sudden load drops. The displacements at the point of failure can be very small. After the maximum load, failure by crack initiation and subsequent crack propagation is observed. The crack can also stop and reinitiate. In this case, the load can decrease in several steps.

As testing with irradiated cladding is both difficult and expensive, it is not possible to cover all possible conditions. Testing with unirradiated material may help bridge the gaps. The precise experimental simulation of the hydride population and geometry observed in irradiated cladding is particularly important in this respect. Novel procedures are needed to experimentally simulate the drying process by independently controlling the internal pressure and the temperature of cladding. In addition, a reliable method is needed to obtain the constitutive equation of cladding (i.e. the stress-strain curve) from unconventional tests such as the ring compression or instrumented indentation tests.

Concerning the state-of-the-art, an analysis of the initiation fracture toughness in the initial elastic region (or just shortly after passing this region) in the ring compression test is missing and should correlate measured load-displacement curves, the observed distribution of hydrides and postulated crack-initiating hydrides. Various failure criteria can be found in literature depending on an "offset strain", strain energy density, or equivalent plastic strain. A complementary assessment method should be developed based on fracture-mechanics methods, especially for potential brittle failure at very small deformation of cladding tubes. A fracture-mechanical analysis of the sudden failure by brittle fracture may help to understand the underlying processes and to develop appropriate failure criteria based on the initiation fracture toughness of the material. The failure criterion to be developed is a necessary link to understanding and predicting the macroscopic behaviour of the cladding under operational and accident conditions on its way towards final disposal.

## 3.4. Numerical methods and analysis

### 3.4.1. Finite element analysis and mechanical state of the fuel

Extensive research studies [SCIP; Billone, 2013a; Billone, 2019] have been performed to investigate phenomena that affect the mechanical state of nuclear fuel and cladding during irradiation. The vast majority of the fuel-performance codes examine mainly the thermo-mechanical properties of the fuel/cladding during irradiation, where numerous models have been developed and validated against experimental data. However, experimental activities using SNF rods experiencing interim and/or long-term dry storage conditions are rather limited. The primary reason is the inherent difficulty of working with highly activated materials in addition to the associated cost of such experiments.

Over the last couple of decades, there has been an increasing need to develop a better phenomenological understanding of the SNF rod mechanical behaviour throughout the different stages of the back-end of the fuel cycle, i.e. during wet/dry storage, transport and handling. This need is mainly associated with the licensing requirements related to the extension of the SNF dry storage periods in transport and storage casks (TSCs) and to their integrity evaluation after transport and/or handling operations related to final disposal. The technical gaps have been identified and presented in [NRC,

2014; UFDC, 2012]. The need to generate experimental data, especially for the high-burnup and MOX cases, was highlighted in order to contribute to the validation and further development of analytical and numerical models. This chapter attempts to provide a review on the SNF rod mechanical-response studies by means of numerical and/or analytical approaches complemented by experimental investigations on irradiated SNF rods.

One of the first integrated programmes addressing SNF integrity after dry storage was developed by Areva TN and International Nuclear Services in the early 2000s. The Fuel Integrity Project (FIP) studied the impact response of both irradiated and unirradiated fuel with the main objective being the development of a methodology to evaluate the nature and extent of damage to SNF assemblies during TSC drop accidents [Purcell, 2004]. The experimental work included an extensive testing programme on both fresh and spent rodlets in order to obtain information on the SNF properties (as a fuel/cladding composite material) and to determine some uncertainties (e.g. pellet/cladding friction coefficients) relative to specific loading configurations of the SNF rods (i.e. static and dynamic bending, buckling). The main results of the experimental campaign are summarised in [Purcell, 2004; Zéachandirin, 2011], where the data obtained are used to develop analytical calculations for the rod behaviour in the elastic domain of the cladding and numerical models for Finite Element Analysis (FEA) of the rod behaviour in the cladding plastic domain. The FEA models were validated against 3-point bending tests on SNF rods and lateral compression tests on claddings [Dallongeville, 2010; Dallongeville, 2005]. The FIP methodology was built upon these results, and it distinguishes cases depending on the type of load (direction), the type of fuel assembly and the irradiation state (fresh or used) of the rod [Zéachandirin, 2011; Dallongeville, 2012]. The major results of this project concerned the uncertainties in the modelling of the fuel rods, the determination of the irradiated cladding properties related to burnup and assumptions on the fuel-mass-release analysis.

Another methodology has been proposed by Structural Integrity Associates, Inc. (former ANATECH) that considers the high-burnup effects mostly associated with the hydrogen concentration and hydride orientation in the cladding [Rashid, 2004a]. A major assumption of this method is the consideration of a static analysis, rather than dynamic, which conservatively bounds the dynamic analysis results. Finite element models have been developed where the essential feature of these models is the damage formulation, which describes the interactions of the cladding response to specific failure modes. Therefore, no a posteriori application of failure criteria is needed in comparison to the FIP methodology. The cladding-failure criteria have been derived from limited experimental data on burst tests of empty claddings [Rashid, 2004b; Rashid, 2004c], with no reference tests used for the finite element model validation. Although this method provides a step towards a quantitative analysis of the SNF rod failures for transport accidents, its application is rather complicated and experimental validation using real SNF rods is still needed.

In order to address some of the aforementioned data gaps, it was necessary to develop experimental campaigns to macroscopically and fundamentally study the mechanical response and failure processes of the fuel/cladding composite system under static and dynamic loads. JRC – Karlsruhe and Oak Ridge National Laboratory (ORNL) were among the first to independently develop such integrated campaigns and make their findings public.

JRC – Karlsruhe initiated an extensive experimental campaign to characterise the quasi-static and dynamic response of surrogate and LWR SNF rodlets using three-point bending and gravitational impact tests, respectively, as described in Section 3.3.5. In collaboration with GNS (Germany) and Areva, the first results of the impact tests were published in [Papaioannou, 2009b; Papaioannou, 2009c; Rondinella, 2012]. These studies focused on the characterisation of the fuel mass release and revealed remarkable similarities among all samples used, corresponding to  $\leq 2$  g of fuel release per fracture, and no indication associated with high-burnup rim structure in the size classification of the released particulates. Investigations following this work included the collaboration with Nagra (Switzerland) and the Federal Institute for Materials Research and Testing (BAM, Germany) aimed at the development of the three-point bending apparatus and the experimental optimisation of the impact tests [Vlassopoulos, 2017b]. Experimental results for the bending tests consist of the flexural stress-strain curves, bending

angles to fracture and fuel mass release characterisation, where a correlation between the level of ductility of the sample and its burnup value was revealed [Nasyrow, 2016; Vlassopoulos 2018b]. To examine the strain-rate dependence of the SNF rod response, an Image Analysis (IA) methodology was developed to analyse the recorded high-speed videos of the impact tests. The experimental campaign is complemented by numerical studies conducted independently by Nagra and BAM using FEA [Vlassopoulos, 2018b; Ballheimer, 2016; Vlassopoulos, 2018a]. Two types of models were developed to simulate the rod response using the simple beam approach or by explicitly modelling the pellets and the cladding. The model validation was performed against the experimental data and the cladding failure criteria were derived by analysing the stresses and strains at the bending angles of fracture.

Another major campaign was established by the U.S. Department of Energy - Office of Nuclear Energy (DOE-NE). The Used Fuel Disposition Campaign (UFDC) [Adkins, 2013] aims to conduct R&D activities related to storage, transport and disposal of SNF and high-level waste. Within this framework, ORNL has developed a SNF-vibration testing procedure to quantify the reliability of the SNF during transport [Jiang, 2014; Wang, 2018]. Experimental activities include static and dynamic SNF testing under simulated transport conditions using a cyclic integrated reversible-bending fatigue tester (CIRFT). The studies revealed a detailed understanding of the mechanical interactions between pellets and cladding, and of the effect of loading rate and loading mode on the fatigue damage evolution of high-burnup SNF under transport conditions [Wang, 2018]. Major findings have shown the importance of the SNF system interface bonding in the vibration performance, the contribution of the fuel to the SNF system stiffness and the SNF failure initiation at the pellet-cladding interface region. FEA was used to investigate the relative importance of the pellet-pellet and pellet-cladding interfacial bonding efficiency with regard to the SNF dynamic system performance, which showed a significant reduction of the SNF system flexural rigidity in case of debonding [Jiang, 2014; Jiang, 2016a; FY2014; Jiang, 2016b; FY2017]. The intensity of the contact interaction as well as the impact loading between spacer grids and SNF rods has also been investigated using FEA. A first approach towards SNF assembly modelling was made by simulating a subassembly model to investigate the SNF system's dynamic stability under normal transport conditions [Jiang, 2016a].

Complementary numerical studies within the UFDC framework, conducted as part of a collaborative effort between different U.S. national laboratories, include FEA on the rod scale [Coleman, 2014] and the SNF assembly level [Sanborn, 2014]. In these studies, the importance of the uncertainties in the SNF material properties and in the non-linear geometric behaviour of the model has been highlighted. For this reason, it was considered necessary to develop the equivalent beam properties of the detailed SNF system. In this respect, the aims of the detailed modelling are to establish reasonable lower/upper bounds and best-estimate material properties. The transport-damage prediction in a worst-case scenario during normal conditions of transport (NCT) was found to be approximately 18 % of the expected SNF fatigue limit, resulting in no SNF rod failures.

For the estimation of the SNF assembly behaviour during handling operations, CEA (with the support of EDF) has conducted three-point bending tests on six-cycle fuel rod segments complemented by FEA [Guerin, 2013]. An equivalent constitutive equation for the SNF rod system has been derived, taking into account the experimental force-displacement curve and maximum failure strain/curvature. The relative contribution of the pellets and cladding to the rod global behaviour has been estimated. The results were used to model a two-dimensional SNF assembly with a beam element in CAST3M. Bending calculations were performed and failure criteria were derived by comparing the calculated bending angles to the experimental ones at failure.

To evaluate the mechanical integrity of high-burnup SNF assemblies under accident transport conditions, BAM has developed an analytical methodology [Ballheimer, 2010; Schrödl, 2010]. The rods are considered as continuous beams, supported at the positions of the grids, and are excited dynamically through the supports (and not by directly applied external loading). The beams are modelled with only elastic material behaviour. This assumption seems to be justified by the drastic decrease in cladding ductility in high-burnup rods. In addition, radial hydrides are not considered to affect the failure mode under bending loadings. Considering certain boundary conditions, an analytical derivation of the

effective static load and the beam's global displacement is possible. To estimate the fuel mass release, the critical deflection of the cladding is compared against the limiting beam deflection, and a bounding release per rod-breakage has been considered. This study clearly highlights the importance of the experimental verification of the approach as well as the importance of the accessibility of data generated by experimental testing of SNF rods.

Another extensive integrated campaign aimed at evaluating the dynamic response of SNF rods has been carried out in a collaborative effort by several Japanese institutions, as was already reported in the SPAR III programme [IAEA, 2015]. The experimental activities include basic mechanical tests on claddings and dynamic impact tests on fuel rods [Ozawa, 2013; Hirose, 2012; Hirose, 2013]. Axial and lateral loading of fuel rods were used to study the rod failure loads, strains, and the fuel mass release. The fuel material release from BWR SNF rods was equivalent to approximately two or three pellets under axial and lateral impact testing, respectively. For the PWR cases, the fuel mass release was bounded to 1.4 g. FEA was used to study the SNF rod buckling behaviour [Minamoto, 2011] as well as the dynamic response of fuel rods under side drop loading [Minamoto, 2015].

### 3.4.2. Fuel performance codes

The key phenomena mentioned above often influence each other so that fuel rod performance can only be properly characterised through their proper integration into analytical tools. The strategy commonly followed to obtain these analytical capabilities is based on the extension to dry storage conditions of in-reactor thermo-mechanical codes. Since the in-reactor end-of-life (EOL) is the final outcome, they are well consolidated and their use is widespread. This extension is based on three main aspects:

- initial conditions (in-reactor EOL) provided by the code itself
- boundary conditions provided by thermal hydraulics or thermal fluid dynamics tools
- fuel performance during dry storage provided by new models implemented in the code extension

Additionally, other minor modifications are needed, such as including suppression of the cladding corrosion modelling during dry storage (i.e. inert atmosphere as coolant). A summary of fuel performance codes extended to dry storage is shown below, based on information available in the open literature.

#### BISON (INL)

Local effects in the cladding, such as hydrogen diffusion and precipitation, cannot be handled rigorously (including e.g. azimuthal variation of hydrides) with traditional 1.5-dimensional fuel performance codes. However, hydrides may be modelled with the thermo-mechanical fuel performance code BISON, developed by the Idaho National Laboratory (INL) since 2009 [Newman, 2009]. BISON employs the finite element method and solves fully coupled thermo-mechanics and species diffusion equation systems in 2D-axisymmetric and 3D geometries. The code has been augmented with hydride modelling capability: hydrogen diffusion, precipitation into hydrides, and dissolution [Courty, 2014; Stafford, 2015]. In order to have a consistent post-irradiation state of the rod (including the cladding stress state) for the study of fuel behaviour in storage, all the successive stages are considered in a single code run: steady-state irradiation, wet storage, drying, and dry storage.

Fuel models in BISON describe temperature- and burnup-dependent thermal properties, swelling, densification, thermal and irradiation creep, relocation, fracture, and fission gas production and release [Hales, 2016]. Cladding mechanical models include plasticity, irradiation growth, and thermal and irradiation creep. The code is also able to simulate gap heat transfer, mechanical contact and the evolution of free volume pressure. With BISON, large problems can be solved as it may be run in parallel, i.e. assumptions on symmetry do not have to be made. The calculation mesh for the FEA is generated with external software such as TRELIS, ABAQUS/CAE, PATRAN or ANSYS, or, in simple cases via the

input file, i.e. 2D-axisymmetric mesh with no pellet chamfers or dishings. Either first- or second-order elements may be used with BISON: 4- or 8-node quad element for 2D, and 8- or 20-node hexahedral element for 3D. In practical applications, it is typical to use 2D simulations for a full-length rod and 3D simulations for a segment of a rod for detailed study.

BISON has a boundary condition option to model the heat flux from, and the peak cladding temperatures of, a rod in the center of a fuel assembly situated in a dry cask storage system [Hales, 2016]. Radiative and conductive effects inside the assembly, and conductive and convective effects from the assembly are considered. The cask-effective heat-transfer coefficient depends on cask type and loading and should be tuned. This option is not applied if the cladding surface temperature is given as a boundary condition. BISON contains a coolant channel model that calculates the heat transfer from cladding to coolant. Again, if the cladding temperature is given, this model is not used.

Currently, the models in BISON cannot predict radial hydride concentrations. Failure estimation due to hydrides can only be studied indirectly by comparing the calculated cladding stress to some stress criteria. The diffusion model implemented in BISON has a shortcoming in that it does not correctly predict the observed (measured) thickness of the hydride rim in the cladding outer periphery if the volume fraction of hydrides in the rim is small [Stafford, 2015]. Therefore, there is an option to limit the peak hydride concentration in the rim by widening the hydride rim region.

For the cladding mechanical behaviour, in order to model the cladding creep-out during interim dry storage, a cladding creep model suitable for out-of-reactor conditions has to be used. Currently in BISON, there are no cladding creep models for dry storage conditions.

## FRAPCON (PNNL)

FRAPCON is a steady-state fuel-performance code developed by PNNL (Pacific Northwest National Laboratory) for the NRC [Geelhood, 2015]; it is applied to light water reactor (LWR) fuel rods. The capability to model spent fuel during dry storage has been added in the last version (4.0) and also in the new code FAST, which merges FRAPCON and the transient code FRAPTRAN. The new capabilities added are:

- coupling with the DATING sub-code, which uses empirical correlations for cladding creep and temperature decay curves for the analysis of fuel cladding under storage conditions
- implementation of the ANS-5.1-2004 Draft Standard to model the decay heat; so far, it is not used to estimate the fuel rod temperature in dry storage
- implementation of empirical correlations to add the effect of helium production and release due to  $\alpha$ -decay and the swelling of the pellets via a build-up of the helium decay product

## FRAPCON-xt (CIEMAT)

FRAPCON-xt is CIEMAT's extension to the FRAPCON code [Herranz, 2010; Feria, 2018]. The extension is based on the inclusion of models (most of them derived from and/or adapted by CIEMAT):

- an empirical cladding creep law that allows a direct feedback with the stress relaxation due to temperature decay and cladding creep-out
- an engineering correlation to calculate the temperature decay (based on thermal fluid dynamics calculations conducted with ANSYS FLUENT for concrete and metallic casks)
- a diffusion/precipitation model that is coupled with the code to estimate the hydrogen distribution throughout the cladding
- an empirical model of hydride radial reorientation in dry storage [Desquines, 2014]
- an empirical criterion based on available data on cladding-defect propagation onset due to UO<sub>2</sub> oxidation

Additionally, a Best Estimate Plus Uncertainty methodology has been set to quantify the code's uncertainties [Feria, 2017].

### ENIGMA (NNL, VTT)

The ENIGMA fuel performance code was originally developed by Berkeley Nuclear Laboratories and Nuclear Electric [Kilgour, 1992] to calculate the thermo-mechanical behaviour of a LWR fuel rod under steady-state conditions.

NNL (UK National Nuclear Laboratory) has extended ENIGMA for modelling dry storage scenarios [Rossiter, 2011], which is mainly based on the incorporation of an empirical creep model valid for dry storage (derived by EDF [Bouffieux, 2001]). The thermal conditions are provided through in-house and commercial thermal analysis or computational fluid dynamics (CFD) codes, including ANSYS FLUENT. The calculation of the decay heat of the spent fuel is based on the FISPIN code, with nuclear cross sections supplied by CASMO.

A recent extension of ENIGMA to dry storage has been carried out by VTT [Arkoma, 2018]. The so-called VTT-ENIGMA was modified in order to model the cladding creep during dry storage. Two creep models were implemented into the code: one from EDF [Bouffieux, 2001] and one from CIEMAT [Feria, 2015]. The thermal conditions were determined by CFD calculations with OpenFOAM, which was fed by decay heat calculations with the SERPENT code.

### TESPA-ROD (GRS)

The TESPA-ROD code analyses the thermo-mechanical behaviour of LWR fuel rods under operational conditions and design-basis accidents (RIA, LOCA), and it was extended to dry storage conditions [Sonnenburg, 2017]. To do this, the creep of the cladding material was modelled under prevailing conditions (implementation of empirical creep law), as well as the pellet swelling due to helium production during long-term storage. The fuel rod temperature was determined through the sub-channel thermal hydraulic code COBRA-SFS and supported by calculations from a burnup code such as KENOREST.

### TRANSURANUS (ITU-JRC)

TRANSURANUS is a fuel-performance code developed by ITU-JRC (Institute for Transuranium Elements-Joint Research Centre) that is applicable to LWR fuel rods. In order to extend the code to dry storage, an analysis of the empirical cladding creep model was used by the code [Lassmann, 1977] and a comparison was performed with other creep models with a wider range of application [Mayuzumi, 1990; Martin, 2007]. With this study, it was possible to identify the best option to apply depending on the prevailing conditions.

## Synthesis

Table 11 provides a synthesis of the information explained above. The following should be highlighted:

- The cladding creep in dry storage is modelled based on practically all the codes shown. In spite of this, further modelling and validation are needed, especially concerning the effect of the irradiation damage annealing and the hydrogen concentration and orientation.
- The in-cladding hydrogen behaviour is only modelled based on BISON and FRAPCON-xt, and further understanding, modelling and validation are needed regarding concerns in dry storage such as hydride radial reorientation or hydride blister formation, for which the accuracy enhancement of the hydrogen migration/precipitation models is of the utmost interest.

- The pellet-related phenomena seem to be less modelled. The  $\alpha$ -decay is only modelled based on two codes; the main research interest is focused on MOX fuel, with significantly higher helium production than UO<sub>2</sub>. Regarding the effect of UO<sub>2</sub> oxidation, only FRAPCON-xt takes it into account with a cladding failure criterion, although supported on a scarce database of low-burnup fuel, and further research is thus needed to model this phenomenon. In the case of the pellet-cladding bonding, only BISON has the capability to analyse its effect; indeed, the complexity of this mechanism requires further research to be done in this regard.

Code	Key phenomena							
	Cladding					Pellet		
	Creep	Hydrogen migration/precipitation	Hydride radial reorientation	Hydride blister formation	DHC	Pellet-cladding bonding	UO <sub>2</sub> oxidation	$\alpha$ decay
FRAPCON-xt (CIEMAT)	X	X	X				X	
FRAPCON/FAST (PNNL)	X							X
ENIGMA (NNL)	X							
VTT-ENIGMA (VTT)	X							
TESPA-ROD (GRS)	X							X
TRANSURANUS (ITU-JRC)	X							
BISON (INL)		X		X	X	X		

Table 11 – Synthesis of fuel performance codes and key phenomena simulated in dry storage

Finally, it should be noted that a proper integrated validation of the codes shown is not possible due to the lack of data. Therefore, further work should be performed to derive qualified experimental databases for the assessment of the code extensions to dry storage.

## 4. Accident scenarios

The term "scenario" means a "*postulated or assumed set of conditions and/or events that can lead to human exposure or environmental contamination*" [IAEA, 2013] or, differently phrased, "a set of conditions and/or events that involves a potential risk of radiation exposure of human beings and/or the environment".

Each scenario must reflect certain conditions arising either during the normal operation of a facility or as a consequence of a specific event leading to a deviation from normal operating conditions. The choice of an appropriate range of scenarios and associated assessment cases is essential for the safety assessment of any nuclear facility (e.g. power plant, wet storage, dry storage, encapsulation facility, etc.) or specific activity/process (e.g. SNF transport, handling, etc.). Once identified, these scenarios should take into account existing and potential hazards arising from the facility/process, and also their interrelation and evolution over the lifetime of the facility or defined processes according to the safety case.

A systematic approach to accident scenarios may be as follows: 1) Identification and screening of hazards with respect to the facility design and defined processes (for instance, the types of hazard have to be identified with respect to the SNF inventory, activity, physical conditions and location, together with any additional hazards arising indirectly from activities or processes for their management); 2) Identification of initiating events with the potential for causing harm to humans and/or the environment; 3) Quantification of the hazards; 4) Safety analysis of all relevant scenarios arising from either processes or accident situations in which the screened hazards could occur.

Unlike the previous chapters, this chapter aims to give a generic overview of accident scenarios that have been identified so far in the pre-disposal activities for SNF. Hazards and initiating events are strongly site-specific and have thus been left out of the scope of this chapter.

### 4.1. Safety standards for pre-disposal management of SNF

The safety requirements for the pre-disposal management of SNF necessitate the development of a safety case – together with the necessary supporting safety assessment – for each facility or activity [IAEA, 2016]. The safety case and supporting safety assessment provide the basis for the demonstration of safety and for licensing (siting, location, design and operation) of SNF dry storage or packaging facilities, as well as other types of nuclear facilities. Spent fuel storage facilities have to demonstrate the safe, stable and secure storage of spent fuel [IAEA, 2020]. The design features and the operation of the facility should be such as to ensure the containment of radioactive material and optimum radiation protection of workers, members of the public and the environment within the dose constraints in accordance with established requirements (see [IAEA, 2009b]), in order to maintain sub-criticality and ensure the removal of decay heat and retrievability of the spent fuel. These safety functions should be maintained during all operational states and accident conditions.

Safety Guides are provided by the IAEA [IAEA, 2013] for guidance and recommendations on the development and review of the safety case and supporting safety assessment prepared or conducted for a pre-disposal waste management facility and related processes/activities. All aspects of the safety case and safety assessment must be covered in a general sense, including planning, design, construction, commissioning, operation and modification of the facility.

This guidance requires demonstration of acceptability following defined accident scenarios (for example SNF transport accidents or a SFA dropping from height). As the IAEA recommendations have a common basis, the Safety Standards are used as the main reference in this report, although certain criteria to be met (such as dose limits) are country-specific.

## 4.2. Accident scenarios for fuel in interim storage

A safety analysis of an interim dry storage facility for SNF must be performed with respect to potential accident scenarios. Several stages, both from the point of view of the design and the site, have to be taken into account: source definition, radioactivity inventory assessment, analysis of the radioactive release scenarios and their consequences in the geosphere and biosphere, dose assessment for preparation, transport/transfer and proper interim storage of spent fuel. The radionuclide inventory and related uncertainty can be evaluated using several methodologies (numerical and experimental), as described in Chapter 2.

According to the IAEA Safety Standards [IAEA, 2013], scenarios should be developed for normal operation, anticipated operational occurrences and accident conditions. The safety analysis should address the consequences of normal operation and the frequencies and consequences associated with all anticipated operational occurrences and accident conditions. The degree of detail of the analysis should depend on the magnitude of the radiation risks associated with the facility or activity, the frequency with which events occur, the complexity of the facility or activity and the uncertainties inherent in the processes.

Three types of potential accident scenarios can be considered according to the nature of the operations:

- I. scenarios for normal operation
- II. scenarios for anticipated operational occurrences and design-basis accidents
- III. scenarios for beyond-design-basis accidents

Scenarios should also be evaluated according to accidents due to natural or man-made events and accidents due to external and internal human-induced events.

In order to analyse the accident scenarios, conservative assumptions should be considered. To perform a probabilistic analysis, the effective doses and risks have to be evaluated. As a consequence of the results obtained and of the measures taken for the design, it must be demonstrated that humans and the environment will remain safe and protected in all cases.

The three above-mentioned scenarios are defined in [IAEA, 2013] in a general context and summarised here as follows.

### I. Scenarios for normal operation

Scenarios for normal operation should address all conditions under which the systems and equipment of the facility operate (activities carried out as expected), with no internal or external challenges [IAEA, 2013]. This includes all aspects of operation for which the facility is designed to conduct over the course of normal operation, including maintenance over the lifetime of the facility and all stages of activities. The effects of variations in the input materials (feedstock, source material, receipts, etc.) on normal operation should be considered.

Scenarios for normal operation should be defined with the goal of assessing whether the activities can be carried out safely or the facility can be operated safely under normal operation. This includes an assessment of whether radiation doses to workers and members of the public and planned discharges will lie within prescribed limits and constraints and can be maintained as low as reasonably achievable. It also includes verification that the elements of defense-in-depth will be maintained and that adequate safety margins will remain at all times.

### II. Scenarios for anticipated operational occurrences and design-basis accidents

The facility conditions considered in the design-basis assessment are typically divided into two categories: anticipated operational occurrences and design-basis accidents. The division between the two categories of scenarios is based on the frequency of occurrence and the extent of the challenge to safety from the initiating events causing the condition [IAEA, 2013].

Anticipated operational occurrences are processes deviating from normal operation that are expected to occur at least once during the operating lifetime of the facility, but which, in view of appropriate design provisions, do not cause any significant damage to items important to safety or do not lead to accident conditions. Scenarios for anticipated occurrences should also be considered for SNF management activities.

A design-basis accident is an accident condition against which a facility is designed according to established design criteria, and for which the damage to the radioactive waste inventory and the release of radioactive material is kept within authorised limits. Design-basis accidents have a lower frequency than anticipated operational occurrences, and they are not expected to occur during the lifetime of the facility but must be considered in its design.

The safety analysis should identify the anticipated operational occurrences and accident conditions. This should include all internal and external events and processes that may impact physical barriers that confine the radioactive material or otherwise increase radiation risks. The selection of events and processes considered in the safety analysis should be based on a systematic, logical and structured approach, and justification should be provided that the identification of scenarios is sufficiently comprehensive. The analysis should be based on an appropriate grouping and bounding of the events and processes, and partial failures of components or barriers as well as complete failures should be considered.

The assessment should demonstrate that the design of the facility and associated safety processes/procedures meet all safety criteria. For instance, the design-basis assessment should demonstrate that the potential for release of radioactive material or loss of shielding is controlled, that any operational discharges of effluents will remain below prescribed limits, that the limiting criteria for design-basis accident conditions will be met and the radiological limits applied will not be exceeded, and that some or all of the barriers put in place to limit exposure and the release of radioactive material from the facility will maintain their integrity to the extent required. A conservative assessment should take account of the uncertainties associated with the assessment itself.

For new facilities or activities, a comprehensive identification and assessment of all design-basis accidents should be carried out. For modifications of existing facilities or activities, the assessment should focus on those design-basis accidents that might either directly or indirectly affect these modifications.

The assessment carried out for anticipated operational occurrences (AOOs) is essentially the same as that for design-basis accidents (DBAs) and requires many of the same conservative assumptions, especially those that relate to the structures, systems and components important to safety. Differences might exist, though, in the consideration of non-safety-related structures, systems and components in safety analyses of AOOs and DBAs.

### III. Scenarios for beyond-design-basis accidents

Accidents beyond the design basis (BDDBA: Beyond-Design-Basis Accident) are those that are not considered for design-basis accidents, but are considered in the design process of the plant in accordance with best-estimate methodology, and for which releases of radioactive material are kept within acceptable limits [IAEA, 2013]. Design-extension conditions can be divided into two general groups: (a) Those with a high enough probability of occurrence and sufficiently severe consequences, for which corrective or remedial actions have to be considered. This may be appropriate even though the probability of occurrence is lower than that of design-basis accidents. (b) Those that have a very low probability of occurrence, but potential consequences could be severe.

The distinction between design-basis accidents (DBA) and accidents beyond design basis is based on the probability of occurrence and the consequences. The distinction is significantly facility- or activity-dependent and site-dependent. If the probability of an accident occurring is considered to be unacceptably high, the design has to make provisions for preventing any significant consequences. If

the probability of occurrence of an accident is much lower but the consequences would be significant, it may be advisable to incorporate features into the design that accommodate this eventuality.

The set of representative fault sequences depends on the design of the facility. These sequences can result in substantial radiological consequences, including those with multiple component failures and/or wrong accident management. Important event sequences that could lead to serious accidents should be identified using a combination of probabilistic and deterministic methods and sound engineering judgement. The details of serious-accident sequences that have to be analysed are unique for each type of facility.

If necessary, the accident assessment should model the wide range of physical processes that could lead to a release of radioactive material to the environment or define the limiting criteria where a release can be assumed.

The assessment should generally be carried out using realistically conservative assumptions, representative data, best-estimate methods and decision criteria. Where this is not possible, reasonably conservative assumptions should be made that take account of the uncertainties in the understanding of any relevant physical process and equipment failure modes being modelled. However, it should be emphasised that the complexity of BDBAs might be such that assumptions made cannot be ensured to be conservative.

## Radiological impact assessment

The assessment of radiological impacts constitutes a major part of the safety case for a pre-disposal SNF management facility and related processes. Qualitative assessments and the quantitative analysis of possible challenges to the safety functions and the resulting potential radiological impacts have to be carried out by means of conceptual and mathematical models. The dose rates for the given assessment endpoint have to be calculated both for workers and the public. For accident scenarios, effective doses (Sv) covering the whole exposure time must be calculated, while for normal operation scenarios the annual effective doses (Sv/year) have to be considered. Doses from internal exposure are generally defined as committed effective doses affecting workers over a period of 50 years and the public over a period of 70 years. The exposure assessment differs from the hazard characterisation in that the assessments do not consider standardised conservative conditions, but realistic conditions expected to occur in the given scenario.

### 4.3. Accident scenarios for SNF during transport

It is assumed that, after dry interim storage, the SNF loaded in the transport and storage casks has to be moved from the interim storage facility to a conditioning facility. These transports must comply with the same requirements as the transports before dry interim storage. This applies to behaviour under normal transport conditions and in the event of transport accidents. The transport of fissile material is governed by the authorities of the individual countries, who generally comply with the requirements specified in IAEA SSR-6 [IAEA, 2018b].

The main focus of the related research activities is on the behaviour and performance of the cladding tubes, i.e. whether they remain intact, only let gas (noble gas and volatiles) escape or whether significant quantities of fissile material can escape from the cladding tubes in addition to the gas (see Chapter 3 for a more detailed description of these activities).

Since cladding tubes are exposed to significantly higher loads in the case of a transport accident than during handling under final conditioning, comparing the analysis of transport accidents can help to conservatively estimate potential SNF damage.

This section focuses on the U.S. NRC approach [NUREG, 2014] as well as on EPRI studies [EPRI, 2007]. The NRC Risk Assessment Report takes into account three different types of containers, various transport routes in the United States and extensive radiological analyses. The guidelines assume a 9-

m drop with an orientation that can cause the greatest damage to the transport/storage cask (TSC) (see Figure 19).

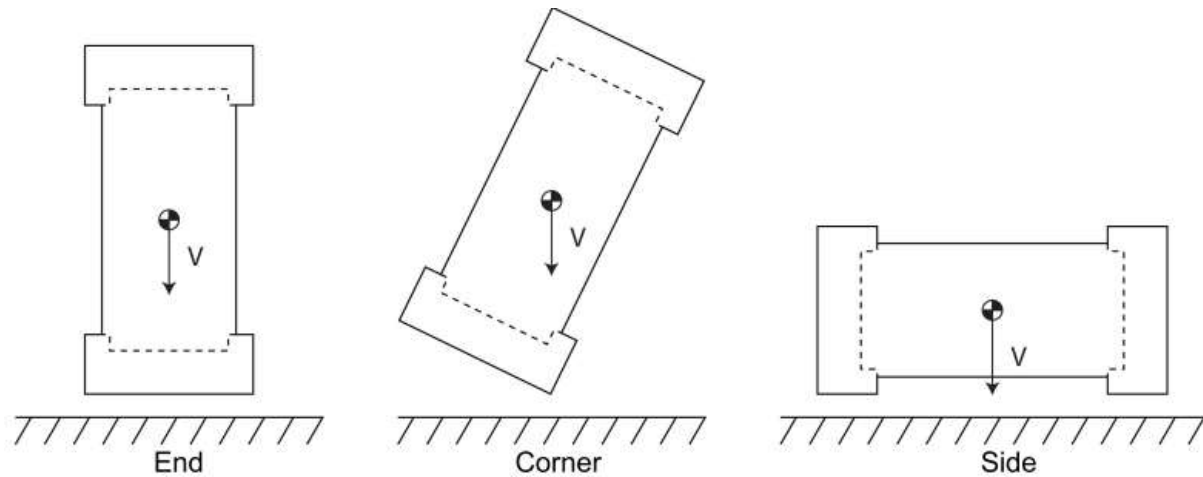


Figure 19 – Different orientations of the TSC for the drop from a 9-m height

[NUREG, 2014]

While a drop on the corner is considered worst for the cask, a drop on the side is more likely to damage the SNF. Therefore, the side case is used for the set of calculations. In the case of the end drop, the fuel rods are guided in the FA structure, which is why the possible failure-relevant bending of the fuel rods, according to the NUREG report, is severely restricted. In addition, the side-drop loads are more relevant in the case of settled formation of radial hydrides in the fuel cladding. The hydride reorientation describes the stress-related rearrangement of hydrides from an orientation in the circumferential direction or from an irregular arrangement into hydride rows which are radially oriented. Such radial hydrides can have an impact on the ductility properties of the cladding (above a certain threshold).

Figure 20 shows different loading modes of a fuel rod.

EPRI also worked extensively on the transport accident behaviour of spent fuel elements (see synthesis report [EPRI, 2007]). This study takes into account the failure modes and the failure criteria for the effects of transport accidents on the fuel rods, including changes in the material of the cladding tube during the dry storage period. The study covers normal transport conditions (falling from a height of 30 cm, according to 10 CFR 71) and accident conditions, as well as an analysis of the cladding behaviour during dry interim storage.

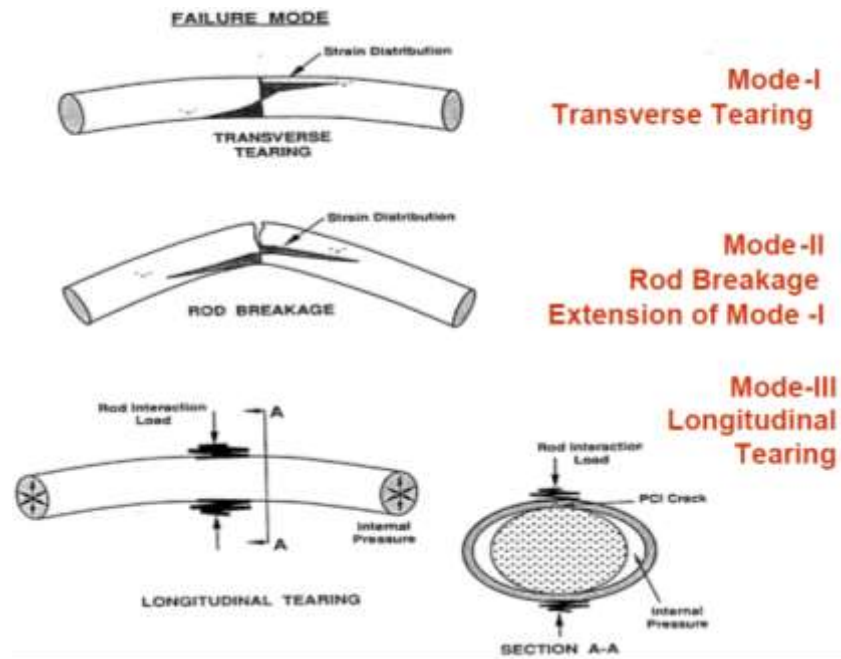


Figure 20 – Different loading modes of the fuel rod

Mode-I describes a bending load that leads to a crack (perpendicular to the rod axis). Mode-II describes the behaviour of the fuel rod under bending load when the above-mentioned crack has passed through the wall thickness: Mode-III describes the loading of the cladding tube under radial pressure (as in the ring compression test).

#### 4.4. Other accident scenarios and the way forward to the final SOTA report

Since this chapter aims to present a general overview, it focuses only on a few scenarios. At this stage, reporting on accident scenarios related to wet storage or other types of storage is not foreseen. Some of those scenarios are expected to be developed and analysed as part of the SFC project (within the framework of Task 4), e.g. hypothetical accidents occurring during fuel handling in a reference SNF encapsulation facility (e.g. FA drop outside TSC). The final SOTA report will include results from Task 4 activities and will thus expand this section to include consequence analysis and mitigation plans.

## 5. Acknowledgements

The authors express their gratitude to Laura Mc Manniman/IAEA and Márton Király/MTA-EK for their extremely valuable contributions to reviewing the manuscript. The authors are also grateful to Linda McKinley and Angela Paulsen/Nagra for the kindly providing comments and an English grammar check, and to Monica Storz/Nagra who supported us to a great extent in the finalisation of the report.

## 6. Conclusions

This report presented an overview of the status of knowledge in the field of spent nuclear fuel characterisation and assessment during the pre-disposal phase. The first part (Chapter 2) focused on the current safety-significant gaps and related challenges in characterisation of SNF properties in terms of source term and inventory assessment, such as neutron, gamma-ray emission, decay heat, radionuclide inventory and elemental content. The status of theoretical methods and codes for estimating the source terms, including their uncertainties, was reviewed and presented, revealing the maturity of these methodologies. However, the main problem in terms of the accurate prediction of source terms with reliable confidence limits is related to the input data, i.e. nuclear data and fuel irradiation history. To reduce bias effects and provide reliable covariance data, improved nuclear data are needed, which implies and requires a dedicated evaluation programme based on sensitivity studies and dedicated experiments. In addition, NDA measurement systems that can be used to verify and improve fuel history data were reviewed. Finally, the importance of experimental programmes (e.g. ARIANE, SKB-50 campaign, ...) and the SFCOMPO data base for code validation was discussed.

The second part of the report (Chapter 3) discussed the SNF in terms of out-of-core fuel performance, focusing on cladding performance and fuel integrity in view of the safety criteria for SNF interim storage, transport and canister packaging, analysing both numerical and experimental approaches and methodologies. The main aim was to report current progress regarding the behaviour of irradiated cladding, the phenomena ruling the potential SNF degradation and the fuel/cladding chemical interaction. Also, the ageing effect under conditions of extended interim storage, transport and emplacement in a final disposal system are considered through experimental as well as modelling studies. The chapter provided an overview of SNF experimental characterisation methodologies, from destructive assays to non-destructive assays.

The last part (Chapter 4) gave a partial status of knowledge on definition and screening of accident scenarios with respect to pre-disposal activities, such as fuel packaging and transport, on the basis of IAEA general assumptions.

This SOTA report is intended as an initial version, to be updated at the end of the WP to become the final SOTA report. The target of the final report is to become a key reference in the field and to gain high recognition and visibility as a key resource for knowledge management programmes and to contribute to demonstrating and documenting the state-of-the-art from a neutral and purely scientific viewpoint.

## A. Relevant Radionuclides

A list of relevant radionuclides for safety studies of a long-term storage installation for Belgian waste was set up by NIRAS/ONDRAF [Vandoorne, 2018]. These radionuclides, together with nuclear properties (half-life and decay mode) and the origin of these nuclides, are listed [Govers, 2019].

Nuclide	Half-life	Decay mode	Major source	Main location	Mostly present as
<sup>54</sup> Mn	312 d	β <sup>+</sup> , EC	<sup>54</sup> Fe	ST, CL, FU	AL/IM, AP
<sup>94</sup> Nb	2.00 10 <sup>4</sup> a	β <sup>-</sup>	<sup>93</sup> Nb	CL	AL, AP
<sup>59</sup> Ni	7.6 10 <sup>4</sup> a	β <sup>+</sup> , EC	<sup>58</sup> Ni	ST, CL, FU	AL/IM, AP
<sup>93</sup> Zr	1.53 10 <sup>6</sup> a	β <sup>-</sup>	<sup>92</sup> Zr, FP	FU, CL	FP, AL, AP.
<sup>63</sup> Ni	101 a	β <sup>-</sup>	<sup>62</sup> Ni	ST, CL, FU	AL/IM, AP
<sup>10</sup> Be	1.6 10 <sup>6</sup> a	β <sup>-</sup>	<sup>9</sup> Be	FU	IM, AP
<sup>14</sup> C	5700 a	β <sup>-</sup>	<sup>14</sup> N, <sup>13</sup> C	FU, CL	IM, AP
<sup>36</sup> Cl	3.01 10 <sup>5</sup> a	β <sup>-</sup> , β <sup>+</sup> , EC	<sup>35</sup> Cl	FU, CL	IM, AP
<sup>41</sup> Ca	1.03 10 <sup>5</sup> a	ec	<sup>40</sup> Ca	FU	IM, AP
<sup>60</sup> Co	5.27 a	β <sup>-</sup>	<sup>59</sup> Co	ST, CL, FU	IM, AP
<sup>93</sup> Mo	4000 a	EC	<sup>92</sup> Mo, <sup>93</sup> Nb	ST, CL	AL/IM, AP
<sup>108m</sup> Ag	418 a	β <sup>-</sup>	<sup>107</sup> Ag	FU, CL	IM, AP
<sup>110m</sup> Ag	250 d	β <sup>-</sup>	FP	FU	FP
<sup>125</sup> Sb	2.76 a	β <sup>-</sup>	FP, <sup>124</sup> Sb	FU, CL	AL/IM, AP, FP
<sup>3</sup> H	12.3 a	β <sup>-</sup>	FP	FU	FP
<sup>79</sup> Se	3.56 10 <sup>6</sup> a	β <sup>-</sup>	FP	FU	FP
<sup>85</sup> Kr	10.8 a	β <sup>-</sup>	FP	FU, plenum	FP
<sup>90</sup> Sr	28.8 a	β <sup>-</sup>	FP	FU	FP
<sup>99</sup> Tc	2.14 10 <sup>5</sup> a	β <sup>-</sup>	FP	FU	FP
<sup>106</sup> Ru	1.06 a	β <sup>-</sup>	FP	FU	FP
<sup>107</sup> Pd	6.5 10 <sup>6</sup> a	β <sup>-</sup>	FP	FU	FP
<sup>126</sup> Sn	2.3 10 <sup>5</sup> a	β <sup>-</sup>	FP	FU	FP
<sup>129</sup> I	1.61 10 <sup>7</sup> a	β <sup>-</sup>	FP	FU	FP

Nuclide	Half-life	Decay mode	Major source	Main location	Mostly present as
<sup>134</sup> Cs	2.07 a	β <sup>-</sup>	FP	FU	FP
<sup>135</sup> Cs	2.3 10 <sup>6</sup> a	β <sup>-</sup>	FP	FU	FP
<sup>137</sup> Cs	30.0 a	β <sup>-</sup>	FP	FU	FP
<sup>144</sup> Ce	285 d	β <sup>-</sup>	FP	FU	FP
<sup>147</sup> Pm	2.62 a	β <sup>-</sup>	FP	FU	FP
<sup>151</sup> Sm	90.0 a	β <sup>-</sup>	FP	FU	FP
<sup>154</sup> Eu	8.59 a	β <sup>-</sup>	FP	FU	FP
<sup>155</sup> Eu	4.75 a	β <sup>-</sup>	FP	FU	FP
<sup>226</sup> Ra	1600 a	β <sup>-</sup>	(4n+2) DS	FU	AC
<sup>229</sup> Th	7340 a	α	(4n+1) DS	FU	AC
<sup>230</sup> Th	7.54 10 <sup>4</sup> a	EC, β <sup>+</sup> , β <sup>-</sup> , α	(4n+2) DS	FU	AC
<sup>232</sup> Th	1.41 10 <sup>10</sup> a	α	(4n) DS	FU	AC
<sup>231</sup> Pa	3.28 10 <sup>4</sup> a	α	(4n+3) DS	FU	AC
<sup>233</sup> U	1.59 10 <sup>5</sup> a	α	(4n+1) DS	FU	AC
<sup>234</sup> U	2.46 10 <sup>5</sup> a	α	(4n+2) DS	FU	AC
<sup>235</sup> U	7.04 10 <sup>8</sup> a	α	Fabrication	FU	AC
<sup>236</sup> U	2.37 10 <sup>7</sup> a	α	<sup>235</sup> U	FU	AC
<sup>238</sup> U	4.47 10 <sup>9</sup> a	α	Fabrication	FU	AC
<sup>237</sup> Np	2.14 10 <sup>6</sup> a	α	<sup>236</sup> U, <sup>241</sup> Am	FU	AC
<sup>238</sup> Pu	87.7 a	α	<sup>237</sup> Np	FU	AC
<sup>239</sup> Pu	2.41 10 <sup>4</sup> a	α	<sup>238</sup> U	FU	AC
<sup>240</sup> Pu	6563 a	α	<sup>239</sup> Pu	FU	AC
<sup>241</sup> Pu	14.3 a	β <sup>-</sup>	<sup>240</sup> Pu	FU	AC
<sup>242</sup> Pu	3.74 10 <sup>5</sup> a	α	<sup>241</sup> Pu	FU	AC
<sup>244</sup> Pu	8.00 10 <sup>7</sup> a	α	<sup>242</sup> Pu	FU	AC
<sup>241</sup> Am	433 a	α	<sup>241</sup> Pu	FU	AC
<sup>242m</sup> Am	141 a	IT	<sup>241</sup> Pu	FU	AC

Nuclide	Half-life	Decay mode	Major source	Main location	Mostly present as
<sup>243</sup> Am	7365 a	α	<sup>242m</sup> Am, <sup>242</sup> Pu	FU	AC
<sup>242</sup> Cm	163 d	α	<sup>242m</sup> Am	FU	AC
<sup>243</sup> Cm	30.0 a	α	<sup>242</sup> Cm	FU	AC
<sup>244</sup> Cm	18 a	α	<sup>243</sup> Cm, <sup>244</sup> Am	FU	AC
<sup>245</sup> Cm	8500 a	α	<sup>244</sup> Cm	FU	AC
<sup>246</sup> Cm	4730 a	α	<sup>245</sup> Cm	FU	AC
<sup>247</sup> Cm	1.6 10 <sup>7</sup> a	α	<sup>246</sup> Cm	FU	AC
<sup>248</sup> Cm	3.4 10 <sup>5</sup> a	α	<sup>247</sup> Cm	FU	AC

EC: Electron Capture  
 IT: Isomeric Transition  
 DS: Decay series  
 FP: Fission Product  
 AL: Alloying  
 IM: Impurity  
 AP: Activation Product  
 ST: Structures  
 CL: Cladding  
 FU: Fuel

## References

- [Adkins, 2013] Adkins, H., Geelhood, K.J., Koeppel, B., Coleman, J., Bignell, J., Flores, G., Wang, J.-A., Sanborn, S., Spears, R., Klymyshyn, N.: Used Nuclear Fuel Loading and Structural Performance Under Normal Conditions of Transport – Demonstration of Approach and Results on Used Fuel Performance Characterization, 2013.
- [Agrenius, 2002] Agrenius, L.: Criticality safety calculations of storage canisters, Technical Report TR02-17, April 2002.
- [Álvarez-Velarde, 2014] Álvarez-Velarde, F., González-Romero, E.M., Rodríguez, I.M.: Validation of the burn-up code EVOLCODE 2.0 with PWR experimental data and with a Sensitivity/Uncertainty analysis, *Annals of Nuclear Energy*, 73 (2014) 175–188.
- [Ancius, 2019] Ancius, D., Aymanns, K., Checcis, P., Gonella, F., Jussofie, A., Montecassiano, F., Murtezi, M., Schwalbach, P., Schoop, K., Vanini, S., Zumerle, G.: Modelling of safeguards verification of spent fuel dry storage casks using muon trackers, *Proceedings 41th ESARDA Symposium*, 14 – 16 May 2019, Stresa, Italy, pp. 142–148, 2019.
- [Anderson, 1955a] Anderson, J.S., Roberts, L.E.J., Harper, E.A.: The oxides of uranium. Part VII: The oxidation of uranium dioxide. *Journal of the Chemical Society (resumed)*, pp. 3946–3959, 1955.
- [Anderson, 1955b] Anderson, J.S., Harper, E.A., Moorbatch, S., Roberts, L.E.J.: The properties and microstructure of uranium dioxide; their dependence upon the mode of preparation. UK Atomic Energy Authority Report, AERE C/R 886, 1955.
- [Andersson, 2016] Andersson, P., Holcombe, S., Tverberg, T.: "Inspection of a LOCA Test Rod at the Halden Reactor Project using Gamma Emission Tomography", *Conference Top Fuel 2016 – LWR Fuels with Enhanced Safety and Performance*, American Nuclear Society, 11 – 16 September 2016 Boise, Idaho, USA.
- [Andersson 2020] Andersson, P., Rathore, B., Senis, L., Anastasiadis, A., Sundén, E.A., Atak, H., Holcombe, S., Håkansson, A., Jansson P., Nyberg, J.: Simulation of the response of a segmented High-Purity Germanium detector for gamma emission tomography of nuclear fuel. Submitted for publication in *SN Applied Sciences*, 2020.
- [Arkoma, 2018] Arkoma, A., Huhtanen, R., Leppänen, J., Peltola, J., Pättikangas, T.: Calculation chain for the analysis of spent nuclear fuel in long-term interim dry storage. *Annals of Nuclear Energy*, Vol. 119, pp. 129–138, 2018.
- [ASTM 1969] ASTM, Standard Test Method for Atom Percent Fission in Uranium and Plutonium Fuel (Neodymium-148 Method), *Annual Book of ASTM Standards 12.02*, E321-69, 1969.
- [ASTM, 2010] ASTM 1562, Standard Guide for Evaluation of Materials Used in Extended Service of Interim Spent Nuclear Fuel Dry Storage Systems, *ASTM C1562-10*, 2010.
- [ASTM, 2012] ASTM, Standard Test Method for Atom Percent Fission in Uranium and Plutonium Fuel (Neodymium-148 Method), *Annual Book of ASTM Standards*, 12.02 E321-96, 2012,
- [Aures, 2017] Aures, A., Bostelmann, F., Hursin, M., Leray, O.: Benchmarking and application of the state-of-the-art uncertainty analysis methods XSUSA and SHARK-X, *Annals of Nuclear Energy* 101 (2017) 262–269.
- [Bae, 1994] Bae, K.K., Kim, B.G., Lee, Y.W., Yang, M.S., Park, H.S.: Oxidation behavior of unirradiated UO<sub>2</sub> pellets. *Journal of Nuclear Materials*, Vol. 209, pp. 274–279, 1994.
- [Baeten, 2003] Baeten, P., D'hondt, P., Sannen, L., Marloye, D., Lance, B., Renard, A., Bassellier, J.: The REBUS Experimental Programme for Burn-up Credit, *Proceedings of the 7<sup>th</sup> International Conference on Nuclear Criticality Safety (ICNC2003)*, Tokai-mura, Japan, 20 – 24 October 2003, JAERI – Conf 2003 – 019, pp. 645–649.

- [Bahadir, 2009] Bahadir, T., Lindahl, S.O.: Studsvik's next generation nodal code SIMULATE-5, in Proceedings of the ANFM-2009 conference, Advances in Nuclear Fuel Management IV, Hilton Head Island, South Carolina, USA, 2009.
- [Ballheimer, 2010] Ballheimer, V., Wille, F., Droste, B.: Mechanical safety analysis for high burn-up spent fuel assemblies under accident transport conditions. Packaging, Transport, Storage & Security of Radioactive Material, Vol. 21, pp. 212–217, 2010.
- [Ballheimer, 2016] Ballheimer, V., Wille, F., Sterthaus, J., Linnemann, K., Rolle, A., Vlassopoulos, E., Nasyrow, R., Papaioannou, D., Rondinella, V.V.: Analysis of parameters affecting the bending behavior of spent fuel rods. In: Proc. 18th International Symposium on the Packaging and Transportation of Radioactive Materials (PATRAM 2016), Kobe, Japan, September 18 – 23, 2016.
- [Bannister, 1968] Bannister, M.J.: The storage behaviour of uranium dioxide powders — review article. Journal of Nuclear Materials, Vol. 26, pp. 174–184, 1968.
- [Barnes, 1970] Barnes, B.K., Hom, D.M., Sanders, W.M., Clinton, D.D., Swansen, J.E.: Techniques for two-dimensional gamma-ray scanning of reactor fuel element sections, Nuclear Applications and Technology 9 (1970) 746 –754.
- [Barnes, 1982] Barnes, B.K., Phillips, J.R., Barnes, M.L.: Reconstruction of radial fission product distributions in reactor fuels from a small number of projections, Journal of Nuclear Materials 106 (1982) 147–156.
- [Bateman, 1910] Bateman, H.: The solution of a system of differential equations occurring in the theory of radioactive transformations, Proc. Cambridge Philos. Soc. 15 (1910) pp. 423–427.
- [Bé, 2015] Bé, M.M., Isnard, H., Cassette, P., Mougeot, X., Lourenço, V., Altitzoglou, T., Pommé, S., Rožkov, A., Auerbach, P., Sochorová, J., Dziel, T., Dersch, R., Kossert, K., Nähle, O., Krivošik, M., Ometáková, J., Stadelmann, G., Nonell, A., Chartier, F.: Determination of the  $^{141}\text{Sm}$  half-life, Radiochimica Acta 103 (2015) 619–626.
- [Becker, 2009] Becker, B., Dagan, R., Lohnert, G.: Proof and implementation of the stochastic formula for ideal gas, energy dependent scattering kernel, Annals of Nuclear Energy, 36 (2009) 470–474.
- [Belgonucléaire, 2000] Belgonucléaire, "ARIANE international programme final report", AR2000/15, BN Ref. 0000253/221, Rev. B, December 2000.
- [Bell, 1973] Bell, M.J.: ORIGEN – The ORNL isotope generation and depletion code, ORNL-4628, May 1973.
- [Berger, 2015] Berger, M.J.: ESTAR, PSTAR, and ASTAR", in: NIST, 2015. <http://physics.nist.gov/Star>.
- [Berndt, 1988] Berndt, R.: Verification of spent PWR fuel data using the  $^{154}\text{Eu}$ ,  $^{134}\text{Cs}$  and  $^{137}\text{Cs}$  activities, Kernenergie 31 (1988) 59–63.
- [Bertolino, 2003] Bertolino, G., Meyer, G., Iping, J.P.: Effects of hydrogen content and temperature on fracture toughness of Zircaloy-4. Journal of Nuclear Materials, Vol. 320, pp. 272–279, 2003.
- [Bevard, 2009] Bevard, B.B., Wagner, J.C., Parks, C.V., Aissa, M.: Review of information for spent nuclear fuel burnup confirmation, Report NUREG/CR-6998, December 2009.
- [Billone, 2013a] Billone, M.C., Burtseva, T.A., Han, Z., Liu, Y.Y.: Used fuel disposition campaign – embrittlement and DBTT of high-burnup PWR fuel cladding alloys. Report FCRD-UFD-2013-000401, ANL-13/16, Argonne National Laboratory, Lemont, 2013.
- [Billone, 2013b] Billone, M.C., Burtseva, T.A., Einziger, R.E.: Ductile-to-brittle transition temperature for high-burnup cladding alloys exposed to simulated drying-storage conditions. Journal of Nuclear Materials, Vol. 433, pp. 431–448, 2013.

[Billone, 2018] Billone, M.C., Burtseva, T.A.: Results of Ring Compression Tests – Spent Fuel and Waste Disposition. Report SFWD-SFWST-2018-000510, ANL-18/36, Argonne National Laboratory, Lemont, 2018.

[Billone, 2019] Billone, M.C.: Ductility of High-Burnup-Fuel ZIRLO™ following Drying and Storage – Spent Fuel and Waste Disposition. Report M2SF-19AN010201011, ANL-19/14, Argonne National Laboratory, Lemont, 2019.

[Bolind, 2014] Bolind, A.M.: Development of an analytical theory to describe the PNAR and CIPN nondestructive assay techniques, *Annals of Nuclear Energy* 66 (2014) 167–176.

[Bolind, 2015] Bolind A.M., Seya, M.: The State of the Art of Nondestructive Assay of Spent Nuclear Fuel Assemblies – A Critical Review of the Spent Fuel NDA Project of the U.S. Department of Energy's Next Generation Safeguards Initiative, JAEA-Review-2015-027, December 2015.

[Borella, 2017] Borella, A., Calleja, A., Fiorito, L.: Sensitivity studies on the production of Cm isotopes in spent fuel for safeguards applications, International Conference on Mathematics and Computational Methods Applied to Nuclear Science & Engineering, Jeju, Korea, April 16 – 20, 2017.

[Borms, 1999] Borms, L., Oeyen, J.: The design of a multipurpose tomography installation, *Nuclear Instruments and Methods in Physics Research A* 422 (1999) 489–492.

[Børresen, 2004] Børresen, S.: Spent Nuclear Fuel Analyses based on In-Core Fuel Management Calculations, in: PHYSOR-2004, Chicago, IL, USA, 2004.

[Borresen, 2014] Borresen, S.: Spent nuclear fuel analyses based on in-core fuel management calculations, in Proceedings of the PHYSOR-2014 conference (The Westin Miyako, Kyoto, Japan, 2014).

[Bosler, 1991] Bosler, G.E., Rinard, P.M.: Burnup measurements with the Los Alamos FORK detector, Report LA-UR-91-2508, December 1991.

[Bouffieux, 2001] Bouffieux, P., Leclercq, S., Cappelaere, C., Bredel, T.: Interim dry storage of PWR spent fuel assemblies – development of a long term creep law to assess the fuel cladding integrity. In: Proc. 8th international conference on radioactive waste management and environmental remediation (ICEM'01), Bruges, Belgium, Sep. 30 – Oct. 4, 2001.

[Boulanger, 2004] Boulanger, D., Lippens, M., Mertens, L., Basselier, J., Lance, B.: High Burnup PWR and BWR MOX Fuel Performance: A Review of Belgonucleaire Recent Experimental Programs, Proceedings. International Meeting LWR Fuel Performance, Orlando, Florida, September 19 – 22, 2004, American Nuclear Society, 2004.

[Bowman, 2011] Bowman, S.M.: SCALE 6: comprehensive nuclear safety analysis code system, *Nuclear Technology* 174 (2011) 126–146.

[Briesmeister, 2000] Briesmeister, J.F.: MCNP - A General Monte Carlo N-Particle Code, Program Manual, LA-13709-M, LANL (2000).

[Broadhead, 1995] Broadhead, B.L., DeHart, M.D., Ryman, J.C., Tang, J.S., Parks, C.V.: Investigation of Nuclide Importance to Functional Requirements Related to Transport and Long-Term Storage of LWR Spent Fuel, Report ORNL/TM-12742, 1995.

[Broustaut, 2012] Broustaut, M.: Benchmarking of the ALEPH Burn-Up code, SCK•CEN/36467063, 2012.

[Brun, 2015] Brun, E., Damian, F., Diop, C.M., Dumonteil, E., Hugot, F.X., Jouanne, C., Lee, Y.K., Malvagi, F., Mazzolo, A., Petit, O., Trama, J.C., Visonneau, T., Zoia, A.: TRIPOLI-4®, CEA, EDF and AREVA reference Monte Carlo code" *Annals of Nuclear Energy*, 82 (2015) 151–160.

[Buurveld, 1993] Buurveld, H.A., Dassel, G.: Emission Computer Tomography on a Dodewaard Mixed Oxide Fuel Pin, Report ECN-C-93065, Petten, 1993.

[Cabellos, 2011] Cabellos, O., Martinez, J.S., Diez, C.J.: Isotopic uncertainty assessment due to nuclear data uncertainties in high-burnup samples, International Conference on Nuclear Criticality, Edinburgh, 19 – 23 September 2011.

[Caldwell, 1986] Caldwell, J.T., Hastings, R.D., Herrera, G.C., Kunz, W.E., Shunk, E.R.: The Los Alamos second-generation system for passive and active neutron assays of drum-size containers, Report LA10774-MS, September 1986.

[Camp, 2002] Camp, D.C., Martz, H.E., Roberson, G.P., Decman, D.J., Bernardi, R.T.: Nondestructive waste-drum assay for transuranic content by gamma-ray active and passive computed tomography, Nuclear Instruments and Methods in Physics Research A495 (2002).

[Campbell, 1989] Campbell, T. K., Gilbert, E. R., White, G. D., Piepel, G. F. and Wrona, B. J.: Oxidation Behavior of Nonirradiated UO<sub>2</sub>, Nuclear Technology, vol. 85, pp. 160-171, 1989.

[Carlson, 2018] Carlson, A.D., Pronyaev, V.G., Capote, R. et al.: Evaluation of the neutron data standards, Nuclear Data Sheets 148 (2018) 143–188.

[Caruso, 2007] Caruso, S., Murphy, M., Jatuff, F., Chawla, R.: Validation of <sup>134</sup>Cs, <sup>137</sup>Cs and <sup>154</sup>Eu single ratios as burnup monitors for ultra-high burnup UO<sub>2</sub> fuel, Annals of Nuclear Energy 34 (2007) 28–35.

[Caruso, 2008] Caruso, S., Günther-Leopold, I., Murphy, M., Jatuff, F., Chawla, R.: Comparison of optimised germanium gamma spectrum try and multicollector inductively coupled plasma mass spectrometry for the determination of <sup>134</sup>Cs, <sup>137</sup>Cs and <sup>154</sup>Eu single ratios in highly-burnt UO<sub>2</sub>, Nuclear Instruments and Methods in Physics Research A589 (2008) 425–435.

[Caruso, 2009] Caruso, S., Murphy, M., Jatuff, F., Chawla, R.: Determination of within-rod caesium and europium isotopic distributions in high burnup fuel rods through computerised gamma-ray emission tomography, Nuclear Engineering and Design 239 (2009) 1220–1228.

[Caruso, 2014a] Caruso, S., Jatuff, F.: Design, development and utilisation of a tomography station for γ-ray emission and transmission analyses of light water reactor spent fuel rods, Progress in Nuclear Energy 72 (2014) 49–54.

[Caruso, 2014b] Caruso, S., Panadero, A.L.: Development and Validation of Ad Hoc ORIGEN-ARP Libraries for Very High Burnup UO<sub>2</sub> PWR Fuel with SCALE/TRITON, PHYSOR 2014, Kyoto, Japan, 28.09-03.10 2014.

[Caruso, 2016] Caruso, S.: Estimation of the radionuclide inventory in LWR spent fuel assembly structural materials for long-term safety analysis, EPJ Nuclear Science and Technology 2 (2016).

[Catherine, 2006] Catherine, C., Le Boulch, D., Carassou, S., Ramasubramanian, N., Lemaignan, C.: An internal conical mandrel technique for fracture toughness measurements on nuclear fuel cladding, Journal of Testing and Evaluation, Vol. 34, pp. 373–382, 2006.

[CEA, 2009] CEA, Nuclear fuels. Paris, 2009.

[Cetnar, 2000] Cetnar, J., Gronek, P.: BISON-C one dimensional transport and burnup calculation code with consideration of actinides and fission, Nuclear Science and Engineering, 134 (2000) 23–25.

[Cetnar, 2006] Cetnar, J.: General solution of Bateman equations for nuclear transformation, Annals of Nuclear Energy 33 (2006) 640–645.

[Chadwick, 2011] Chadwick, M.B. et al.: ENDF/B-VII.1 Nuclear Data for Science and Technology: Cross Sections, Covariances, Fission Product Yields and Decay Data, Nuclear Data Sheets. 112 (2011) 2887–2996. doi:10.1016/j.nds.2011.11.002.

[Chatzidakis, 2016] Chatzidakis, S., Choi, C.K., Tsoukalas, L.H.: Interaction of cosmic ray muons with spent fuel dry casks and determination of lower detection limit, Nuclear Instruments and Methods in Physics Research A 828 (2016) 37–45.

[Checchia, 2017] Checchia, P., Gonella, F., Rigoni, A., Vanini, S., Zumerle, G.: Muon tomography for

spent nuclear fuel control, ESARDA Bulletin 54 (2017) 2– 5.

[Checchia, 2018] Checchia, P., Ancius, D., Goonella, F., Zumerle, G., Aymanns, K., Erdmann, N. Schwalbach, P., Vanini, S.: Muography of spent fuel containers for Safeguards purposes, IAEA Symposium on International Safeguards, IAEA-CN-267–048, 2018.

[Choi, 1996] Choi, J.-W., McEachern, R.J., Taylor, P., Wood, D.D.: The effect of fission products on the rate of U<sub>3</sub>O<sub>8</sub> formation in SIMFUEL oxidized in air at 250°C. Journal of Nuclear Materials, Vol. 230, pp. 250–258, 1996.

[Choi, 2018] Choi, H. et al.: Benchmarking DRAGON/PARCS Against KRITZ and FFTF Measurements, Journal of Nuclear Technology 205 (2018) 486–505.

[Cobos, 1998] Cobos, J., Papaioannou, D., Spino, J., Coquerelle, M.: Phase characterisation of simulated high burn-up UO<sub>2</sub> fuel. Journal of Alloys and Compounds, Vol. 271–273, pp. 610–615, 1998.

[Coleman, 2014] Coleman, J.L., Spears, R.E.: Detailed PWR Fuel Rod and Grid Finite Element Analysis to Provide Equivalent Rod Stiffness and Damping and Equivalent Grid Shell Thickness to PWR Used Nuclear Fuel (UNF) Assembly – 14525 Idaho National Laboratory. In: Proc. Waste Management Symposia 2014 (WM2014), Phoenix, Arizona, USA, March 2 – 6, 2014.

[Courty, 2014] Courty, O., Motta, A.T., Hales, J.D.: Modeling and simulation of hydrogen behavior in Zircaloy-4 fuel cladding. Journal of Nuclear Materials, Vol. 452, pp. 311–320, 2014.

[Croff, 1983] Croff, A.G.: ORIGEN2: a versatile computer code for calculating the nuclide compositions and characteristics of nuclear materials, Nuclear Technology, 62 (1983) 335–352.

[Dagan, 2005] Dagan, R.: On the use of S(a,b) tables for nuclides with well pronounced resonances, Annals of Nuclear Energy 32 (2005) 367–377.

[Dallongeville, 2005] Dallongeville, M., Werle, J., McCreesh, G.: Fuel Integrity Project: Analysis of Results of Tests on Light Water Reactor Fuel Rods. Packaging, Transport, Storage & Security of Radioactive Material, Vol. 16, pp. 125–134, 2005.

[Dallongeville, 2010] Dallongeville, M., Zeachandirin, A., Purcell, P., Cory, A.: Finite elements analysis of intergrid bending tests on used fuel rods samples. In: Proc. 16th International Symposium on the Packaging and Transportation of Radioactive Materials (PATRAM 2010), London, UK, October 3–8, 2010.

[Dallongeville, 2012] Dallongeville, M., Zeachandirin, A., Laurent, M.: Simplified approach to study fuel rod rupture risks by bending or Euler buckling, Proc. 9th International Conference on the Radioactive Materials Transport and Storage (RAMTRANSPORT 2012), Kensington, London, UK, 22–24 May, 2012.

[Degueldre, 2016] Degueldre, C., Bertsch, J., Martin, M.: Post irradiation examination of nuclear fuel: Toward a complete analysis, Progress in Nuclear Energy 92 (2016) 242–253.

[Desquines, 2014] Desquines, J., Drouan, D., Billone, M., Puls, M.P., March, P., Fourgeaud, S., Getrey, C., Elbaz, V., Philippe, M.: Influence of temperature and hydrogen content on stress-induced radial hydride precipitation in Zircaloy-4 cladding. Journal of Nuclear Materials, 453, 131–150, 2014.

[Díez, 2015] Díez, C.J., Buss, O., Hofer, A., Porsch, D., Cabellos, O.: Comparison of nuclear data uncertainty propagation methodologies for PWR burn-up simulations, Annals of Nuclear Energy 77 (2015) 101–114.

[Dilg, 1973] Dilg, W., Mannhart, W., Steinchele, E., Arnold, P.: Precision neutron total cross section measurements on gold and cobalt in the 40 µeV – 5 meV range, Zeitschrift für Physik 264 (1973) 427–444.

[Dilg, 1974] Dilg, W., Mannhart, W.: Neutron total cross sections of Sc, V, Cu and Rh at µeV energies, Zeitschrift für Physik 266 (1974) 157–160.

[Dimitriou, 2014] Dimitriou, P., Nichols, A.L.: Total absorption gamma-ray spectroscopy for decay heat calculations and other applications, Summary report of a consultants' Meeting, 15 – 17 December 2014, IAEA, Vienna, INDC(NDS) – 0676.

[Dobrin, 1997] Dobrin, R., Craciunescu T., Tuturici, I.L.: The Analysis of Failed Nuclear Fuel Rods by Gamma Computed Tomography, *Journal of Nuclear Materials* 246 (1997) 37–42.

[Dokhane, 2018] Dokhane, A., Grandi, G., Vasiliev, A., Rochman, D., Ferroukhi, H.: Validation of PSI best estimate plus uncertainty methodology against SPERT-III reactivity initiated accident experiments, *Annals of Nuclear Energy* 118 (2018) 178.

[Donnelly, 2000] Donnelly, J.V. abd, Ovanes, M.: Validation of 3-Dimensional Neutron Transport Calculations of CANDU Reactivity Devices, 2000 ANS International Topical Meeting on Advances in Reactor Physics and Mathematics and Computation into the Next Millenium (PHYSOR 2000), May 7 – 12, 2000. Pittsburg, OA, USA, 2000.

[Dostal, 2015] Dostál, M., Klouzal, J., Valach, M., Magnusson, P., Corleoni, F.: FEM modelling of the expanding mandrel test simulating out-of-pile PCI SCC of fuel cladding. Proc. 23rd Conference on Structural Mechanics in Reactor Technology (SMiRT-23), Manchester, UK, August 10 – 14, 2015.

[Ducros, 1985] Ducros, G.: ISARD, a method of tomographic reconstruction of the position of gamma emitters in a nuclear fuel pin from transversal gamma scanning, *Nuclear Technology* 68 (1985) 370–384.

[Durham, 2018] Durham, J.M., Poulson, D., Bacon, J., Chichester, D.L., Guardincerri, E., Morris, L., Plaud-Ramos, K., Schwendiman, W., Tolman, J.D., Winston, P.: Verification of Spent Nuclear Fuel in Sealed Dry Storage Casks via Measurements of Cosmic-Ray Muon Scattering, *Physical Review Applied* 9 (2018) 044013.

[Ebiwonjumi, 2019] Ebiwonjumi, B., Choi, S., Lemaire, M., Lee, D., Shin, H.C., Lee, H.S.: Verification and validation of radiation source term capabilities in STREAM, *Annals of Nuclear Energy* 124 (2019) 80–87.

[Eigenbrodt, 2014] Eigenbrodt, J., Tobin, S.J., Charlton, W.S., Bolind, A.M., Menlove, H.O., Seya, M., Trelue, H.R.: PNAR Measurements of Fugen Fuel, 55<sup>th</sup> Annual Meeting of the Institute of Nuclear Materials Management, Atlanta, Georgia, 20 – 14 July 2014.

[Eigenbrodt, 2016] Eigenbrodt, J., Menlove, H.O.: Spent fuel measurements: passive neutron albedo reactivity (PNAR) and photon signatures, Report LA-UR-16-22112, May 2016.

[Eloirdi, 2018] Eloirdi, R., Cakir, P., Huber, F., Seibert, A., Konings, R., Gouder, T.: X-ray photoelectron spectroscopy study of the reduction and oxidation of uranium and cerium single oxide compared to (U-Ce) mixed oxide films. *Applied Surface Science*, Vol. 457, pp. 566–571, 2018.

[Elorrieta, 2016] Elorrieta, J. M., Bonales, L. J., Rodriguez-Villagra, N. Baonza, V. G., Cobos, J.: A detailed Raman and X-ray study of UO<sub>2+x</sub> oxides and related structure transitions. *Physical Chemistry Chemical Physics*, Vol. 18, pp. 28209–28216, 2016.

[Elorrieta, 2017] Elorrieta, J.M., Manara, D., Bonales, L.J., Vigier, J.F., Dieste, O., Naji, M., et al.: Raman study of the oxidation in (U, Pu)O<sub>2</sub> as a function of Pu content. *Journal of Nuclear Materials*, Vol. 495, pp. 484–491, 2017.

[Elorrieta, 2018a] Elorrieta, J.M., Bonales, L.J., Baonza, V.G., Cobos, J.: Temperature dependence of the Raman spectrum of UO<sub>2</sub>. *Journal of Nuclear Materials*, Vol. 503, pp. 191–194, 2018.

[Elorrieta, 2018b] Elorrieta, J.M., Bonales, L.J., Fernández, S., Rodríguez-Villagra, N., Cobos, J.: Pre- and post-oxidation Raman analysis of (U, Ce)O<sub>2</sub> oxides. *Journal of Nuclear Materials*, Vol. 508, pp. 116–122, 2018.

[EPRI, 2007] Spent Fuel Transportation Applications - Assessment of Cladding Performance under normal and hypothetical accident conditions, EPRI Synthesis Report 1015048, 2007.

- [Espriu-Gascon, 2015] Espriu-Gascon, A. Llorca, J., Domínguez, M., Giménez, J., Casas, I., de Pablo, J.: UO<sub>2</sub> surface oxidation by mixtures of water vapor and hydrogen as a function of temperature. *Journal of Nuclear Materials*, Vol. 467, pp. 240–243, 2015.
- [Ewing, 2015] Ewing, R. C.: Long-term storage of spent nuclear fuel. *Nat Mater*, Vol. 14, pp. 252–257, 2015.
- [Faridani, 2011] Faridani, M.N.: Classification and probabilistic model development for creep failures of structures: Study of X-70 carbon steel and 7075-T6 aluminum alloys. University of Maryland, 2011.
- [Feria, 2015] Feria, F., Herranz, L.E., Penalva, J.: On the way to enabling FRAPCON-3 to model spent fuel under dry storage conditions: the thermal evolution. *Annals of Nuclear Energy* 85, 995–1002, 2015.
- [Feria, 2017] Feria, F., Herranz, L.E.: Application of the BEPU methodology to assess fuel performance in dry storage. *Annals of Nuclear Energy*, 99, 240–246, 2017.
- [Feria, 2018] Feria, F., Herranz, L.E.: Effect of the oxidation front penetration on in-clad hydrogen migration. *Journal of Nuclear Materials*, Vol. 500, pp. 349–360, 2018.
- [Ferroukhi, 2008] Ferroukhi, H., Hofer, K., Hollard, J.M., Vasiliev, A., Zimmermann, M.A.: Core Modelling and Analysis of the Swiss Nuclear Power Plants for Qualified R& D Applications, in Proc. Int. Conf. on the Physics of Reactors, PHYSOR'08, 2008, Interlaken, Switzerland.
- [Fiorito, 2014] Fiorito, L., Diez, C.J., Cabellos, O., Stankovskiy, A., Van den Eynde, G., Labeau, P.S.: Fission yield covariance generation and uncertainty propagation through fission pulse decay heat calculation, *Annals of Nuclear Energy* 69 (2014) 331–343.
- [Fiorito, 2015] Fiorito, L., Piedra, D., Cabellos, O., Diez, C.J.: Inventory calculation and nuclear data uncertainty propagation on light water reactor fuel using ALEPH-2 and SCALE 6.2, *Annals of Nuclear Energy* 83 (2015) 137–146.
- [Fiorito, 2016] Fiorito, L., Stankovskiy, A., Van den Eynde, G., Diez, C.J., Cabellos, O. and Labeau, P.E.: Generation of fission yield covariances to correct discrepancies in the nuclear data libraries, *Annals of Nuclear Energy* 88 (2016) 12–23.
- [Fiorito, 2017] Fiorito, L., Žerovnik, G., Stankovskiy, A., van den Eynde, G., Labeau, P.E.: Nuclear data uncertainty propagation to integral responses using SANDY, *Annals of Nuclear Energy* 101 (2017) 359–366
- [Fiorito] Fiorito, L.: Private communication.
- [Foster,1987] Foster, J.P.: Segmented expanding mandrel test methods (letter to editors). *Journal of Nuclear Materials*, Vol. 150, pp. 342–350, 1987.
- [Fröhner, 2000] Fröhner, F.H.: Evaluation and analysis of nuclear resonance data, JEFF Report 18, NEA/OECD, 2000.
- [Fujino, 1992] Fujino, T., Sato, N.: Analyses of the oxygen potential of the solid solutions MyU<sub>1</sub>–yO<sub>2</sub>+x (M = M<sub>3</sub>+andM<sub>2</sub>+) by statistics of defects and defect complexes. *Journal of Nuclear Materials*, Vol. 189, pp. 103–115, 1992.
- [FY2014] FY 2014 Status Report : Quantification of CIRFT System Biases and Uncertainties When Testing High-Burnup Spent Nuclear Fuel, 2014.
- [FY2017] FY 2017 Status Report : CIRFT Data Update and Data Analyses for Spent Nuclear Fuel Vibration Reliability Study, 2017.
- [Gandini, 1975] Gandini, A.: Time-dependent generalized perturbation methods for burn-up analysis, NEACRP-L-130, 1975.

[Gauld, 2001] Gauld, I.C., Ryman, J.C.: Nuclide importance to criticality safety, decay heating, and source terms related to transport and interim storage of high-burnup LWR fuel, Report NUREG/CR-6700, January 2001.

[Gauld, 2003] Gauld, I.C.: Strategies for Applications of Isotopic Uncertainties in Burnup Credit, Report NUREG/CR-6811, June 2003.

[Gauld, 2005] Gauld, I.C. Mueller, D.E.: Evaluation of Cross-Section Sensitivities in Computing Burnup Credit Fission Product Concentrations, ORNL/TM-2005/48, August 2005.

[Gauld, 2006] Gauld, I.C., Bowman, S.M., Murphy, B.D., Schwalbach, P.: Applications of ORIGEN to spent fuel safeguards and non-proliferation", in Proceedings of the INMM 47<sup>th</sup> Annual Meeting, 16 – 20 July 2006, Nashville, Tennessee.

[Gauld, 2010] Gauld, I.C., Ilas, G., Murphy, B.D., Weber, C.F.: Validation of SCALE 5 decay heat predictions for LWR spent nuclear fuel, Report, TM-2008/015, February 2010.

[Gauld, 2011a] Gauld, I.C., Ilas, G., Radulescu, G.: Uncertainties in predicted isotopic compositions for high burnup PWR spent nuclear fuel, Report NUREG/CR-7012, January 2011.

[Gauld, 2011b] Gauld, I.C., Radulescu, G., Ilas, G., Murphy, B.D., Williams, M.L., Wiarda, D.: Isotopic depletion and decay methods and analysis capabilities in scale, Nuclear Technology 174 (2011) 169–195.

[Gauld, 2015] Gauld, J.C., Hu, J., DeBaere, P., Vaccaro, S., Schwalbach, P., Liljenfeldt, H., Tobin, S.: In-field performance testing of the FORK detector for quantitative spent fuel verification, in Proceedings of the 37<sup>th</sup> Annual ESARDA Symposium, Manchester, 2015.

[Gauld, 2016] Gauld, I.C., Giaquinto, J.M., Delashmitt, J.S., Hu, J., Ilas, G., Haverlock, T.J., Romano, C.: Re-evaluation of spent nuclear fuel assay data for the Three Mile Island unit reactor 1 and application to code validation, Annals of Nuclear Energy 87 (2016) 267–281.

[Gauld, 2017] Gauld, I.C., Williams, M.L., Michel-Sendis, F., Martinez, J.S.: Integral nuclear data validation using experimental spent nuclear fuel compositions, Nuclear Engineering and Technology 49 (2017) 1226–1233.

[Gauld, 2019] Gauld, I.C. Merturek, U.: Validation of BWR spent nuclear fuel isotopic predictions with applications to burnup credit, Nuclear Engineering and Design 345 (2019) 110–124.

[Geelhood, 2015] Geelhood, K.J., Luscher, W.G., Raynaud, P.A., Porter, I.E.: FRAPCON-4.0: A Computer Code for the Calculation of Steady-State, Thermal–Mechanical Behavior of Oxide Fuel Rods for High Burnup. PNNL-19418, Vol. 1, Rev. 2, 2015.

[Gérard, 2018] Gérard, D.: Validation expérimentale du code ALEPH2 d'évolution du combustible pour le calcul de chaleur résiduelle, UCL 17217, 2018.

[Gómez, 2008] Gómez, F., Quiñones, J., Iglesias, E., Rodriguez, N.: Dependence of the specific surface area of the nuclear fuel with the matrix oxidation. In: ATALANTE 2008: Nuclear Fuel Cycle for a Sustainable Future, Montpellier, France, 2008.

[Gomez, 2017] Gomez, F.J., Rengel, M.A.M., Ruiz-Hervias, J., Puerta, M.A.: Study of the hoop fracture behaviour of nuclear fuel cladding from ring compression tests by means of non-linear optimization techniques. Journal of Nuclear Materials, Vol. 489, pp. 150–57, 2017.

[Govers, 2015] Govers, K., Dobney, A., Gysemans, M., Verwerft, M.: Technical scope of the REGAL base program, Revision 1.2, External Report SCK•CEN-ER-110, January 2015.

[Govers, 2019] Govers, K., Boulanger, D., Meert, K., Leinders, G., Verwerft, M.: Characterization of Belgian spent fuel assemblies, SCK•CEN, Mol, Report BLG-1142, 2019.

- [Grandi, 2011] Grandi, G., Lindahl, S.O.: Benchmark of SIMULATE5 thermal hydraulics against the Frigg and NUPEC full bundle test experiments, International Topical Meeting on Nuclear Reactor Thermalhydraulics, Toronto, Ontario (Canada), 25 – 30 September 2011, NURETH-14.
- [Gruel, 2011] Gruel, A., Leconte, P., Bernard, D., Archier, P., Noguère, G.: Interpretation of Fission Product Oscillations in the MINERVE Reactor, from Thermal to Eprithermal Spectra, Nuclear Science and Engineering 169 (2011) 229–244.
- [Guerin, 2013] Guerin, C., Laporte, T., Cappelaere, C., Vaille, C., Mongabure, P., Miquet, A., Bouffieux, P.: CAST3M modelling of a spent fuel assembly bending during a handling accident. Rod failure risk evaluation from the experimental results of spent fuel rod bending test, Mechanics & Industry, Vol. 305, pp. 301–305, 2013.
- [Haeck, 2012] Haeck, W., Cochet, B., Aguiar, L.: Monte Carlo depletion calculations using VESTA 2.1 new features and perspectives, International Conference on the Physics of Reactors 2012, PHYSOR 2012, Advances in Reactor Physics.
- [Hairer, 1996] Hairer, E., Wanner, G.: 'Solving Ordinary Differential Equations II: Stiff and Differential-Algebraic Problems', Springer Series in Computational Mathematics 14, Springer-Verlag, Second Edition (1996).
- [Hairer, 1999] Hairer, E., Wanner, G.: Stiff differential equations solved by Radau methods, Journal of Computational and Applied Mathematics 111 (1999) 93–111.
- [Hales, 2016] Hales, J.D., Gamble, K. A., Spencer, B. W., Novascone, S. R., Pastore, G., Liu, W., Stafford, D. S., Williamson, R. L., Perez, D. M., Gardner, R. J., Casagrande, A., Galloway, J., Matthews, C., Unal, C., Carlson, N.: BISON Users Manual, BISON Release 1.3. INL/MIS-13-30307 Rev. 3, 2016.
- [Ham, 2011] Ham, Y.S., Sitaraman, S.: Partial defect tester: a novel approach to detect partial defects in pressurized water reactor spent fuel, Nuclear Technology 175 (2011) 401–418.
- [Ham, 2015] Ham, Y., Sitaraman, S., Kerr, P., Rossa, R.: Partial defect verification of spent fuel assemblies by PDET: principle and field testing in interim fuel storage facility (CLAB) Sweden, ANIMMA conference, April 2015.
- [Ham, 2019] Ham, Y., Sitaraman S., Kerr, P.: Verification of spent fuel inside dry storage casks using fast neutrons, ESARDA Bulletin 59 (2019) 47–56.
- [Hanson, 1998] Hanson, B.D.: The Burnup Dependence of Light Water Reactor Spent Fuel Oxidation. Report PNNL-11929, Pacific Northwest National Laboratory, 1998.
- [Hanson, 2003] Hanson, B.D., Cumblidge, S.E., Scheele, R.D., Sell, R.L.: The Effect of Rare Earth Dopants on UO<sub>2</sub> Oxidation. United States, 2003.
- [Hanson, 2012] Hanson, B., Alsaed, H., Stockman, C., Enos, D., Meyer, R., Sorenson, K.: Gap analysis to support extended storage of used nuclear fuel. Report PNNL-20509, Pacific Northwest National Laboratory, 2012.
- [Harkness, 2018] Harkness, Zhu, T., Liang, Y., Rauch, E., Enqvist, A., Jordan, K.A.: Development of neutron energy spectral signatures for passive monitoring of spent fuel nuclear fuels in dry cask storage, EPJ Web of Conferences 170 (2018) 07004.
- [Hautamäki, 2000] Hautamäki, J., Tiitta, A.: Spent fuel verification options for final repository safeguards in Finland, STUK-YTO – TR 173, December 2000.
- [Hébert, 2006] Hébert, A.: 'Towards DRAGON Version4', Proceedings of Topical Meeting on Advances in Nuclear Analysis and Simulation (PHYSOR), Vancouver, Canada, September 10 – 14, 2006.

[Heck, 1974] Heck, D., Börner, H.R., Rousille, R.: Neutron capture cross section of  $^{147}\text{Nd}$ , *Atomkernenergie* 24 (1974) 141.

[Henzl, 2013] Henzl, V., Croft, S., Richard, J., Swinhoe, M.T., Tobin, S.J.: Determination of the plutonium content in a spent fuel assembly by passive and active interrogation using a differential die-away instrument", *Nuclear Instruments and Methods in Physics Research A* 712 (2013) 83–92.

[Herb, 2014] Herb, J., Sievers, J., Sonnenburg, H.G.: A new cladding embrittlement criterion derived from ring compression tests, *Nuclear Engineering and Design*, Vol. 273, pp. 615–630, 2014.

[Herranz, 2009] Herranz, E., Fera, F.: Spent fuel rod splitting due to  $\text{UO}_2$  oxidation during dry storage: Assessment of the database. *Progress in Nuclear Energy*, Vol. 51, pp. 201–206, 2009.

[Herranz, 2010] Herranz, L.E., Fera, F.: Extension of the FRAPCON-3.3 creep model to dry storage conditions. *Progress in Nuclear Energy* 52, 634–639, 2010.

[Herrero, 2015] Herrero, J.J., Pecchia, M., Ferrouki, H., Canepaad, S., Vasiliev, A., Caruso, S.: Computational Scheme for Burnup Credit Applied to Long Term Waste Disposal, *Proceeding International Conference on Nuclear Criticality Safety, ICNC 2015, Charlotte, US, 2015.*

[Herrero, 2017] Herrero, J.J., Vasiliev, A., Pecchia, M., Rochman, D., Ferroukhi, H., Johnson, L., Caruso, S.: Criticality Safety Assessment for Geological Disposal of spent Fuel using the PSI BUCSS R Methodology, *Nagra Arbeitsbericht NAB 17-23, October 2017.*

[Hicks, 2018] Hicks, T.W., Baldwin, T.D.: Review of Burn-up Credit Applications in Criticality Safety Assessments for Spent Fuel Management and Disposal, *Contractor Report to RWM, Contractor Report no. GSL-1649-4-V3.1, January 2018.*

[Higham, 2005] Higham, N.J.: The scaling and squaring method for the matrix exponential revisited, *SIAM Journal on Matrix Analysis and Applications*, 2 (2005) 1179–1193.

[Higham, 2009] Higham, N.: *Cholesky Factorization*, Vol. 1, John Wiley & Sons, Inc., 2009, pp. 251–254.

[Hirose, 2012] Hirose, T., Ozawa, M., Miura, H., Baba, T., Kamimura, K.: Dynamic load impact tests on high burnup spent fuel rods of BWR and PWR. In: *Proc. The Nuclear Materials Conference (NuMat 2012), Osaka, Japan, 2012.*

[Hirose, 2013] Hirose, T., Ozawa, M., Miura, H., Baba, T., Kamimura, K.: Research on integrity of high burnup spent fuel under long term dry storage and transport. In: *OECD/NEA International Workshop on Safety of Long Term Interim Storage Facilities, Munich, Germany, 2013.*

[Hoekstra, 1961] Hoekstra, H.R., Santoro, A., Siegel, S.: The low temperature oxidation of  $\text{UO}_2$  and  $\text{U}_4\text{O}_9$ . *Journal of Inorganic and Nuclear Chemistry*, Vol. 18, pp. 166–178, 1961.

[Holcombe, 2015] Holcombe, S., Jacobsson, S., Svärd, J., Hallstadius, L.: A novel gamma emission tomography instrument for enhanced fuel characterization capabilities within the OECD Halden Reactor Project, *Annals of Nuclear Energy* 85 (2015) 837–845.

[Holcombe, 2016] Holcombe, S., Andersson, P., Svärd, S.J., Hallstadius, L.: Determination of the rod-wise fission gas release fraction in a complete fuel assembly using non-destructive gamma emission, *Nuclear Instruments and Methods in Physics Research A* 337 (2016) 99–108.

[Hong, 2002] Hong, I.S.: Validation of DRAGON code in Connection with WIMS-AECL/RFSP Code System based on ENDF/B-VI Library and Two Group Model, *Report KAERI/TR-2218/2002, Korean Atomic Energy Research Institute (2002).*

[Honkamaa, 2014] Honkamaa, T., Lévy, F., Berndt, R., Schwalbach, P., Vaccaro, S., Turunen, A.: A Prototype for Passive Gamma Emission Tomography, *Symposium on International Safeguards, IAEA, Vienna, 2014.*

- [Hsu, 2012] Hsu, H.H., Tsay, L.W.: Fracture properties of hydrided Zircaloy-4 cladding in recrystallization and stress-relief anneal conditions. *Journal of Nuclear Materials*, Vol. 422, pp. 116–123, 2012.
- [Hu, 2014] Hu, J., Gauld, I.C.: Impact of nuclear data uncertainties on calculated spent fuel nuclide inventories and advanced NDA instrument response, *ESARDA Bulletin 51 (2014)* 9–18.
- [Hu, 2016] Hu, J., Gauld, I.C., Peterson, J.L., Bowman, S.M.: "US commercial spent nuclear fuel assembly characteristics: 1968 – 2013", Report NUREG/CR-7227, September 2016.
- [Hu, 2017] Hu, J., Giaquinto, J.M., Gauld, I.C., Ilas, G., Keever, T.J.: Analysis of new measurements of Calvert Cliffs spent fuel samples using SCALE 6.2, *Annals of Nuclear Energy* 106 (2017) 221–234.
- [Hue, 1978] Hue, S.T., Crane, T.W., Talbert Jr. W.L., Lee, J.C.: Nondestructive assay methods for irradiated nuclear fuels, Report LA – 6923, January 1978.
- [Hykes, 2013] Hykes, J.M., Ferrer, R.M.: Solving the Bateman equations in CASMO5 using implicit ODE numerical methods for stiff systems, M&C 2013, International Conference on Mathematics & Computational Methods Applied to Nuclear Science & Engineering, Sun Valley, Idaho, US, 5 – 9 May, 2013.
- [IAEA, 2009] International Atomic Energy Agency, *Predisposal Management of Radioactive Waste*, IAEA Safety Standards Series No. GSR Part 5, IAEA, Vienna, 2009.
- [IAEA, 2013] International Atomic Energy Agency, *General Safety Guide GSG-3, "The Safety Case and Safety Assessment for the Predisposal Management of Radioactive Waste"*, 2013.
- [IAEA, 2015] IAEA: *Final Report CRP Spent Fuel Performance Final Report of a Coordinated Assessment and Research SPAR III (2009 – 2014)*. IAEA-Tecdoc-1771, IAEA, Vienna, 2015.
- [IAEA, 2016] International Atomic Energy Agency, *Safety Assessment for Facilities and Activities*, IAEA Safety Standards Series No. GSR Part 4 – Rev.1, IAEA, Vienna, 2016.
- [IAEA, 2018a] IAEA Safeguards, *Research and Development Plan, Enhancing capabilities for nuclear verification*, Report STR-385, January 2018.
- [IAEA, 2018b] IAEA Safety Standards SSR-6 Rev.1 "Regulations for the Safe Transport of Radioactive Material", 2018.
- [IAEA, 2019a] IAEA: *Behaviour of spent power reactor fuel during storage extracts from the final reports of coordinated research projects on behaviour of spent fuel assemblies in storage (BEFAST I–III) and spent fuel performance assessment and research (SPAR I–III) – 1981–2014*. IAEA-Tecdoc-1862, Vienna, 2019.
- [IAEA, 2019b] IAEA: *Demonstrating Performance of Spent Fuel and Related Storage System Components during Very Long Term Storage*, Vienna, 2019.
- [IAEA, 2020] IAEA Safety Standards SSG-15 "Storage of Spent Nuclear Fuel (Rev.1)", 2020.
- [Iglesias, 2008] Iglesias, E., Quiñones, J.: Analogous materials for studying spent nuclear fuel: The influence of particle size distribution on the specific surface area of irradiated nuclear fuel. *Applied surface science*, Vol. 254, pp. 6890–6896, 2008.
- [Ilas, 2008] Ilas, G., Gauld, I.C.: SCALE analysis of CLAB decay heat measurements for LWR spent fuel assemblies, *Annals of Nuclear Energy* 35 (2008) 37–48.
- [Ilas, 2010] Ilas, G., Gauld, I.C., Murphy, B.D.: Analysis of experimental data for high burnup PWR spent fuel isotopic validation) ARIANE and REBUS programs (UO<sub>2</sub> fuel), Report NUREG/CR-6969, February 2010.
- [Ilas, 2011] Ilas, G., Gauld, I.C.: Analysis of experimental data for high-burnup PWR spent fuel isotopic validation – Vandellós II reactor, Report NUREG/CR – 7013, January 2011.
- [Ilas, 2012] Ilas, G., Gauld, I.C., Radulescu, G.: Validation of new depletion capabilities and ENDF/B-

VII data libraries in SCALE, *Annals of Nuclear Energy* 46 (2012) 43–55.

[Ilas, 2014] Ilas, G., Gauld, I.C., Lijenfeldt, H.: Validation of ORIGEN for LWR used fuel decay heat analysis with SCALE, *Nuclear Engineering and Design* 273 (2014) 58–67.

[Ilas, 2017] Ilas, G., Liljenfeldt, H.: Decay heat uncertainty for BWR used fuel due to modeling and nuclear data uncertainties, *Nuclear Engineering and Design* 319 (2017) 176–184.

[ISO 7438, 2016] ISO 7438:2016. Metallic materials - Bend test.

[Isotalo, 2011] Isotalo, A.E., Aarnio, P.A.: Comparison of depletion algorithms for large systems of nuclides, *Annals of Nuclear Energy* 38 (2011) 261–268.

[Isotalo, 2015] Isotalo, A.E., Wieselquist, W.A.: A method for including external feed in depletion calculations with CRAM and implementation in ORIGEN, *Annals of Nuclear Energy* 85 (2015) 68–77.

[Isotalo, 2016] Isotalo, A., Pusa, M.: Improving the accuracy of the Chebyshev Rational Approximation Method using substeps, *Nuclear Science and Engineering* 183 (2016) 65–77.

[Ito, 2004] Ito, K., Kamimura, K., Tsukuda, Y.: Evaluation of irradiation effect on spent fuel cladding creep properties. *Proceedings of the 2004 International Meeting on LWR Fuel Performance*, Orlando, Florida, September 19 – 22, 2004.

[Ivanov, 2013] Ivanov, K., Avramorva, M., Kamerow, S., Kodeli, I., Sartori, E., Ivanov, E., Cabellos, O.: Benchmarks for Uncertainty Analysis in Modelling (UAM) for the design, operation and safety analysis of LWRs, *NEA/NSC/DOC(2013)7*, May 2013.

[Jaboulay, 2012] Jaboulay, J.C., Bourganel, S.: Analysis of MERCI decay heat measurements for PWR UO<sub>2</sub> fuel rod, *Nuclear Technology* 177 (2012) 73–82.

[Jansson, 2020] Jansson, P., Bengtsson, M., Bäckström, U., Svensson, K., Lycksell, M., Sjöland, A.: Data from calorimetric decay heat measurements of five used PWR 17x17 nuclear fuel assemblies, *Data in Brief* 28 (2020) 104917.

[Jaynes, 1968] Jaynes, J.E.T.: Prior Probabilities, *IEEE T. Syst. Sci. Cyb.*, 4 (1968) 227–241.

[Jessee, 2014] Jessee, M.A., Wieselquist, W.A., et. al.: Polaris: A New Two-Dimensional Lattice Physics Analysis Capability for the SCALE Code System, *PHYSOR 2014*, Kyoto, Japan.

[Jiang, 2014] Jiang, H., Wang, J.J.: Methodology for mechanical property testing of fuel cladding using an expanding plug wedge test. *Journal of Nuclear Materials*, Vol. 446, pp. 27–37, 2014

[Jiang, 2016a] Jiang, H., Wang, J.A.J.: Spent nuclear fuel system dynamic stability under normal conditions of transportation. *Nuclear Engineering and Design*, Vol. 310, pp. 1–14, 2016.

[Jiang, 2016b] Jiang, H., Wang, J.A.J., Wang, H.: The impact of interface bonding efficiency on high-burnup spent nuclear fuel dynamic performance. *Nuclear Engineering and Design*, Vol. 309, pp. 40–52, 2016.

[Jordan, 2008] Jordan, K.A., Gozani, T., J. Vujic, J.: Differential die-away analysis system response modeling and detector design, *Nuclear Instruments and Methods in Physics Research A* 598 (2008) 436 – 444.

[Jung, 2013] Jung, H., Shukla, P., Ahn, T., Tipton, L., Das, K., He, X., et al.: Extended storage and transportation: Evaluation of drying adequacy. In: *14th International High-Level Radioactive Waste Management Conference (IHLRWMC)*, Albuquerque, New Mexico, 2013.

[Kaiser, 2018] Kaiser, R.: Muography: overview and future directions, *Philosophical Transactions A* 377 (2018) 20180049.

[Kamimura, 2003] Kamimura, K., Kohno, N., Itoh, K., Tsukuda, Y., Aomi, M., Yasuda, T., Murai, K., Fujii, H., Irida, Y.: Thermal creep tests of BWR and PWR spent fuel cladding. Proc. International conference on storage of spent fuel from power reactors (Vienna, Austria, 2-6 Jun 2003), pp. 50–51, 2003.

[Kamimura, 2004] Ito, K., Kamimura, K., Tsukuda, Y.: Evaluation of irradiation effect on spent fuel cladding creep properties. Proc. 2004 International Meeting on LWR Fuel Performance, Orlando, Florida, September 19 – 22, 2004.

[Kapklan, 2014] Kapklan, A.C., Henzl, V., Menlove, H.O., Swinhoe, M.T., Belian, A.P., Flaska, M., Pozzi, S.A.: Determination of total plutonium content in spent nuclear fuel assemblies with the differential die-away self-interrogation instrument, Nuclear Instruments and Methods in Physics Research A 764 (2014) 347–351.

[Kashima, 2015] Kashima, T., Suyama, K., Mochizuli, H.: Validation of burnup calculation code SWAT4 by evaluation of isotopic composition data of mixed oxide fuel irradiated in pressurized water reactor, Energy Procedia 71 (2015) 159–167.

[Kellett, 2017] Kellett, M.A., Bersillon, O.: The Decay Data Evaluation Project (DDEP) and the JEFF-3.3 radioactive decay data library: combining international collaborative effort on evaluated data, EPJ Web of Conferences 146 (2017) 02009.

[Kępisty, 2007] Kępisty, G., Cetnar, J.: On the discrepancies between FIMA and specific burnup", Progress in Nuclear Energy 98 (2007) 187–192.

[Kilgour, 1992] Kilgour, W.J., White, R.J., Shea, J.H., Turnbull, J.A.: The ENIGMA fuel performance code, code description, version 5.8d. Berkeley Nuclear Laboratories, TD/NS/REP/0035, 1992.

[Kim, 1995] Kim, H.S., Yoon, Y.K., Lee, Y.W.: Defect structures of  $U_{1-y}Er_yO_{2-x}$  solid solutions. Journal of Nuclear Materials, Vol. 226, pp. 206–215, 1995.

[Kim, 2001] Kim, J.-G., Ha, Y.-K., Park, S.-D., Jee, K.-Y., Kim, W.-H.: Effect of a trivalent dopant, Gd<sup>3+</sup>, on the oxidation of uranium dioxide. Journal of Nuclear Materials, Vol. 297, pp. 327–331, 2001.

[Kim, 2007] Kim, J.S., Jeon, Y.S., Park, S.D., Han, S.H., Kim, J.G.: Burnup determination of high burnup a dry processed fuels based on isotope dilution mass spectrometric measurements, Journal of Nuclear Science and Technology, 44 (2007) 1015–1023.

[Kim, 2015] Kim, J.S., Jeon, Y.S., Park, S.D., Ha, Y.K., Song, K.: Analysis of high burnup pressurized water reactor fuel using uranium, plutonium, neodymium and cesium isotope correlations with burnup, Nuclear Energy Technology 47 (2015) 924–933.

[Kleykamp, 1979] Kleykamp, H.: The chemical state of LWR high-power rods under irradiation. Journal of Nuclear Materials, Vol. 84, pp. 109–117, 1979.

[Koch, 1981] Koch, J.L., Schoof, S.: The Isotope Correlation Experiment ICE – Final Report, Technical Report EUR 7766 EN, 1981.

[Kodeli, 2001] Kodeli, I.: Multidimensional deterministic nuclear data sensitivity and uncertainty code system: method and application, Nuclear Science and Engineering 138 (2001) 45–66.

[Koning, 2012] Koning, A.J., Rochman, D.: Modern Nuclear Data Evaluation with the TALYS Code System, Nuclear Data Sheets. 113 (2012) 2841–2934. doi:10.1016/j.nds.2012.11.002.

[Kromar, 2015] Kromar, M., Kurinčič, B.: Determination of the NPP Krško Spent Fuel Activity, Proceedings of 24th International Conference Nuclear Energy for New Europe – NENE 2015, Portorož, Slovenia, 2015, pp. 410.1-410.9.

[Kromar, 2017] Kromar, M., Kurinčič, B.: Determination of the NPP Krško spent fuel decay heat, Proceedings of AIP conference: Thermophysics 2017, 22nd International Meeting of Thermophysics 2017, Terchova, Slovakia, 2017, pp. 050005-1.

[Kromar, 2019] Kromar, M., Kurinčič, B.: Determination of the NPP Krško spent fuel characteristics with

the Serpent and SCALE code systems, Proceedings of the 28th International Conference Nuclear Energy for New Europe – NENE 2019, Portorož, Slovenia, 2019 (to be published).

[Krzykacz, 1994] Krzykacz, B., Hofer, E., Kloos, M.: A Software System for Probabilistic Uncertainty and Sensitivity Analysis of Results from Computer Models, Proceedings of International Conference on Probabilistic Safety Assessment and Management (PSAM-II), San Diego, USA, 1994.

[Kum, 2018] Kum, O.: Development of easy-to-use interface for nuclear transmutation computing, VCINDER code, Nuclear Engineering and Technology 50 (2018) 25–34.

[Kvashnina, 2013] Kvashnina, K.O., Butorin, S.M., Martin, P., Glatzel, P.: Chemical State of Complex Uranium Oxides. Physical Review Letters, Vol. 111, p. 253002, 2013.

[Lahaye, 2017] Lahaye, S., Tsilanizara, A., Bellier, P., Bittar, T.: Implementation of a CRAM solver in MENDEL depletion code system, M&C 2017, International Conference on Mathematics & Computational Methods Applied to Nuclear Science and Engineering, Jeju, Korea, 16 – 20 April, 2017.

[Langlade, 2006] Langlade, C., Bouffioux, P., Clavel, M.: Fracture toughness of hydrided Zircaloy-4 experimental and numerical study. Springer Netherlands, Dordrecht, pp. 1133–1134, 2006.

[Lassmann, 1977] Lassmann, K., Moreno, A.: The light-water-reactor version of the URANUS integral fuel-rod code, Atomkernenergie, Vol. 30, p. 207–215, 1977.

[Le Saux, 2015] Le Saux, M., Besson, J., Carassou, S.: A model to describe the mechanical behavior and the ductile failure of hydrided Zircaloy-4 fuel claddings between 25 °C and 480 °C. Journal of Nuclear Materials, Vol. 466, pp. 43–55, 2015.

[Lebrun, 2001a] Lebrun, A., Bignan, G.: Nondestructive Assay of Nuclear Low-Enriched Uranium Spent Fuels for Burnup Credit Application, Nuclear Technology 13 (2001) 216–229.

[Lebrun, 2001b] Lebrun, A., Merelli, M., Szabo, J.L., Huver, M., Arlt, R., Areans-Carrasco, J.: SMOPY a new NDA tool for safeguards of LEU and MOX spent fuel, Report IAEA-SM-367/CD, IAEA, 2001.

[Lebrun, 2013] Lebrun, A., Jung, S., Zykov, S., Berlizov, A.: Status of NDA techniques in use for IAEA verification of light water reactor spent fuel, in: Proceedings of the 54<sup>th</sup> Annual Meeting of the Institute of Nuclear Materials Management, INMM 2013, Atlanta, Georgia, July 2013.

[Lee, 1982] Lee, D.M., Lindqvist, L.O.: Self-interrogation of spent fuel, Report LA-9494-MS, August 1982

[Lee, 2015] Lee, Y.G., Jagenbrein, S., Kamy, S., Kamy, S.A., Ahn, S.H., Kim, K.H., Park, J.B., Lee, N.Y.: Development of "Fission Chamber Free" Fork Detector (FDET) for Safeguards Measures on LWR Spent Fuel Assemblies, Report IAEA-CN-220, March 2015.

[Leinders, 2016a] Leinders, G., Pakarinen, J., Delville, R., Cardinaels, T., Binnemans, K., Verwerft, M.: Low-Temperature Oxidation of Fine UO<sub>2</sub> Powders: A Process of Nanosized Domain Development. Inorganic Chemistry, Vol. 55, pp. 3915–3927, 2016.

[Leinders, 2016b] Leinders, G., Delville, R., Pakarinen, J., Cardinaels, T., Binnemans, K., Verwerft, M.: Assessment of the U<sub>3</sub>O<sub>7</sub> Crystal Structure by X-ray and Electron Diffraction. Inorganic Chemistry, Vol. 55, pp. 9923–9936, 2016.

[Leinders, 2016c] Leinders, G.: Low-temperature oxidation of fine UO<sub>2</sub> powders. KU Leuven, Belgium, 2016.

[Leppänen, 2010] Leppänen, J.: Performance of Woodcock delta-tracking in lattice physics applications using the Serpent Monte Carlo reactor physics burnup calculation code, Annals of Nuclear Energy 37 (2010) 715–722.

[Leppänen, 2015a] Leppänen, J.: Serpent – a Continuous-energy Monte Carlo Reactor Physics Burnup Calculation Code, User's Manual, VTT Technical Research Centre of Finland (2015a).

[Leppänen, 2015b] Leppänen, J., Pusa, M., Viitanen, T., Valtavirta, V., Kaltiaisenaho, T.: 'The Serpent

Monte Carlo code: Status, development and applications in 2013,' *Annals Nuclear Energy* 82 (2015b) 142–150.

[Leray, 2016] Leray, O., Rochman, D., Grimm, P., Ferroukhi, H., Vasiliev, A., Hursin, M., Perret, G., Pautz, A.: Nuclear data uncertainty propagation on spent fuel nuclide compositions, *Annals of Nuclear Energy* 94 (2016) 603–611.

[Leray, 2017a] Leray, O., Ferroukhi, H., Hursin, M., Vasiliev, A., Rochman, D.: Methodology for Core Analyses with Nuclear Data Uncertainty Quantification and Application to Swiss PWR Operated Cycles, *Annals of Nuclear Energy* 110 (2017) 547.

[Leray, 2017b] Leray, O., Fiorito, L., Rochman, D., Ferroukhi, H., Stankovskiy, A., Van den Eynde, G.: Uncertainty propagation of fission product yields to nuclide composition and decay heat for a PWR UO<sub>2</sub> fuel assembly, *Progress in Nuclear Energy* 101 (2017) 488–495.

[Lévy, 1993] Lévy, F., Dési, S., Tarvainen, M., Arlt, R.: Use of high energy gamma emission tomography for partial defect verification of spent fuel assemblies, Report STUK-YTO-TR 56, November 1993.

[Lindgren, 2019] Lindgren, S., af Ekenstam, G., Hildingsson, L., Fagerholm, R., Sjöland, A., Stål, J.O.: Aspects on declared accountancy data for the Final Spent Fuel Disposal in Sweden, Presented at the 41<sup>st</sup> ESARDA annual meeting symposium on safeguards and nuclear material management, 14 – 16 May, Stresa, Italy, 2019.

[Lyon, 2018] Lyon, W., Mai, A, Liu, W., Capps, N., Rashid, J., Machiels, A., Waldrop, K.: Impact of Fuel-Cladding Bonding on the Response of High Burnup Spent Fuel Subjected to Transportation Accidents. Top Fuel meeting, paper A0118, 2018.

[Ma, 2019] Ma, F., Kopecky, S., Alaerts, G., Harada, H., Heyse, J., Kitatani, F., Noguere, G., Paradela, C., Šalamon, L., Schillebeeckx, P., Tsuchiya, H, Wynants, R.: Non-destructive analysis of samples with a complex geometry by NRTA, accepted for publication in *Journal of Analytical and Atomic Spectrometry* (2019).

[MacFarlane, 2010] MacFarlane, R.E., Kahler, A.C.: Methods for processing ENDF/B-VII with NJOY, *Nuclear Data Sheets* 111 (2010) 2739–2890.

[Maeda, 2004] Maeda, S., Sekine, T., Aoyala, T.: Measurement and analysis of decay heat of fast reactor spent MOX fuel, *Annals of Nuclear Energy* 31 (2004) 1119–1133.

[Martin, 1948] Martin, G.L.: The deterioration of UO<sub>2</sub> in storage. Mallinckrodt Chemical Works, USA, 1948.

[Martin, 2007] Martin, O., Nilsson, K.F., Györi, C., van Uffelen, P., Schubert, A.: Creep Simulation of Nuclear Fuel Cladding under long term storage conditions with TRANSURANUS. JRC Scientific and Technical Reports, EUR 23926 EN, 2007.

[Martin, 2011] Martin, N.: Application de la méthode des sous-groupes au calcul Monte-Carlo multigroupe, EPM PhD Thesis, 2011.

[Martinik, 2015] Martinik, T., Henzl, V., Grape, S., Svärd, S.J., Jansson, P., Swinhoe, M.T., Tobin, S.J.: Simulation of differential die-away instrument's response of asymmetrically burned spent nuclear fuel, *Nuclear Instruments and Methods in Physics Research A* 788 (2015) 79–85.

[Martinik, 2016] Martinik, T., Henzl, V., Grape, S., Jansson, P., Swinhoe, M.T., Goodsell, A.V., Tobin, S.J.: Design of a prototype Differential Die-Away instrument proposed for Swedish spent nuclear fuel characterization, *Nuclear Instruments and Methods in Physics Research A* 821 (2016) 55–65.

- [Martin-Rengel, 2012] Martin-Rengel, M.A., Sanchez, F.J.G., Ruiz-Hervias, J., Caballero, L., Valiente, A.: Revisiting the method to obtain the mechanical properties of hydrided fuel cladding in the hoop direction. *Journal of Nuclear Materials*, Vol. 429, pp. 276–283, 2012.
- [Martin-Rengel, 2013] Martin-Rengel, M.A., Sanchez, F.J.G., Ruiz-Hervias, J., Caballero, L.: Determination of the hoop fracture properties of unirradiated hydrogen-charged nuclear fuel cladding from ring compression tests. *Journal of Nuclear Materials*, Vol. 436, pp. 123–129, 2013.
- [Martin-Rengel, 2017] Martin-Rengel, M.A., Gomez, F.J., Rico, A., Ruiz-Hervias, J., Rodriguez, J.: Obtention of the constitutive equation of hydride blisters in fuel cladding from nanoindentation tests. *Journal of Nuclear Materials*, Vol. 487, pp. 220–228, 2017.
- [Massih, 2018] Massih, A.R.: UO<sub>2</sub> fuel oxidation and fission gas release. Quantum Technologies AB. Uppsala Science Park, Uppsala, Sweden, 2018.
- [Massinon, 2018] Massinon, L.: Validation of ALEPH2 depletion code on the spent fuel isotopic content of samples irradiated in Gösgen PWR core, UCL 13305, 2018.
- [Matsson, 1997] Matsson, I., Grapengiesser, B.: Developments in gamma scanning of irradiated nuclear fuel, *Applied Radiation Isotopes* 48 (1997) 1289–1298.
- [Mayuzumi, 1990] Mayuzumi, M., Onchi, T.: Creep deformation of an unirradiated Zircaloy nuclear fuel cladding tube under dry storage conditions. *Journal of Nuclear Materials*, Vol. 171, 1990, p. 381–388, 1990.
- [McEachern, 1998] McEachern, R.J., Taylor, P.: A review of the oxidation of uranium dioxide at temperatures below 400°C. *Journal of Nuclear Materials*, Vol. 254, pp. 87–121, 1998.
- [McKinnon, 1986] McKinnon, M.A., Doman, J.W., Heeb, C.M., Creer, J.M.: Monticello BWR spent fuel assembly decay heat predictions and measurements, Report PNL-5799, June 1986.
- [Menlove, 1997] Menlove, H.O., Beddingfield, D.H.: Passive neutron reactivity measurement technique. In *Proceedings of the Institute of Nuclear Materials Management Annual Meeting*, 1997.
- [Menlove, 2009] Menlove, H.O., Menlove, S.H., Tobin, S.J.: Fissile and fertile nuclear material measurements using a new differential die-away-self-interrogation technique, *Nuclear Instruments and Methods in Physics Research A* 602 (2009) 588–593.
- [Michel-Sendis, 2017] Michel-Sendis, F. et al.: SFCOMPO-2.0: An OECD NEA database of spent nuclear fuel isotopic assays, reactor design specifications, and operating data, *Annals of Nuclear Energy* 110 (2017) 779–788.
- [Minamoto, 2011] Minamoto, H., Yasuda, T., Nakatsuka, M., Kawamura, S.: Buckling behavior of fuel rods under impact loads (numerical study on the effect of material properties). *Nihon Kikai Gakkai Ronbunshu, A Hen/Transactions of the Japan Society of Mechanical Engineers, Part A*, Vol. 77, pp. 16–26, 2011.
- [Minamoto, 2015] Minamoto, H., Nakatsuka, M.: Numerical analysis on the dynamic response of nuclear fuel rods under side drop loading. *Transactions of the JSME (in Japanese)*, Vol. 81, pp. 14–00676, 2015.
- [Moler, 2003] Moler, C., Van Loan, C.: Nineteen dubious ways to compute the exponential of a matrix, twenty-five years later, *SIAM Review* (2003) 3–49.
- [Mongiello, 2013] Mongiello, R., Finch, R., Baldwin, G.: Safeguards approaches for geological repositories: status and gap analysis, Technical report, SAND 2013-5185P, June 2013.
- [Moore, 1995] Moore, L., Schnitzler, B.G., Wemple, C.A., Babcock, R.S., Wessol, D.E.: MOCUP: MCNP-ORIGEN2 coupled utility program, INEL-95/0523, September 1995.
- [Morgan, 2015] Morgan, L.W.G., Kotlyar, D.: 'Weighted-delta-tracking for Monte Carlo particle transport,' *Annals of Nuclear Energy* 85 (2015) 1184–1188.

[Murphy, 2009] Murphy, B.D., Gauld, I.C.: Spent fuel decay heat measurements performed at the Swedish central interim storage facility, Report NUREG/CR-6971, June 2009.

[Nagai, 1983] Nagai, M., Shimada, S., Nishimura, S., Amano, K.: Elucidating the iodine stress corrosion cracking (SCC) process for zircaloy tubing. Pellet Cladding Interaction in Water Reactor Fuel, International Working Group On Water Reactor Fuel Performance and Technology, IWGFPT/18, Proceedings of IAEA Specialists' Meeting (3 – 5 October 1983, Seattle, USA), pp. 89–102, 1983.

[Nakatsuka, 1987] Nakatsuka, M., Nagai, M.: Reduction of plastic anisotropy of zircaloy cladding by neutron irradiation (I). Journal of Nuclear Science and Technology, Vol. 24, pp. 832–838, 1987.

[Nasyrow, 2016] Nasyrow, R., Papaioannou, D., Rondinella, V.V., Vlassopoulos, E., Linnemann, K., Ballheimer, V., Sterthaus, J., Rolle, A., Wille, F., Caruso, S.: Bending test device for mechanical integrity studies of spent nuclear fuel rods, In: Proc. 18th International Symposium on the Packaging and Transportation of Radioactive Materials (PATRAM 2016), Kobe, Japan, September 18–23, 2016.

[NEA, 2007] NEA/OECD, WPEC Subgroup 25, "Assessment of fission product decay data for decay heat calculations", Nuclear Science Report, NEA/WPEC-25, ISBN 978-92-64-99034-0, 2007.

[NEA, 2011] NEA Nuclear Science Committee, "Spent Nuclear Fuel Assay Data for Isotopic Validation, State-of-the-art Report", Nuclear Science, NEA/NSC/WPNC/DOC(2011)5, June 2011.

[NEA, 2018] OECD-NEA, Pellet-Clad Interaction (PCI) in Water-Cooled Reactors, Vol. NEA/CSNI/R (2018) 9, 2018.

[Newman, 2009] Newman, C., Hansen, G., Gaston, D.: Three dimensional coupled simulation of thermomechanics, heat, and oxygen diffusion in UO<sub>2</sub> nuclear fuel rods. Journal of Nuclear Materials, Vol. 392, pp. 6–15, 2009.

[Nichols, 2002] Nichols, A.L.: Nuclear data requirements for decay heat calculations, Lectures at the Workshop on Nuclear Reaction Data and Nuclear Reactors: Physics, Design and Safety, Trieste, Italy, 25 February – 28 March 2002.

[Niemeyer, 2016] Niemeyer, I., Deissmann, G.: Bridging nuclear safety, security and safeguards at geological disposal of high-level radioactive waste and spent nuclear fuel, Presented at the International Conference on the Safety of Radioactive Waste Management, Vienna, Austria, 21 – 25 November 2016.

[Nilsson, 2010] Nilsson, K.F., Jaksic, N., Vokal, V.: An elasto-plastic fracture mechanics based model for assessment of hydride embrittlement in zircaloy cladding tubes. Journal of Nuclear Materials, Vol. 396, pp. 71–85, 2010.

[Nilsson, 2011] Nilsson, K.-F., Martin, O., Chenel-Ramos, C., Mendes, J.: The segmented expanding cone-mandrel test revisited as material characterization and component test for fuel claddings. Nuclear Engineering and Design, Vol. 241, pp. 445–458, 2011.

[Nobrega, 1985] Nobrega, B.N., King, J.S., Was, G.S., Wisner, S.B.: Improvements in the design and analysis of the segmented expanding mandrel test. Journal of Nuclear Materials, Vol. 131, pp. 99–104, 1985.

[Norris, 1983] Norris, D.I.R., Kay, P.: Oxygen potential and lattice parameter measurements in (U, Ce)O<sub>2</sub> – zirconia. Journal of Nuclear Materials, Vol. 116, pp. 184–194, 1983.

[NRC, 2014] US NRC: Identification and Prioritization of the Technical Information Needs Affecting Potential Regulation of Extended Storage and Transportation of Spent Nuclear Fuel. Washington, DC, 2014. <https://www.nrc.gov/docs/ML1404/ML14043A423.pdf>.

[NRC, 2019] US NRC: Managing Aging Processes In Storage (MAPS) Report. Washington, DC, 2019.

[NSFPOISG, 2006] N. S. F. P. O. I. S. G.-22: Potential rod splitting due to exposure to an oxidizing atmosphere during short-term cask loading operations in LWR or other uranium oxide based fuel. ed., 2006.

[NUREG, 2014] Spent Fuel Transportation Risk Assessment, U.S. NRC NUREG-2125, 01/2014.

[Olander, 1976] Olander, D.R.: Fundamental aspects of nuclear reactor fuel elements, chapter 15. In: Technical Information Center - Energy Research and Development Administration, ed. University of California, Berkeley, 1976.

[Olander, 1999] Olander, D.R., Soo Kim, Y., Wang, W.-E., Yagnik, S.K.: Steam oxidation of fuel in defective LWR rods. *Journal of Nuclear Materials*, Vol. 270, pp. 11–20, 1999.

[Olsen, 2018] Olsen, A.M., Schwerdt, I.J., Richards, B., McDonald, L.W.: Quantification of high temperature oxidation of U<sub>3</sub>O<sub>8</sub> and UO<sub>2</sub>. *Journal of Nuclear Materials*, Vol. 508, pp. 574–582, 2018.

[Ortensi, 2010] Ortensi, J. et al.: Deterministic Modeling of the High Temperature Test Reactor, INL/EXT-10-18969, Idaho National Laboratories, 2010.

[Ozawa, 2013] Ozawa, M., Hirose, T., Miura, H., Baba, T., Kamimura, K., Yasuda, T., Murakami, T.K., Shinohara, Y.: Fuel rod mechanical performance under dynamic load condition on high burn-up spent fuel of BWR and PWR. In: Proc. 17th International Symposium on the Packaging and Transportation of Radioactive Materials (PATRAM 2016), San Francisco, California, USA, August 18 – 25, 2013.

[Papaioannou, 2009b] Papaioannou, D., Nasyrow, R., Rondinella, V.V.: Fuel release experiments on irradiated fuel rodlets under transient impact conditions. Report JRC-ITU-TPW-2009/01, Joint Research Centre of the European Commission, Karlsruhe, 2009.

[Papaioannou, 2009c] Papaioannou, D., Nasyrow, R., Rondinella, V.V., Goll, W., Winkler, H.P., Liedtke, R., Hoffmann, D.: Fuel release experiments on irradiated fuel rodlets under transient impact conditions. Proc. KTG 2009, May 12-14, 2009, Dresden, Germany, INIS Vol.42, INIS Issue.16, 2009.

[Park, 1992] Park, K., Olander, D.R.: Defect models for the oxygen potentials of gadolinium-and europium-doped urania. *Journal of Nuclear Materials*, Vol. 187, pp. 89–96, 1992.

[Parker, 2015] Parker, H., Joyce, M.J.: The use of ionising radiation to image nuclear fuel: A review, *Progress in Nuclear Energy* 85 (2015) 297–318.

[Patterson, 2015] Patterson, C., Garzarolli, F.: Dry Storage Handbook. Performance of Spent Nuclear Fuel during Dry Storage, 2015.

[Peerani, 2007] Peerani, P., Galletta, M.: Re-establishment of the continuity of knowledge in the safeguards interim storages using NDA techniques, *Nuclear Engineering and Design* 237 (2007) 94–99.

[Petit, 2008] Petit, O., Hugot, F.X., Lee, Y.K., Jouanne, C., Mazzolo, A.: TRIPOLI-4 version 4 User Guide, Report CEA-R-6169, E. Brun, E. dumonteil and F. Malvagi, "Systematic uncertainty due to statistics in Monte Carlo burnup codes: application to a simple benchmark with TRIPOLI-4-D, Janvier 2008.

[Phillips, 1979] Phillips, J.R.: Passive Nondestructive Assay of Nuclear Materials, LA-UR-90-732, p. 529.

[Phillips, 1983] Phillips, J.R., Bosler, G.E., Halbig, J.K., Klosterbuer, S.F., Menlove, H.O., Rinard, P.M.: Experience using a spent fuel measurement system, *Nuclear Materials Management XII* (1983) 175–181.

[Poston, 1999] Poston, D.L., Trellue, H.R.: User's Manual, Version 2.0 for MONTEBURNS Version 1.0, LA-UR-99-4999, September 1999.

- [Poulson, 2018] Poulson, D., Bacon, J., Durham, M., Guardincerri, E., Morris, C.L., Trelue, H.R.: Application of muon tomography to fuel cask monitoring, *Philosophical Transactions A* 377 (2018) 20180052.
- [Purcell, 2004] Purcell, P.C., Dallongeville, M: Testing of Lwr Fuel Rods to Support Criticality Safety Analysis of Transport Accident Conditions. *Packaging, Transport, Storage & Security of Radioactive Material*, Vol. 15, pp. 265–272, 2004.
- [Pusa, 2010] Pusa, M., Leppänen, J.: Computing the matrix exponential in burnup calculations", *Nuclear Science and Engineering* 164 (2010) 140–150.
- [Pusa, 2013] Pusa, M., Leppänen, J.: Solving linear systems with sparse Gaussian elimination in the Chebyshev Rational Approximation Method, *Nuclear Science and Engineering* 175 (2013) 250–258.
- [Pusa, 2016] Pusa, M.: Higher-order Chebyshev Rational Approximation Method and applications to burnup equations, *Nuclear Science and Engineering* 182 (2016) 297–318.
- [Puse, 2011] Pusa, M.: Rational approximations to the matrix exponential in burnup calculations, *Nuclear Science and Engineering* 169 (2011) 155–167.
- [Ramthum, 1967] Ramthum, H.: Microcalorimetric determination of the mean  $\beta$ -energy of  $^{90}\text{Sr} + ^{90}\text{Y}$ , *Proceedings of a Symposium on Standardisation of radionuclides*, 10 – 14 October 1967, IAEA Vienna (AU), pp. 589–599.
- [Rashid, 2004a] Rashid, J.Y.R., Machiels, J.: A methodology for the evaluation of fuel rod failures under transportation accidents. In: *Proc. 14th International Symposium on the Packaging and Transportation of Radioactive Materials (PATRAM 2004)*, Berlin, Germany, September 19 – 24, 2004.
- [Rashid, 2004b] Rashid, J., Rashid, D.R.M.: Failure Criteria for Zircaloy Cladding Using a Damage-based Metal/Hydride Mixture Model. EPRI, Palo Alto, CA, 1009693, 2004.
- [Rashid, 2004c] Rashid, J., Rashid, D.R.M.: Development of a Metal/Hydride Mixture Model for Zircaloy Cladding With Mixed Hydride Structure. EPRI, Palo Alto, CA, 1009694, 2004.
- [Rearden, 2011] Rearden, B.T., Williams, M.L., Jesse, M.A., Mueller, D.E., Wiarda, D.A.: Sensitivity and uncertainty analysis capabilities and data in SCALE, *Nuclear Technology* 174 (2011) 236–288.
- [Rearden, 2015] Rearden, B., Bekar, K., Celik, C., Clarno, K., Dunn, M., Hart, S., Ibrahim, A., Johnson, S., Langley, B., Lefebvre, J., Lefebvre, R., Marshall, W., Mertzyurek, U., Mueller, D., Peplow, D., Perfetti, C., Petrie, L., Thompson, A., Wiarda, D., Wieselquist, W., Williams, M.: Criticality safety enhancements for SCALE 6.2 and beyond, *Proceedings of ICNC 2015*, Charlotte, NC, USA, 2015, pp. 1255–1269
- [Rearden, 2016] Rearden, B.T., Jesse, M.A.: SCALE Code System, ORNL/TM-2005/39 Version 6.2, April 2016.
- [Rhodes, 2006] Rhodes, J., Smith, K., Lee, D.: CASMO-5 development and applications, in *Proceedings of the PHYSOR-2006 conference, ANS Topical Meeting on Reactor Physics*, Vancouver, BC, Canada, 2006, p. B144.
- [Rimpler, 2002] Rimpler, A.: Bonner sphere neutron spectrometry at spent fuel casks, *Nuclear Instruments and Methods in Physics Research A* 476 (2002) 468–473.
- [Rinard, 1988] Rinard, P.M., Bosler, G.E.: Safeguarding LWR spent fuel with the FORK detector, Report LA-11096-MS, March 1988.
- [Ro, 2009] Ro, T.I.K., Danon, Y., Liu, E., Barry, D., Dagan, R.: Measurements of the Neutron Scattering Spectrum from U238 and Comparison of the results with a Calculation at the 36.68-eV Resonance, *Journal of the Korean Physical Society* Vol. 55 No.4 October 2009.
- [Rochman, 2011] Rochman, D., Koning, A.J., van der Marck, S.C., Sciolla, C.M.: Nuclear data uncertainty propagation: perturbation vs. Monte Carlo, *Annals of Nuclear Energy* 38 (2011) 942–952.

- [Rochman, 2013] Rochman, D., Sciolla, C.M.: Nuclear data uncertainty propagation for a typical PWR fuel assembly with burnup, *Nuclear Engineering and Technology* 46 (2013) 353–362.
- [Rochman, 2016a] Rochman, D., Leray, O., Perret, G., Vasiliev, A., Ferroukhi, H., Koning, A.J.: Re-evaluation of the thermal neutron capture cross section of  $^{147}\text{Nd}$ , *Annals of Nuclear Energy* 94 (2016) 612–617.
- [Rochman, 2016b] Rochman, D., Leray, O., Vasiliev, A., Ferroukhi, H., Koning, A.J., Fleming, M., Sublet, J.C.: A Bayesian Monte Carlo method for fission yield covariance information, *Annals of Nuclear Energy* 95 (2016) 215–134.
- [Rochman, 2018a] Rochman, D., Vasiliev, A., Ferroukhi H., Pecchia, M.: Consistent criticality and radiation studies of Swiss spent nuclear fuel: the CS2M approach, *Journal of Hazardous Materials* 357 (2018) 384.
- [Rochman, 2018b] Rochman, D.A., Vasiliev, A., Dkhane, A., Ferroukhi, H.: Uncertainties for Swiss LWR spent nuclear fuels due to nuclear data, *European Physics Journal Nuclear Science and Technology*, 4 (2018) 6–15.
- [Rochman, 2019a] Rochman, D.: Validation of CASMO5/SIMULATE5 models for KKB2 from Cycle 12 to Cycle 42, PSI Internal Report, TM-41-18-22, April 2019.
- [Rochman, 2019b] Rochman, D.: Validation of CASMO5/SIMULATE5 models for KKB1 from Cycle 16 to Cycle 42, PSI Internal Report, TM-41-18-21, April 2019.
- [Rochman, 2020a] Rochman, D., Dokhane, A., Vasiliev, A., Ferroukhi, H., Hursin, M.: Nuclear data uncertainties for Swiss BWR spent nuclear fuel characteristics, to be published in EPJ, 2020.
- [Rochman, 2020b] Rochman, D., Vasiliev, A., Ferroukhi, H., Seidl, M., Basualdo, J.: Improvement of PIE analysis with a full core simulation: the U1 case, to be submitted in ANE, January 2020.
- [Rondinella, 2011] Rondinella, V.V.: Effects of Helium Build-up on Nuclear Fuel Evolution During Storage. In: Proc. of the 13th International High-Level Radioactive Waste Management Conference (IHLRWMC), Albuquerque, New Mexico, American Nuclear Society, April 10 – 14, 2011.
- [Rondinella, 2012] Rondinella, V.V., Wiss, T., Papaioannou, D., Nasyrow, R.: Studies on nuclear fuel evolution during storage and testing of used fuel response to impact loadings. Proc. 11th International Probabilistic Safety Assessment and Management Conference and the Annual European Safety and Reliability Conference 2012, PSAM11 ESREL 2012, 2012.
- [Rondinella, 2017] Rondinella, V.V., Nasyrow, R., Papaioannou, D., Vlassopoulos, E., Cappia, F., Dieste-Blanco, O., Wiss, T.A.G.: Mechanical integrity studies on spent nuclear fuel rods, Proc. IHLRWMC 2017, Charlotte, North Carolina, American Nuclear Society, April 9 – 13, 2017.
- [Rossiter, 2011] Rossiter, G.: Development of the ENIGMA fuel performance code for whole core analysis and dry storage assessment. *Nuclear Engineering and Technology*, 43, 489, 2011.
- [Rothenstein, 1998] Rothenstein, W., Dagan, R.: Ideal gas scattering kernel for energy dependent cross-sections, *Annals of Nuclear Energy* 25 (1998) 209–222.
- [Rothenstein, 2004] Rothenstein, W.: Proof of the formula for the ideal gas scattering kernel for nuclides with strongly energy dependent scattering cross sections, *Annals of Nuclear Energy* 31 (2004) 9–23.
- [Ruiz, 2015] Ruiz-Hervias, J., Martin-Rengel, M.A., Gomez-Sanchez, F.J.: Failure criteria for unirradiated PWR cladding subjected to ring compression tests. Paper PVP2015-45793, Proc. of the ASME 2015 Pressure Vessels and Piping Conference, Boston, 2015.
- [Šalamon, 2019] Šalamon, L.: Neutron resonance transmission analysis of cylindrical samples used for reactivity worth measurements, *Journal of Radioanalytical and Nuclear Chemistry* 321 (2019) 519–530.
- [Sanborn, 2014] Sanborn, S. Koepfel, B., Klymyshyn, N., Adkins, H., Geelhood, K.: Assembly Level Modeling and Transportation Damage Prediction of Used Nuclear Fuel (UNF) Cladding – 14569. In:

Proc. Waste Management Symposia 2014 (WM2014), Phoenix, Arizona, USA, March 2 – 6, 2014.

[Sanders, 1990] Sanders, T.L., Westfall, R.M.: Feasibility and Incentives for Burnup Credit in Spent-Fuel Transport Casks", Nuclear Science and Engineering 104 (1990) 66–77.

[Sani, 2010] Santi, P.A., Browne, M.C., Parker, R.F., Williams, R.B.: Testing of the dual slab verification detector for attended measurements of the BN-530 dry storage casks, Report LA-UR-09-03480, 2010.

[Sanz, 2008] Sanz, J.: ACAB-2008: Activation Abacus Code V2008", NEA Data Bank NEA-1839.

[Scaglione, 2009] Scaglione, J.M., Wagner, J.C.: Burnup Credit Approach used in the Yucca Mountain License Application, International Workshop on Advances in Applications of Burnup Credit for Spent Fuel Storage, Transport, Reprocessing, and Disposition, Córdoba, Spain, 27 – 30 October 2009.

[Schillebeeckx, 2012] Schillebeeckx, P., Becker, B., Danon, Y., Guber, K., Harada, H., Heyse, J., Junghans, A.R., Kopecky, S., Massimi, C., Moxon, M., Otuka, N., Sirakov, I., Volev, K.: Determination of resonance parameters and their covariance from neutron induced reaction cross section data, Nuclear Data Sheets, 113 (2012) 3054–3100.

[Schillebeeckx, 2018] Schillebeeckx, P., Alaerts, G., Borella, A., Fiorito, L., Govers, K., Paepen, J., Pedersen, B., Stankovskiy, A., Van den Eynde, G., Verwerft, M., Wynants, R., Žerovnik, G.: Characterisation of spent nuclear fuel by theoretical calculations and non-destructive analysis, Proceedings of the International Workshop on Numerical Modelling of NDA Instrumentation and Methods for Nuclear Safeguards, 16 – 17 May 2018, Luxembourg, pp. 101–113.

[Schrödl, 2010] Schrödl, E., Brücher, W., Koch, W., Ballheimer, V.: Experimentelle Untersuchungen zum Verhalten von Brennstäben mit hohem Abbrand bei mechanischen Unfallbelastungen beim Transport, GRS - A – 3490, 2010.

[SCIP] SCIP III – Technical Description, Studsvik Report, STUDSVIK/N-13/172.

[Simakov, 2017] Simakov, S.P., van den Berg, Q.Y.: Update of the  $\alpha$ -n yields for reactor fuel materials for the interest of nuclear safeguards, Nuclear Data Sheets 139 (2017) 190–203.

[Simeonov, 2017] Simeonov, T., Wemple, C.: Update and Evaluation of Decay Data for Spent Nuclear Fuel Analyses, EPJ Web of conferences 146 (2017) 09011.

[Sirakov, 2017] Sirakov, I., Capote, R., Gritzay, O., Kim, H.I., Kopecky, S., Kos, B., Paradela, C., Pronyaev, V., Schillebeeckx, P., Trkov, A.: Evaluation of cross sections for neutron interactions with  $^{238}\text{U}$  in the energy region between 5 keV and 150 keV, European Physics Journal A 53 (2017) 199.

[SKB, 2006] SKB, Measurements of Decay Heat in Spent Nuclear Fuel at the Swedish Interim Storage Facility, Clab", SKB report R-05-62, December 2006 <https://www.skb.se/publikation/1472024/R-05-62.pdf>.

[Smith, 2011] Smith, R.E.: Annotated Bibliography for Drying Nuclear Fuel. United States, 2011.

[Smith, 2013] Smith, H.J., Gauld, I.C., Mertyutrk, U.: Analysis of experimental data for high burnup BWR spent fuel isotopic validation – SVEA-96 and GE14 assembly designs, Report NUREG/CR-7162, March 2013.

[Sonnenburg, 2017] Sonnenburg, H.G., Boldt, F.: Brennstabverhalten im Normalbetrieb, bei Störfällen und bei Langzeitlagerung. GRS-Bericht: GRS – 464, ISBN 978-3-946607-47-2, 2017.

[Stafford, 2015] Stafford, D.S.: Multidimensional simulations of hydrides during fuel rod lifecycle. Journal of Nuclear Materials, Vol. 466, pp. 362–372, 2015.

[Stankovskiy, 2011] Stankovskiy, A., Van den Eynde, G., Vidmar, T.: Development and validation of ALEPH Monte Carlo burnup code, Proc. Int. Workshop NEMEA-6, Krakow, Poland, 25 – 28 October 2010, NEA/NSC/DOC(2011)4, pp. 161–169, 2011.

[Stankovskiy, 2012] Stankovskiy, A., Van den Eynde, G.: 'Advanced Method for Calculations of Core

Burn-Up, Activation of Structural Materials, and Spallation Products Accumulation in Accelerator-Driven Systems, Science and Technology of Nuclear Installations 2012 (2012) 545103.

[Sublet, 2009] Sublet, J.C., Blomquist, R.N., Goluoglu, S., Macfarlane, R.E.: Unresolved resonance range cross section probability and self-shielding factors, CEA Cadarache, Report CEA-R-6227, Juillet 2009.

[Sublet, 2017] Sublet, J.Ch., Eastwood, J.W., Morgan, J.G., Gilbert, M.R., Fleming, M., Arter, W.: FISPACT-II: An Advanced Simulation System for Activation, Transmutation and Material Modelling, Nuclear Data Sheets 139 (2017) 77-137

[Suman, 2018] Suman, S., Khan, M.K., Pathak, M., Singh, R.N.: Effects of hydrogen on thermal creep behaviour of Zircaloy fuel cladding. Journal of Nuclear Materials, Vol. 498, pp. 20–32, 2018.

[Suresh, 2004] Suresh Kumar, K., Mathews, T., Nawada, H.P., Bhat, N.P.: Oxidation behaviour of uranium in the internally gelated urania–ceria solid solutions – XRD and XPS studies. Journal of Nuclear Materials, Vol. 324, pp. 177–182, 2004.

[Suyama, 2005] Suyama, K., Mochizuki, H.: Effect of neutron induced reactions of neodymium-147 and 148 on burnup evaluation, Journal of Nuclear Science and Technology 42 (2005) 661–669.

[Suyama, 2006] Suyama, K., Mochizuki, H.: Corrections to the  $^{148}\text{Nd}$  method evaluation of burnup for the PIE damples from Mihama-3 and Genkai-1, Annals of Nuclear Energy 33 (2006) 335–342.

[Svärd, 2005] Svärd, S.J., Håkansson, A., Bäcklin, A., Osifo, O., Willman, Ch.: Nondestructive experimental determination of the pin-power distribution in nuclear fuel assemblies, Nuclear Technology 151 (2005) 70–76.

[Talip, 2018] Talip, Z., Peugeot, S., Magnin, M., Tribet, M., Valot, C., Vauchy, R., et al.: Characterization of un-irradiated MIMAS MOX fuel by Raman spectroscopy and EPMA. Journal of Nuclear Materials, Vol. 499, pp. 88–97, 2018.

[Tanke, 1991] Tanke, R.H., Jasper, J.E., Gaalman, P.A.M., Killian, D.: Applications of tomography in nuclear research, Kerntechnik, 56, 1991.

[Tardy, 2015] Tardy, M., Kitsos, S., Grassi, G., Santamarina, A., San Felice, L., Riffard, C.: First burnup credit application including actinides and fission products for transport and storage cask by using French experiments, Journal of Nuclear Science and Technology 52 (2015) 1008–2017.

[Tarvainen, 1997] Tarvainen, M., Lévy, F., Valentine, T.E., Abhold, M., Moran, B.: NDA techniques for spent fuel verification and radiation monitoring, STUK-YTO-TR 133, August 1997.

[Taylor, 1980] Taylor, P., Burgess, E.A., Owen, D. G.: An X-ray diffraction study of the formation of  $\beta\text{UO}_2$  on  $\text{UO}_2$  pellet surfaces in air at 229 to 275°C. Journal of Nuclear Materials, Vol. 88, pp. 153–160, 1980.

[Thomas, 1993] Thomas, L.E., Einziger, R.E. Buchanan, H.C.: Effect of fission products on air-oxidation of LWR spent fuel. Journal of Nuclear Materials, Vol. 201, pp. 310–319, 1993.

[Tiitta, 2001] Tiitta, A., Hautamäki, J., Turunen, A., Arlt, R., Carrasco, J.A., Esmailpour-Kazerouni, K., Schwalbach, P.: "Spent BWR fuel characterisation combining a FORK detector with gamma spectrometry, Report STUK-YTO-TR 175, February 2001.

[Tiitta, 2002] Tiitta, A., Saarinen, J., Tarvainen, M., Axell, K., Jansson, P., Carchon, R., Gerits, J., Kulikov, Y., Lee, Y.G.: Investigation on the possibility to use FORK detector for partial defect verification of spent LWR fuel assemblies, Report STUK-YTO-TR 191, September 2002.

[Tobin, 2009] Tobin, S.J.: Determination of plutonium content in spent fuel with non-destructive assay, Presented at the 50<sup>th</sup> INMM Annual Meeting, Tucson, AZ, 11 – 17 July 2009, Report LA-UR- 09-03748 (2009).

[Tobin, 2011] Tobin, S.J., Menlove, H.O., Swinhoe, M.T., Schear, M.A.: Next Generation Safeguards

Initiative research to determine the Pu mass in spent fuel assemblies: purpose, approach, constraints, implementation and calibration, Nuclear Instruments and Methods in Physics Research A 652 (2011) 73–75.

[Tobin 2016] Tobin, S.J., Fugate, M.L., Trelue, H.R., DeBaere, P., Sjöland, A., Liljenfeldt, H., Hu, J., Backstrom, U., Bengtsson, M., Burr, T., Eliasson, A., Favalli, A., Gauld, I., Grogan, B., Jansson, P., Junell, H., Schwalbach, P., Vaccaro, S., Vo, D.T., Wildlestrant, H.: Nondestructive assay data integration with the SKB-50 assemblies – FY16 update, Report LA-UR-16-28290, October 2016.

[Tobin, 2018a] Tobin, S.J., Peura, P., Bélanger-Champagne, C., Moring, M., Dendooven, P., Honkamaa, T.: Utility of including Passive Neutron Albedo Reactivity in an integrated NDA system for encapsulation safeguards, ESARDA Bulletin 56 (2018) 12–18.

[Tobin, 2018b] Tobin, S.J., Peura, P., Bélanger-Champagne, C., Moring, M., Dendooven, P., Honkamaa, T.: Measuring spent fuel assembly multiplication in borated water with a passive neutron albedo reactivity instrument, Nuclear Instruments and Methods in Physics Research A 897 (2018) 32–37.

[Tobin, 2018c] Tobin, S.J., Peura, P., Honkamaa, T., Dendooven, P., Moring, M., Bélanger-Champagne, C.: Passive Neutron Albedo Reactivity in the Finnish encapsulation context, Finnish Radiation and Nuclear Safety Authority, ISBN 978-952-309-406-2, January 2018.

[Tobin, 2019] Tobin, S.J., Tupasela, T., Dendooven, P., Honkamaa, T.: PNAR measurement report, Report LA-UR-19-30861, October 2019.

[Töre, 2013] Töre, C., Rodríguez, A.: Evaluation of REBUS measurements, sample M11, Technical Report SEA – 45, Rev. B, October 2013.

[Trahan, 2020] Trahan, A.C., McMath, G.E., Mendoza, P.M., Trelue, H.R., Backstrom, U., Balkeståhl, L.P., Grape, S., Henzl, V., Leyba, D., Root, M.A., Sjöland, A.: Results of the Swedish spent fuel measurement field trials with the Differential die-Away Self-interrogation Instrument, Nuclear Instruments and Methods in Physics Research A 955 (2020) 163329.

[Trelue, 2013] Trelue, H.R., Galloway, J.D., Fischer, N.A., Tobin, S.: Advances in spent fuel libraries, in Proceedings of the 54<sup>th</sup> Annual Meeting of the Institute of Nuclear Materials Management, pp. 1603–1612, 2013.

[Tsilanzara, 2000] Tsilanzara, A., Diop, C.M., Nimal, B., Detoc, M., Lunéville, L., Chiraon, M., Huynh, T.D., Brésard, I., Eid, E., Klein, J.C., Roque, B., Marimbeau, P., Garzenne, C., Parize, J.M., Vergne, C.: DARWIN: An evaluation code system for a large range of applications, Journal Nuclear Science and Technology, 37 (Supp. 1) (2000) 845–849.

[Tsilanzara, 2016] Tsilanzara, A., Gilardi, N., Huynh, T.D., Jouanne, C., Lahaye, S., Martinez, J., Diop, C.M.: Probabilistic approach for decay heat uncertainty estimation under URANIE platform by using MENDEL depletion code, Annals of Nuclear Energy 90 (2016) 62–70.

[Tuli, 2001] Tuli, J.K.: Evaluated Nuclear Structure Data File, BNL-NCS-51655-01/02-Rev, BNL, 2001.

[Tupasela, 2009] Tupasela, T.: Passive neutron albedo reactivity assay of spent nuclear fuel, Master Thesis, Aalto University, 2 July, 2009.

[UFDC, 2012] UFDC: Review of Used Nuclear Fuel Storage and Transportation Technical Gap Analyses, United States of America - Department of Energy, 2012.  
[https://www.energy.gov/sites/prod/files/Gap Comparison Rev 0.pdf](https://www.energy.gov/sites/prod/files/Gap%20Comparison%20Rev%200.pdf).

[Vaccaro, 2016] Vaccaro, S., Tobin, S.J., Favalli, A., Grogan, B., Jansson, P., Liljenfeldt, H., Mozin, V., Hu, J., Schwalbach, P., Sjöland, A., Trelue, H., Vo, D.: PWR and BWR spent fuel assembly gamma spectra measurements", Nuclear Instruments and Methods in Physics Research A 833 (2016) 208–225.

[Vaccaro, 2018] Vaccaro, S., Gauld, I.C., Hu, J., DeBaere, P., Petersen, J., Schwalbach, P., Smejkal, A., Tomanin, A., Sjöland, A., Tobin, S., Wiarda, D.: Advancing the FORK detector for quantitative spent

nuclear fuel verification, Nuclear Instruments and Methods in Physics Research A 888 (2018) 202–217.

[Vandoorne, 2018] Vandoorne, T.: Calculation of spent fuel and reprocessing waste inventory for SFC-1, ONDRAF/NIRAS, Report 2017-1497 rev1), 2018.

[Vasiliev, 2019] Vasiliev, A., Herrero, J., Pecchia, M., Rochman, D., Ferroukhi, H., Caruso, S.: Preliminary Assessment of Criticality Safety Constraints for Swiss Spent Nuclear Fuel Loading in Disposal Canisters, Materials 12 (2019) 494.

[Viitanen, 2009] Viitanen, T.: Implementing a Doppler-preprocessor of cross section libraries in reactor physics code Serpent, M.Sc. Thesis, Helsinki University of Technology, 2009.

[Vlassopoulos, 2017b] Vlassopoulos, E., Nasyrow, R., Papaioannou, D., Rondinella, V.V., Caruso, S., Pautz, A.: Destructive tests for determining mechanical integrity of spent nuclear fuel rods. In: ANS IHLRWM 2017 - 16th International High-Level Radioactive Waste Management Conference: Creating a Safe and Secure Energy Future for Generations to Come - Driving Toward Long-Term Storage and Disposal, pp. 726–733, 2017.

[Vlassopoulos, 2018a] Vlassopoulos, E., Papaioannou, D., Nasyrow, R., Caruso, S., Raffuzzi, V., Gretter, R., Fongaro, L., Somers, J., Rondinella, V.V., Grünberg, P., Pautz, A., Helfenstein, J., Schwizer, P.: Mechanical Integrity of Spent Nuclear Fuel: From Experimental to Numerical Studies. TOPFUEL 2018, ENS, Prague, 2018.

[Vlassopoulos, 2018b] Vlassopoulos, E., Nasyrow, R., Papaioannou, D., Gretter, R., Fongaro, L., Somers, J., Rondinella, V.V., Caruso, S., Grünberg, P., Helfenstein, J., Schwizer, P., Pautz, A.: Response of irradiated nuclear fuel rods to quasi-static and dynamic loads. Kerntechnik, Vol. 83, pp. 507–512, 2018.

[Wang, 2018] Wang, J., Wang, H., Jiang, H., Bevard, B.: High burn-up spent nuclear fuel transport reliability investigation. Nuclear Engineering and Design, Vol. 330, pp. 497–515, 2018.

[Wasywich, 1993] Wasywich, K. M., Hocking, W. H., Shoesmith, D. W., and Taylor, P.: Differences in Oxidation Behavior of Used CANDU Fuel During Prolonged Storage in Moisture-Saturated Air and Dry Air at 150°C, Nuclear Technology, vol. 104, pp. 309-329, 1993.

[Werner, 2017] Werner, C.: MCNP6 User's Manual, Code version 6.2, Report. LA-UR-17-29981, 2017.

[White, 2018] White, T., Mayorov, M., Lebrun, A.R., Peura, P.: Verification of Spent Nuclear Fuel Using Passive Gamma Emission Tomography (PGET), IAEA Symposium on International Safeguards, 2018,

[Wieselquist, 2013] Wieselquist, W., Zhu, T., Vasiliev, A., Ferroukhi, H.: PSI methodologies for nuclear data uncertainty propagation with CASMO-5M and MCNPX: results for OECD/NEA UAM benchmark phase I, Science and Technology of Nuclear Installations, 2013 (2012) 549793.

[Wigner, 1944] Wigner, E.P., Wilkins, E.J.: AECD-2275, Clinton Laboratory, 1944,

[William, 2006a] William, C., Håkansson, A., Osifo, O., Bäcklin, A., Svärd, S.J.: Nondestructive assay of spent nuclear fuel with gamma-ray spectroscopy, Annals of Nuclear Energy 33 (2006) 427–438.

[William, 2006b] William, C., Håkansson, A., Osifo, O., Bäcklin, A., Svärd, S.J.: A non-destructive method for discriminating MOX fuel from LEU fuel for safeguards purposes, Annals of Nuclear Energy 33 (2006) 766–773.

[Williams, 1978] Williams, M.L., Weisbin, C.R.: Sensitivity and uncertainty analysis for functionals of the time-dependent nuclide density field, ORNL-5393, April 1978.

[Williams, 2011] Williams, M.L.: Resonance Self-Shielding Methodologies in SCALE6, Nuclear Technology 174 (2011) 149–168.

[Williams, 2013a] Williams, M.L., Kim, K.S.: The Embedded Self-Shielding Method, PHYSOR 2012, Knoxville, Tennessee, USA.

- [Williams, 2013b] Williams, M.L., Ilas, G., Jesse, M.A., Rearden, B.T., Wiarda, D., Zwermann, W., Gallner, L., Klein, M., Krzykarcz-Hausmann, B., Pautz, A.: A Statistical Sampling Method for Uncertainty Analysis with SCALE and XSUSA, Nuclear Technology 183 (2013) 515–526. xxx
- [Wilson, 1961] Wilson, W.B., Alexander, C.A., Gerds, A.F.: Stabilization of UO<sub>2</sub>. Journal of Inorganic and Nuclear Chemistry, Vol. 20, pp. 242–251, 1961.
- [Wilson, 2008] Wilson, W.B., Cowell, S.T., England, T.R., Hayes, A.C., Moller, P.: A Manual for CINDER'90 Version 07.4 Codes and Data, LA-UR-07-8412 (December 2007, Version 07.4.2 updated March 2008).
- [Wiss, 2014] Wiss, T., Hiernaut, J.-P., Roudil, D., Colle, J.-Y., Maugeri, E., Talip, Z., et al.: Evolution of spent nuclear fuel in dry storage conditions for millennia and beyond, Journal of Nuclear Materials, vol. 451, pp. 198-206, 2014.
- [Wood, 1986] Wood, P., Banniste, G.H.: Release of Fission Products During and After Oxidation of Trace-Irradiated Uranium Dioxide at 300 – 900 °C. In: Proceedings of IAEA Specialists' Meeting on Fission Product Release and Transport in Gas Cooled Reactors (Berkeley, United Kingdom, October 22 –25,1985), Austria, 1986.
- [Woodcock, 1965] Woodcock, E.R. et al.: Techniques used in the GEM code for Monte Carlo neutronics calculations in reactors and other systems of complex geometry, ANL-7050, Argonne National Laboratory, 1965.
- [Yaakoubi, 2019] Yaakoubi, H.E. et al.: Validation study of the reactor physics lattice transport code DRAGON5 & the Monte Carlo code OpenMC by critical experiments of light water reactors", Journal of King Saud University, Vol. 33 (1), pp. 1271–1275, 2019.
- [Yamamoto, 2007] Yamamoto, A., Tatsumi, M., Sugimura, N.: Numerical solution of stiff burnup equation with short half lived nuclides by the Krylov subspace method, Journal of Nuclear Science and Technology 44 (2007) 147–154.
- [You, 2000] You, G.-S., Kim, K.-S., Min, D.-K., Ro, S.-G.: Oxidation kinetic changes of UO<sub>2</sub> by additive addition and irradiation. Journal of Nuclear Materials, Vol. 277, pp. 325–332, 2000.
- [Zain, 2018] Zain, J.A. et al.: Validation of DRAGON4/DONJON4 simulation methodology for a typical MNSR by calculating reactivity feedback coefficient and neutron flux, Journal of Results in Physics 9 (2018) 1155–1160.
- [Zéachandirin, 2011] Zéachandirin, A., Dallongeville, M., Purcell, P., Cory, A.: Description of Fuel Integrity Project methodology principles. Packaging, Transport, Storage & Security of Radioactive Material, Vol. 22, pp. 184–191, 2011.
- [Žerovnik, 2018] Žerovnik, G., Schillebeeckx, P., Govers, K., Borella, A., Čalić, D., Fiorito, L., Kos, B., Stankovskiy, A., Van den Eynde, G., Verwerf, M.: Observables of interest for the characterisation of Spent Nuclear Fuel, JRC Technical Reports, EUR 29301 EN, 2018.
- [Žerovnik, 2019] Žerovnik, G., Ambrožič, K., Čalić, D., Fiorito, L., Govers, K., Hernandez Solis, A., Kos, B., Kromar, M., Schillebeeckx, P., Stankovskiy, A.: Characterization of spent PWR fuel for decay heat, neutron and gamma-ray emission rate: code comparison,' Proceedings of the International Conference on Mathematics and Computational Methods applied to Nuclear Science and Engineering (M&C 2019), Portland, USA, 25 – 29 August 2019, pp. 2736–2745.
- [Zhu, 2015] Zhu, T., Vasiliev, A., Ferroukhi, H., Pautz, A.: NUSS: A tool for propagating multigroup nuclear data covariances in pointwise ACE-formatted nuclear data using stochastic sampling method, Annals of Nuclear Energy 75 (2015) 713-722.

[Ziock, 2005] Ziock, K.P., Vanier, P., Forman, L., Caffrey, G., Wharton, J., Lebrun, A.: The feasibility of cask "Fingerprinting" as a spent-fuel, dry-storage cask safeguards technique, Report UCRL-TR-215943, 5 October, 2005.

[Zoia, 2013] Zoia, A., Brun, E., Jouanne, C., Malvagi, F.: Doppler broadening of neutron elastic scattering kernel in TRIPOLI-4, *Annals of Nuclear Energy* 54 (2013) 218–226.

[Zu, 2016] Zu, T., Yang, C., Cao, L., Wu, H.: Nuclear data uncertainty propagation analysis for depletion calculation in PWR and FR pin-cells, *Annals of Nuclear Energy* 94 (2016) 399–408.

[Zwermann, 2014] Zwermann, W., Aures, A., Gallner, L., Hannstein, V., Krzykacz-Hausmann, B., Velkov, K., Martinez, J.: Nuclear data uncertainty and sensitivity analysis with XSUSA for the fuel assembly depletion calculations, *Nuclear Engineering Technology* 46 (2014) 343–352.

[Zwicky, 2010] Zwicky, H.U., Low, J., Granfors, M., Alejano, C., Conde, J.M., Casado, C., Sabater, J., Lloret, M., Quecedo, M., Gago, J.A.: Nuclide analysis in high burnup fuel samples irradiated in Vandellós 2, *Journal of Nuclear Materials* 402 (2010) 60–73.

<http://www.oecd-nea.org/dbdata/data/evaluated.htm>

<https://www-nds.iaea.org/>